A SEARCH FOR LEPTON FLAVOUR VIOLATION IN Z^0 DECAYS WITH THE DELPHI DETECTOR AT LEP

Cand. Scient. Thesis in Experimental Particle Physics

Department of Physics
University of Oslo
Norway

Øystein Krogen

April 27, 1995

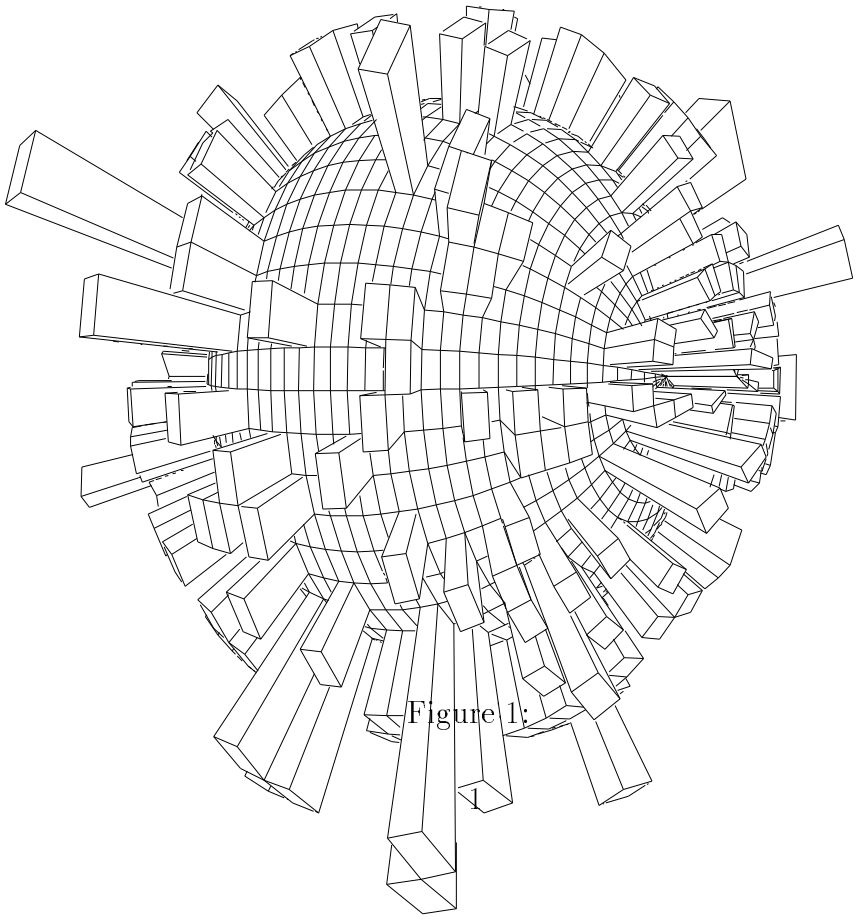

Figure 1:

Contents

List of Figures

List of Tables

1 INTRODUCTION

In this thesis a search for lepton-flavour-violating Z^0 boson decays into lepton pairs is described. All data, collected with the DELPHI detector at LEP during 1991, 1992, and 1993 runs, corresponding to 2.2×10^6 Z^0's, were used.

The number of candidates was consistent with the estimated background. At the 95% confidence level the upper limits on the branching ratios for $\mu\tau$ was 2.9×10^{-5}, eτ was 4.5×10^{-5}, and eμ was 0.4×10^{-5}.

CHAPTER 2 gives a short introduction to the subject with references to previous searches.

The theory which this thesis is based upon, the so called Standard Model, and also possible extensions to it which again could lead to lepton flavour violating processes, are presented in CHAPTER 3.

In CHAPTER 4 the LEP accelerator and the DELPHI detector are described.

CHAPTER 5 describes the search.

Estimation of background from -, and smearing of Monte Carlo simulated events are described in CHAPTER 6, where also the upper limit calculations are given.

The final results are presented in CHAPTER 7

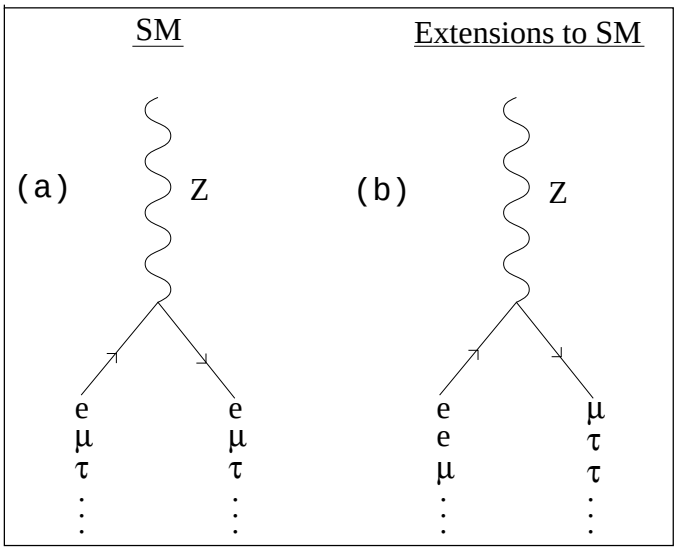

Figure 2: *a) Standard Model neutral currents. b) Lepton flavour changing neutral currents.*

2 MOTIVATION

2.1 Test of the Standard Model

Despite the success of the Standard Model there seems to be consensus that it is not the final theory.

It is important to search for phenomena which can lead one beyond the standard model.

The decays of $Z^0 \rightarrow e\mu$, $\mu\tau$, and $e\tau$ due to lepton-flavour-violating-current are strictly forbidden in the standard model, but are allowed in several extension models (figure 2). If they exist they should show clear signals in the experimental apparatus, and could be testable if the rate is high enough.

Violation of lepton flavour conservation would indicate new physics beyond the Standard Model, possibly related to the properties of the neutrinos, and the leptonic weak interaction.

A search for lepton flavour violating decays might be a test of the Standard Model and/or different models beyond it.

2.2 Models beyond Standard Model

Lepton flavour violation could arise from the existence of non-zero neutrino masses and the possible related existence of neutral singlet heavy leptons such as right-handed neutrinos

By extending the standard $SU(2)\otimes U(1)$ electro-weak theory leptonic flavour violation may arise even if the neutrinos are strictly massless. The effects are potentially large and may be manifested either in the domain of low energy processes or at the Z peak.

Existing models beyond the Standard Model are predicting lepton flavour violating processes up to an order of 10^{-4} for some minimal supersymmetric models. But for most models, the upper limits for these lepton flavour violating processes, are still out of reach for this and other direct searches.

Also if not finding any evidence for lepton flavour violation, a search for, and hopefully a lowering of the existing upper limits for lepton flavour violation processes, will possibly at least exclude some of the models proposed.

2.3 LEP

The Large Electron Positron accelerator LEP(section: 4) with its four experiments is a high-luminosity Z^0 factory. It is working for long periods at the Z^0 resonance, and thereby gives an excellent opportunity to test fundamental symmetries of the standard electro-weak theory, and thus the standard model. By 1993 the experiments had produced close to 3 million observed Z^0 in each of the four detectors.

LEP experiments

In this thesis the DEtector with Lepton, Photon and Hadron Identification - DELPHI was used (section: 4.3). The three detectors ALEPH, The (Omni-Purpose Apparatus at LEP -) OPAL and DELPHI have a similar structure, consisting of mainly the same detector types and magnetic field, while L3 is slightly different. The speciality of the DELPHI detector is the Cerenkov counter, a very good instrument for tagging, especially hadrons. Unfortunately for this thesis it is not very useful for lepton tagging, and also was not working until the 1993 data taking.

2.4 Previous experimental results

Previous searches for lepton flavour violating events at LEP has been published for all the four Detectors; ALEPH, L3 [7], OPAL [8, 9], and DELPHI [5]. No evidence of lepton flavour violating events were found. Upper limits at 95% confidence level are given in table 1.

Upper limits for the $Z^0 \rightarrow \mu\tau$ and $Z^0 \rightarrow$eτ channels based on tau decay were reported from the CLEO collaboration [12]. The upper limits are also given in table 1 ([21]).

Low energy experiments have already given limits in the $Z^0 \rightarrow \mu$e channel out of reach for the kind of search described in this thesis at LEP.

Low energy experimental results are mainly based on the failure to observe the neutrinoless $\mu \rightarrow$eee, $\tau \rightarrow$eee, $\tau \rightarrow \mu\mu\mu$ decays and indirectly give limits on $Z^0 \rightarrow \mu$e, $Z^0 \rightarrow \tau$e, $Z^0 \rightarrow \tau\mu$ [32].

A μe branching fraction upper limit of 10^{-13} from the SINDRUM collaboration will not be possible to match even with 100% efficiency in particle identification.

But low energy experiments might not be sufficient since lepton flavour violating processes might in some models be energy dependent.

Other possible lepton flavour violation channels like $\tau \rightarrow \mu\gamma$ and $\tau \rightarrow$eγ have been searched for at LEP with no evidence of lepton flavour violation. Upper limits at 90% confidence level of 1.3×10^{-4} and 9.4×10^{-5} were obtained in the $\mu\gamma$ and eγ

channels respectively [25]. Other lepton flavour violation searches in tau decay are also published [12, 6].

Experiment	decay mode			Data sample
	$Z^0 \to \mu\tau$	$Z^0 \to e\tau$	$Z^0 \to \mu e$	
L3 95% CL	1.1×10^{-5}	0.87×10^{-5}	0.39×10^{-5}	90-93
OPAL 95% CL	2.9×10^{-5}	2.3×10^{-5}	0.36×10^{-5}	91-93
ALEPH 95% CL	3.5×10^{-5}	1.7×10^{-5}	0.37×10^{-5}	90-92
DELPHI 95% CL	8.0×10^{-5}	7.0×10^{-5}	1.9×10^{-5}	90-92
LOW E. 90% CL	6.0×10^{-5}	10.0×10^{-5}	7.5×10^{-13}	(SINDRUM) (CLEO)

Table 1: *Previous experimental results LEP and low energy. The results for L3, ALEPH, and OPAL in this table are preliminary.*

3 THEORETICAL FOUNDATION

In this section a short introduction to the Standard Model, concentrating on leptons, is given in sections 3.1.

A short description of models which are extensions of -, and beyond the standard model, like Supersymmetry, GUT, and String theories, are presented in section 3.2.

Finally section 3.3 gives an introduction to massive neutrinos.

3.1 The STANDARD MODEL

The underlying principle of the Standard Model is spontaneously broken local gauge symmetries (see sections 3.1.7 and 3.1.8): [29] [16] [17]

$$SU_c(3) \otimes SU_I(2) \otimes U_Y(1) + Higgssector \quad (1)$$

- The Standard Model accomodate all quarks, leptons and bosons except the graviton (G)
- The Model enables us to calculate cross sections, lifetimes etc to high precision.
- The Model can accomodate all experimental data so far. If not, the model would be dead.
- The Model predicts the existence of the Higgs boson. Previous predictions of W, Z, and top were confirmed.

3.1.1 Problems

- Why precisely the symmetry in Equation 1
- Why particle masses ?

  The model works perfectly well without masses. The Electro Weak broken symmetry which introduces masses, is only introduced to get mass terms to the Lagrangian and is no consequence of the theory which works perfectly well without.
- Why 3[1] generations ?

  It is nothing in the theory which tells how many families.
- The Standard Model says nothing about the Gravitation.
- The number of free parameters are large. (21).

[1] A very important result obtained at LEP, assuming a light neutrino in each family [19].

3.1.2 Feynman Diagrams

The language of the Standard Model is Feynman Diagrams.

The Feynman rules are derived from a Lagrangian, based on criteria of gauge symmetry and renormalisation.

Given Feynman rules, one can in principle calculate all experimentally observable quantities in any model.

3.1.3 Invariance/Symmetries

Manipulations that leave the Lagrangian ($\int$d^{4}xL) numerical invariant do not have any physical effect. A good Lagrangian should allow some obvious manipulation like Lorentz-invariance which implies momentum/energy conservation etc.

GAUGE SYMMETRIES

In Quantum Electro Dynamics - QED, the electron field Ψ has a complex phase which is unobservable. The physics should therefore not change if phase is changed from point to point:

$$\Psi(x) \rightarrow e^{-iq\alpha(x)}\Psi(x), \bar{\Psi}(x) \rightarrow e^{-iq\alpha(x)}\bar{\Psi}(x) \tag{2}$$

But then is the Lagrangian for a free electron no longer invariant because of an unwanted term. To compensate for this an extra field A$^\mu$, which add an interaction term in the Lagrangian, is introduced. By definition;

$$A^\mu(x) \rightarrow A^\mu(x) + \partial^\mu_\alpha(x) \tag{3}$$

The combined Lagrangian

$$L = \bar{\Psi}(i\gamma^\mu\partial_\mu + m)\Psi + \bar{\Psi}\gamma^\mu\Psi A_\mu - \frac{1}{4}F^{\mu\nu}F_{\mu\nu} \tag{4}$$

($F_{\mu\nu} = \partial_\mu A_\nu(x) - \partial_\nu A_\mu(x)$ is invariant)
is invariant under local phase transformations.

This predicts:

- The gauge field A_μ must be a spin -1 field
- The gauge field must be massless
- The transformation property $A^\mu \rightarrow A^\mu + \partial^\mu_\alpha$ is required.

There are more complicated possibilities for invariance:

- Colour for quarks SU(3) $\rightarrow$ gluons
- Weak Isospin and weak hypercharge SU(2)$_I \otimes$U$_Y$(1) $\rightarrow$ W^{+-}, Z^0

But W^{+-} and Z^0 are not massless so something else is needed; which introduces spontaneously broken symmetry, the Higgs field (section: 3.1.8).

3.1.4 Particles

The current picture is postulating fermions as the fundamental particles in nature. The fermions known as quarks and leptons can be grouped into three generations or families table 2. The first generation with up and down quark, electron and electron neutrino builds all matter in nature. The second and third generations are unstable and therefore only observed through interaction processes.

FERMIONS (S=1/2)				
part. type	1.family	2.family	3.family	Q
Leptons	ν_e	ν_μ	ν_τ	0
	e	μ	τ	-1
Quarks	up	charm	top	+2/3
	down	strange	bottom	-1/3

Table 2: *Particles in the Standard Model*

3.1.5 Forces

Interaction between fermions occur via four principal forces: gravity, electromagnetism, the strong force, and the weak force. Forces, having particle-nature can be traced to fundamental bosons:

- Vector bosons(S=1)
  1. Electromagnetic force - photon
  2. Weak force - W^+, W^-, Z^o
  3. Strong force - 8 gluons
- Tensor Bosons(S=2)
  1. Gravitation force - (G)
- Scalar boson
  1. Higgs - (H)

3.1.6 QED/Electromagnetism

Electromagnetic interaction is introduced into the free-fermion Lagrangian density:

$$L_0 = \bar{\psi}(x)(i\gamma^\mu \partial_\mu - m)\psi(x) \tag{5}$$

through the minimal substitution:

$$\partial_\mu \rightarrow D_\mu = [\partial_\mu + iqA_\mu(x)] \tag{6}$$

(Where q is the charge of the particle annihilated by the field $\psi(x)$.)

The Lagrangian density is required to be invariant under gauge transformation of the electromagnetic field:

$$A_\mu \rightarrow A'_\mu(x) = A_\mu + \partial_\mu f(x) \tag{7}$$

(f(x) is a real differentiable function)

This invariance is ensured if the Dirac fields undergo the gauge transformation[2]:

$$\psi(x) \rightarrow \psi'(x) = \psi(x)e^{-iqf(x)} \tag{8}$$

$$\bar{\psi}(x) \rightarrow \bar{\psi}'(x) = \bar{\psi}(x)e^{-iqf(x)} \tag{9}$$

QED is the simplest example of a gauge theory.

[2] Also called a local phase transformation

3.1.7 Weak interaction

In this chapter a short description of the weak interaction leading to the electroweak theory is given. Only leptons are considered. The starting point will be the Intermediate Vector Boson theory IVB. Problems arising in the IVB theory will then lead to the gauge theory, and finally to generate masses in a renormalizable theory, the spontaneous symmetry breaking in the so called Higgs model [16] [17].

Coupling strengths are inversely related to lifetimes. Observations of lifetimes of the order of 10^{-6} - 10^{-8} compared to the lifetimes of 10^{-23} in Strong and of 10^{-16} in electromagnetic interaction processes, were evidence of another type of interaction, with a weaker coupling.

All hadrons and leptons experience this weak interaction, and can undergo weak decay, but are often hidden by the much more rapid color or electromagnetic decays.

Neutrinos can only interact by weak interactions. They are colorless, electrical neutral, and within experimental limits massless.

IVB THEORY

The IVB theory is the basis of modern theory of weak interaction. The weak interaction Hamiltonian density responsible for leptonic processes is constructed from bilinear forms of the leptonic field operator assuming that the lepton field only enter the interaction in the combination:

$$\begin{array}{l} J_\alpha(x) = \sum_l \bar{\psi}_l(x)\gamma_\alpha(1-\gamma_5)\psi_{\nu_l}(x) \\ J^\dagger_\alpha(x) = \sum_l \bar{\psi}_{\nu_l}(x)\gamma_\alpha(1-\gamma_5)\psi_l(x) \end{array} \tag{10}$$

(Where l labels the various charged lepton fields, l=e,μ,τ, and ν_l the corresponding neutrino fields.)

The term:

$$\bar{\psi}_e(x)\gamma_\alpha(1-\gamma_5)\psi_{\nu_e}(x)$$

is linear in electron creation and positron absorption operators and in ν_e absorption and $\bar{\nu}_e$ creation operators. Any interaction built up from these leptonic currents conserves lepton numbers (section 3.1.11).

In analogy with the electromagnetic interaction as being transmitted by photons, weak interaction is described as due to transmission of quanta, called W particles. The leptonic interaction of IVB is:

$$H_I(x) = g_W J^{\alpha\dagger}(x)W_\alpha(x) + g_W J^\alpha(x)W^\dagger_\alpha(x) \tag{11}$$

(Where g_W is a coupling constant and the field $W_\alpha(x)$ describes the W particles.)

The interaction of equation 11 couples the field $W_\alpha(x)$ to the leptonic vector current, it must be a vector field, and the W particles are vector bosons with spin 1. Each term in the leptonic current involves a charged and a neutral lepton, therefore

the W particles are electrically charged. From general arguments relating the range of a force to the mass of the quanta transmitting it, the W bosons must be very massive.

The interaction in equation 11 is known as V-A (Vector - axial vector) interaction since it can be written as the difference between a vector current and an axial vector current. Parity is not conserved under these interactions, a characteristic of all weak interactions.

The term $\frac{1}{2}(1-\gamma_5)$ is a helicity projection operator for zero mass particles (like neutrinos). Since ψ_{ν_l}(x)is linear in neutrino absorption operators and in antineutrino creation operators, it follows that in the interaction in equation 11 only negative helicity neutrinos can be annihilated and positive helicity antineutrinos can be created. In weak interaction only these states play a role, and positive helicity neutrinos and negative helicity antineutrinos do not take part.

For particles of non-zero mass the states projected out by the helicity projection operators $P_L=\frac{1}{2}(1-\gamma_5)$ and $P_R=\frac{1}{2}(1+\gamma_5)$ are helicity eigenstates only in the high-energy limit in which the particle energy is very large compared to the particle mass. This will always be a good approximation for neutrinos even if their masses are not precisely zero.

The left handed charged lepton field is defined:

$$\psi_l^L(x) \equiv P_L \psi_l(x)$$

And the leptonic current can be written:

$$J_\alpha(x) = 2\sum_l \bar{\psi}_l^L(x)\gamma_\alpha \psi_{\nu_l}^L(x) \tag{12}$$

This means that only the left-handed fields are involved for the charged leptons.

The IVB theory represent a phenomenological theory, and only processes which do not involve loop integrals in the lowest order of perturbation theory, can be calculated. The IVB theory is not renormalizable.

It fails to describe processes like ν_μ - e scattering, ($\nu_\mu + e^- \rightarrow \nu_\mu + e^-$) where the measured cross-section are comparable to the cross-sections for processes like ν_e - e scattering. This suggest that the IVB interaction is not complete, and that the leptonic interaction contains additional terms which allow ν_μ - e scattering to occur as a one-boson-exchange process. To retain lepton number conservation, the extra terms will involve the exchange of a neutral vector boson Z^0.

The existence of the Z^0 boson and the presence of neutral-current terms in the interaction, are required by the standard electro-weak theory, to be renormalizable.

The renormalizability of the theory of weak interaction is achieved by formulating it as a gauge theory.

GAUGE THEORY OF WEAK INTERACTION

The requirement of of gauge invariance leads to the neutral leptonic current. At the same time a unification of electromagnetic and weak interaction is achieved

in a natural way. The gauge invariance described here necessitate all leptons and vector bosons to be massless. In section 3.1.8 this problem will be solved introducing spontaneously broken symmetry, the so called Higgs mechanism.

To formulate the theory of weak interaction as a gauge theory, one need to find a set of global phase transformations, which leave the free-lepton Lagrangian density invariant, leading to conservation of the weak currents of equation 12.

Assuming all leptons to be massless, and since the leptonic current and leptonic interaction involve only left-handed lepton fields, a splitting of the field in left- and right-handed terms ψ^L(x)=P$_L\psi$(x), and ψ^R(x)=P$_R\psi$(x). Combining the fields ψ_l^L and $\psi_{\nu_l}^L$ into a two-component field

$$\Psi_l^L(x) = \begin{pmatrix} \psi_{\nu_l}^L \\ \psi_l^L \end{pmatrix}$$

the free-lepton Lagrangian density then becomes:

$$L_0 = i[\bar{\Psi}_l^L(x)\ \not{\partial}\Psi_l^L(x) + \bar{\psi}_l^R(x)\ \not{\partial}\psi_l^R(x) + \bar{\psi}_{\nu_l}^R(x)\ \not{\partial}\psi_{\nu_l}^R(x)] \tag{13}$$

The left-right asymmetry of weak interaction can be described in terms of different transformation properties of the left- and right-handed fields.

The set of transformations

$$\Psi_l^L(x) \rightarrow \Psi_l^{L'}(x) = U(\vec{\alpha})\Psi_l^L(x)$$
$$\bar{\Psi}_l^L(x) \rightarrow \bar{\Psi}_l^{L'}(x) = \bar{\Psi}_l^L(x)U^\dagger(\vec{\alpha})$$

leaves the term i$\bar{\Psi}_l^L$(x)$\not{\partial}\Psi_l^L$(x) in eq: 13 invariant.

(The operators U($\vec{\alpha}$)$\equiv exp[\frac{i}{2}\alpha_j\tau_j]$ is unitary for any three real numbers $\vec{\alpha} \equiv (\alpha_1, \alpha_2, \alpha_3)$, τ_j are the 2x2 Hermitian Pauli spin matrices.)

The operators U($\vec{\alpha}$) are 2x2 unitary matrices with det U($\vec{\alpha}$)=1 called SU(2) transformations.

The two-component lepton-field transformations correspond to two-dimensional global phase transformations with properties identical to those of the two-component isospinors describing the nucleon. Ψ_l^L is therefore called a weak isospinor. Each right-handed lepton field is defined to be a weak isoscalar i.e. to be invariant under any SU(2) transformation:

$$\psi_l^R(x) \rightarrow \psi_l^{R'}(x) = \psi_l^R(x) \quad \psi_{\nu_l}^R(x) \rightarrow \psi_{\nu_l}^{R'}(x) = \psi_{\nu_l}^R(x)$$

$$\bar{\psi}_l^R(x) \rightarrow \bar{\psi}_l^{R'}(x) = \bar{\psi}_l^R(x) \quad \bar{\psi}_{\nu_l}^R(x) \rightarrow \bar{\psi}_{\nu_l}^{R'}(x) = \bar{\psi}_{\nu_l}^R(x)$$

From the invariance of the Lagrangian density the conservation of three weak isospin currents follows:

$$J_i^\alpha(x) = \frac{1}{2}\bar{\Psi}_l^L(x)\gamma^\alpha\tau_i\Psi_l^L(x) \tag{14}$$

and conserved quantities called weak isospin charges:

$$I_i^W = \frac{1}{2}\int d^3x\Psi_l^{L\dagger}(x)\tau_i\Psi_l^L(x) \tag{15}$$

The leptonic currents of equation 10 can be written as linear combinations of the conserved weak isospin currents $J_1^\alpha(x)$ and $J_2^\alpha(x)$:

$$\begin{array}{l} J^\alpha(x) = 2[J_1^\alpha(x) - iJ_2^\alpha(x)] = \bar{\psi}_l(x)\gamma^\alpha(1-\gamma_5)\psi_{\nu_l}(x) \\ J^{\alpha\dagger}(x) = 2[J_1^\alpha(x) + iJ_2^\alpha(x)] = \bar{\psi}_{\nu_l}(x)\gamma^\alpha(1-\gamma_5)\psi_l(x) \end{array} \tag{16}$$

But this also lead to the conservation of a third current:

$$J_3^\alpha(x) = \frac{1}{2}\bar{\Psi}_l^L(x)\gamma^\alpha\tau_3\Psi_l^L(x) \tag{17}$$

This is a so called neutral current since it couples either electrically neutral leptons or electrically charged leptons.

The weak hypercharge current is defined by:

$$J_Y^\alpha(x) = -\frac{1}{2}\bar{\Psi}_l^L(x)\gamma^\alpha\Psi_l^L(x) - \bar{\psi}_l^R(x)\gamma^\alpha\psi_l^R(x) \tag{18}$$

The corresponding conserved weak hypercharge Y is related to the electric charge Q and the weak isocharge I_3^W by:

$$Y = \frac{Q}{E} - I_3^W$$

3.1.8 Electro-weak interaction

To generalize the SU(2) and U(1) transformations from global to local phase transformations, and to retain invariance under local phase transformations one have to introduce gauge fields which will automatically generate the interactions.

This is obtained by starting with the SU(2) transformations, and replacing the global transformations by local phase transformations:

$$\begin{array}{ll} \Psi_l^L(x) \to \Psi_l^{L'}(x) = e^{\frac{i}{2}g\tau_j\omega_j(x)}\Psi_l^L(x) & \\ \bar{\Psi}_l^L(x) \to \bar{\Psi}_l^{L'}(x) = \bar{\Psi}_l^L(x)e^{-\frac{i}{2}g\tau_j\omega_j(x)} & \\ \psi_l^R(x) \to \psi_l^{R'}(x) = \psi_l^R(x), & \psi_{\nu_l}^R(x) \to \psi_{\nu_l}^{R'}(x) = \psi_{\nu_l}^R(x) \\ \bar{\psi}_l^R(x) \to \bar{\psi}_l^{R'}(x) = \bar{\psi}_l^R(x), & \bar{\psi}_{\nu_l}^R(x) \to \bar{\psi}_{\nu_l}^{R'}(x) = \bar{\psi}_{\nu_l}^R(x) \end{array} \tag{19}$$

(Where $\omega_j(x)$ are three arbitrary real differentiable functions, and g the coupling constant.)

The differential operator $\not{\partial}$ of the spinor term in the free-lepton Lagrangian density (L) will also act on the function ω_j(x) and L will no longer be invariant

under this transformation. The invariance is obtained by replacing the the ordinary derivatives $\partial^\mu \Psi_l^L$(x) by the covariant derivatives:

$$\partial^\mu \Psi_l^L(x) \to D^\mu \Psi_l^L(x) = [\partial^\mu + \frac{i}{2} g \tau_j W_j^\mu(x)] \Psi_l^L(x) \tag{20}$$

The corresponding local phase transformations for U(1) transformations are:

$$\begin{array}{l} \psi(x) \to \psi'(x) = e^{ig'Yf(x)}\psi(x) \\ \bar{\psi}(x) \to \bar{\psi}'(x) = \bar{\psi}(x) e^{-ig'Yf(x)} \end{array} \tag{21}$$

The Lagrangian density is invariant under local phase transformations if the ordinary derivatives are replaced by covariant derivatives:

$$\partial^\mu \psi(x) \to D^\mu \psi(x) = [\partial^\mu + ig'YB^\mu(x)]\psi(x) \tag{22}$$

The real gauge field B^μ(x) introduced transforms like:

$$B^\mu(x) \to B^{\mu'}(x) = B^\mu(x) - \partial^\mu f(x) \tag{23}$$

The SU(2)$\otimes$U(1) gauge-invariant leptonic Lagrangian density becomes:

$$L^L = i[\bar{\Psi}_l^L(x) \not{D} \Psi_l^L(x) + \bar{\psi}_l^R(x) \not{D} \psi_l^R(x) + \bar{\psi}_{\nu_l}^R(x) \not{D} \psi_{\nu_l}^R(x)] \tag{24}$$

Where

$$\begin{array}{l} D^\mu \Psi_l^L(x) = [\partial^\mu + \frac{i}{2} g \tau_j W_j^\mu(x) - \frac{i}{2} g' B^\mu(x)] \Psi_l^L(x) \\ D^\mu \psi_l^R(x) = [\partial^\mu - ig' B^\mu(x)] \psi_l^R(x) \\ D^\mu \psi_{\nu_l}^R(x) = \partial^\mu \psi_{\nu_l}^R(x) \end{array} \tag{25}$$

From this one obtains:

$$\begin{array}{l} W_\mu^\pm(x) = \frac{1}{\sqrt{2}}[W_{1\mu}(x) \pm iW_{2\mu}(x)] \\ W_{3\mu}(x) = \cos\theta_W Z_\mu(x) + \sin\theta_W A_\mu(x) \\ B_\mu(x) = -\sin\theta_W Z_\mu(x) + \cos\theta_W A_\mu(x) \end{array} \tag{26}$$

(The angle θ_W is known as the weak mixing angle, or Weinberg angle and specifies the mixture of the two different Hermitian fields $A_\mu(x)$ and $Z_\mu(x)$.)

The gauge field A_μ(x) is required to be the electromagnetic field and is coupled to electric charges through the term -s^μ(x)A_μ(x) in the Lagrangian density.

The mixing angle θ_w is given by the ratio of the coupling constants of the two independent groups U(1) and SU(2):

$$g \sin\theta_W = g' \cos\theta_W = e \tag{27}$$

The final expression for the interaction Lagrangian density is:

$$L_I = -s^\mu(x)A_\mu(x) - \frac{g}{2\sqrt{2}}[J^{\mu\dagger}(x)W_\mu(x) + J^\mu(x)W_\mu^\dagger(x)] - \frac{g}{\cos\theta_W}[J_3^\mu(x) - \frac{\sin^2\theta_W s^\mu(x)}{2}]Z_\mu(x) \tag{28}$$

The SU(2)⊗U(1) gauge-invariant interaction of equation 28 first introduced by Glashow describes the electromagnetic and weak interactions of leptons. The first term is the interaction of QED, and the second the IVB interaction Lagrangian density provided $g_W = \frac{g}{2\sqrt{2}}$.

The quanta of the gauge field W(x) are the $W^\pm$ vector bosons, and the third term represent a neutral current coupled to a real vector field $Z_\mu(x)$ where the quanta of this field are the electrical neutral vector bosons Z^0.

SPONTANEOUS SYMMETRY BREAKING

The gauge-invariant and renormalizable unified theory of weak and electromagnetic interactions has so far only massless leptons and gauge bosons. In order to obtain a renormalizable theory, the masses has to be introduced by a mechanism which retains the gauge invariance of the Lagrangian density. The spontaneous symmetry breaking is such a mechanism.

To break the gauge invariance spontaneously, a Higgs field is introduced. The Higgs field is a scalar field with non-vanishing vacuum expectation value which is not invariant under the gauge transformations. To break the SU(2) symmetry the field must have several components, and non-zero isospin, the simplest possibility is a weak isospin doublet:

$$\Phi(x) = \begin{pmatrix} \phi_a(x) \\ \phi_b(x) \end{pmatrix} \tag{29}$$

(Where $\phi_a(x)$ and $\phi_b(x)$ are scalar fields under Lorentz transformations.)

Φ(x) transforms analogously to equation 19 under SU(2) transformations, and to equation 21 under U(1) weak hypercharge transformations.

The generalize Lagrangian density which include the Higgs field Φ(x) and is SU(2)⊗U(1) gauge-invariant is:

$$L = L^L + L^B + L^H \tag{30}$$

Where L^L is the leptonic Lagrangian density, L^B is the gauge boson Lagrangian density, and:

$$L^H(x) = [D^\mu\Phi(x)]^\dagger[D_\mu\Phi(x)] - \mu^2\Phi^\dagger(x)\Phi(x) - \lambda[\Phi^\dagger(x)\Phi(x)]^2 \tag{31}$$

The covariant derivative is defined by:

$$D^\mu\Phi(x) = [\partial^\mu + \frac{i}{2}g\tau_j W_j^\mu(x) + ig'YB^\mu(x)]\Phi(x) \tag{32}$$

For $\lambda > 0$ and $\mu^2 < 0$ the classical energy density is a minimum for a constant Higgs field:

$$\Phi(x) = \Phi_0 = \begin{pmatrix} \phi_a^0 \\ \phi_b^0 \end{pmatrix}$$

with:

$$\Phi_0^\dagger \Phi_0 = |\phi_a^0|^2 + |\phi_b^0|^2 = \frac{-\mu^2}{2\lambda} \tag{33}$$

and all other fields vanishing. Choosing for the ground state a particular value ϕ_0 leads to spontaneous symmetry breaking.

One can choose:

$$\Phi_0 = \begin{pmatrix} \phi_a^0 \\ \phi_b^0 \end{pmatrix} = \begin{pmatrix} 0 \\ \frac{v}{\sqrt{2}} \end{pmatrix} \tag{34}$$

(Where $v = \frac{-\mu^2}{\lambda}^{\frac{1}{2}} (> 0)$*.)*

The Higgs field of the vacuum state is in general not invariant under SU(2)×U(1) gauge transformations, but it must be invariant under U(1) electromagnetic gauge transformations to ensure zero mass for the photon and conservation of the electric charge conservation to hold exactly.

An arbitrary Higgs field can again be parameterized in terms of its deviation from the vacuum field Φ_0 in the form:

$$\Phi(x) = \frac{1}{\sqrt{2}} \begin{pmatrix} \eta_1(x) + i\eta_2(x) \\ v + \sigma(x) + i\eta_3(x) \end{pmatrix} \tag{35}$$

The Lagrangian density L^H can be expressed in terms of the four real fields σ(x) and η_i(x). The fields η_i(x) are unphysical fields, and in the unitary gauge they are transformed away. The two fields $W_\mu^\pm = \frac{1}{\sqrt{2}}(W_{1\mu} \pm iW_{2\mu})$ describing the charged $W^\pm$ bosons acquire mass. The neutral fields W_μ^3 and B_μ don't correspond to mass eigenstates. But the admixture

$$\begin{aligned} A_\mu &= cos\theta_W B_\mu + sin\theta_W W_{3\mu} \\ Z_\mu &= -sin\theta_W B_\mu + cos\theta_W W_{3\mu} \end{aligned} \tag{36}$$

are physical states, Z_μ acquire mass, but A_μ, the photon, remains massless since the electromagnetic gauge symmetry has not been spontaneously broken.

The Higgs field are after symmetry breaking reduced to:

$$\phi = \frac{1}{\sqrt{2}} \begin{pmatrix} 0 \\ v + \sigma(x) \end{pmatrix} \tag{37}$$

Only a neutral Higgs field h(x) of the Higgs doublet survives and gives rise to spin 0 particles, occurring in several terms of the Lagrangian. σ(x) is massive, but the mass depends on the strength of the Higgs self coupling λ which is unknown.

Non-vanishing lepton masses are obtained by adding a suitable term L^{LH} to the Lagrangian density (Weinberg-Salam).

$$L^{LH}(x) = -g_l[\bar{\Psi}_l^L(x)\psi_l^R(x)\Phi(x)+\Phi^\dagger(x)\bar{\psi}_l^R(x)\Psi_l^L(x)]-g_{\nu_l}[\bar{\Psi}_l^L(x)\psi_{\nu_l}^R(x)\tilde{\Phi}(x)+\tilde{\Phi}^\dagger(x)\bar{\psi}_{\nu_l}^R(x)\Psi_l^L(x)] \tag{38}$$

g_l and g_{ν_l} are dimensionless coupling constants and:

$$\tilde{\Phi}(x) = -i[\Psi^\dagger(x)\tau_2]^T = \begin{pmatrix} \psi_b^*(x) \\ -\psi_a^*(x) \end{pmatrix}$$

Assuming g_{ν_l}=0 leads to zero neutrino masses. A non-zero value for g_{ν_l}=0 represents the simplest way of introducing non-zero neutrino masses.

The introduction of the Higgs field also generates the fermion masses. Yukawa coupling between the Higgs field and each fermion field with strength G_f produces through symmetry breaking fermion masses proportional to G_f. The coupling constant G_f is arbitrary so the actual fermion masses are not predicted.

3.1.9 QCD/Strong interaction

Interaction between the constituent quarks which make up the hadron. The coupling of the quarks mediated via bosons called gluons; the neutral massless carriers of the strong force. There are six types of strong charge or color, number of internal degrees of freedom. Three colors carried by the quarks and three anticolors by the antiquarks. Gluons are also carrying colorcharge. Color symmetry is supposed to be exact, quark-quark force is independent of the quark colors involved.

3.1.10 Gravity

Gravity is not described in the Standard Model. One has to use String theory or other extensions to be able to describe it in a sufficient way. But gravity is unimportant in particle physics at accelerator energies.

3.1.11 Leptons

Leptons are all those fermions which participate in weak and electromagnetic interactions only. Within experimental accuracy the three known charged leptons $e^{\pm}$, $\mu^{\pm}$, and $\tau^{\pm}$ exhibit properties of particles whose interaction are identical except for their masses. Within experimental limits leptons are pointlike.

Under the assumption of a light neutrino ($M_\nu < \frac{M_Z}{2}$)in all generations, the LEP experiments has shown that only three families exist [19]. [there is still the possibility of heavy families with heavy neutrinos]

In principle the muon lepton - μ could decay electromagnetic to the lighter electron $\mu \rightarrow e\gamma$ but this decay mode is not seen. This is taken as evidence for additive conserved lepton numbers L_e,L_μ, and L_τ. All known reactions conserve these three lepton numbers seperatly.

$$\begin{aligned} L_e &= N(e^-) - N(e^+) + N(\nu_e) - N(\bar{\nu_e}) \\ L_\mu &= N(\mu^-) - N(\mu^+) + N(\nu_\mu) - N(\bar{\nu_\mu}) \\ L_\tau &= N(\tau^-) - N(\tau^+) + N(\nu_\tau) - N(\bar{\nu_\tau}) \end{aligned}$$

There are no flavour changing neutral current in the lepton sector similar to the one in the quark sector (GIM).

$$\begin{pmatrix} \nu_e \\ e \end{pmatrix} \begin{pmatrix} \nu_\mu \\ \mu \end{pmatrix} \tag{39}$$

A Cabbibo like angle in the leptonic sector would be unobservable if ν_e and ν_μ are massless, since a Cabbibo like rotation would leave the neutrino mass eigenstates.

3.1.12 Summary

The current picture:

- All matter composed of spin $\frac{1}{2}$ particles.

- Interaction is a consequence of exact local gauge symmetries. Gauge bosons (Color and Electro-weak) are spin 1 particles
- Spontaneous symmetry breaking introduces mass to fermions and Weak bosons. And makes the theory renormalizable.

3.2 Models beyond the Standard Model

A number of more or less successful attempts to make models beyond and instead of S.M. has been introduced. Most of these are extensions of the standard model and unification theories, trying to include gravity and or unify all parts to one whole theory, like the grand unification theory (GUT), and supersymmetrical models. Some theories have already been abandoned, but most such theories have in common the problem of verification, at least at the energies which are possible at any experiment today.

Also therefore the need of building new and more energetic colliders like Large Hadron Collider - LHC.

The common approach in most of these new models are the need of adding new particles.

Some theories beyond the Standard Model are listed below. A short introduction, and the corresponding possible lepton flavour violation rates, for some of the models in the channels searched for in this thesis, are also given.

3.2.1 Supersymmetry

Geometrical structure of space experienced by a fermion differs fundamentally from that experienced by a boson. Algebra of geometrical symmetry operations such as rotations is radically different, and this is one of the reasons why the distinction between bosons and fermions is so fundamental.

Supersymmetry[28] provides a geometrical framework, within which fermions and bosons receive a common description. This cannot be achieved within the context of familiar geometrical operations in ordinary space. Supersymmetricall operations can mathematical be represented by attaching to the four dimensions of ordinary spacetime another four dimensions, forming a 'superspace', with the purpose of accomodate the geometrical properties of fermions.

The additional 'fermionic' dimensions are not space or time dimensions as known.

The geometric rules in the extra dimensions are very different, commutators replaced with anticommutators, introducing a dramatic difference in the mathematical description, leading to a unified description of bosons and fermions.

Supersymmetry operations rotate from the ordinary spacetime of experience into these extra fermionic dimensions.

Thus one can regard fermions and bosons as two different projections of a single underlying geometrical unity.

If the world is Supersymmetric one should expect to see direct physical evidence for the link between fermions and bosons. Each particle would have a Supersymmetric partner. Every known type of fermion should be matched with a boson, and every boson with a fermion in a systematic way.

It is not possible to pair up the current known particles in this fashion, but this does not necessarily mean that Supersymmetry is irrelevant since underlying symmetries often are broken in the real world. And/or there is no reason why the currently known fermions have to be superpartners of the known bosons.

(The Undiscovered superpartners to the known particles are named: Photinos [which interacting very weak with ordinary matter], Gluinos, Gravitinos, Squarks, and Sleptons).

3.2.2 GUT

Grand Unified Theory aims to unify the electro-weak force with QCD [28].

This is done by finding a larger group which embodies SU(3) of QCD and the SU(2) and U(1) gauge groups of the weak and electromagnetic forces as subgroups.

GUT mixes together the identities of the sources of the three forces. Leptons associated with quarks. (assumed to be equal number of quarks and leptons today).

Mixing, by exchange of a new set of messenger particles known as χ particles. χ can turn a quark into a lepton or vice versa. One should expect to see proton decay, but at a very low rate, possibly unobservable. And GUT also predicts magnetic monopoles which neither have been observed.

At low energy the forces will have distinct identities, at high energies they will merge.

3.2.3 Superstring

String theories [28] were originally an attempt to understand the strong force. It was never completely successful and therefore almost forgotten when Quantum Chromodynamics (QCD) were introduced in the mid 1970s. But not completely.

It was noticed that the string theory always gave rise to a particle with no mass and spin=2, not corresponding to any strong interaction particle, but exact like the graviton. The new approach was to use it to describe gravity, and at the same time other fundamental forces.

- Original picture (for strong interaction):

  Hadrons made of quarks held together by some force called strings, like bits of elastic. Quarks attached to the ends.

- Problems:

  The massless spin 2 particle.

  The spacetime consisted of more than four dimensions. In the first attempts 26, but reduced to ten in the later and more promising theories.

  The 26 dimension theories contained tachyonic particles (v>c).

TEN-DIMENSIONAL STRING THEORIES: These theories have supersymmetry, and therefore called SUPERSTRING THEORIES. Incorporated in the Superstring theory is SUPERGRAVITY, which is a supersymmetric generalization of gravity.

Quantum calculations of gravity give rise to divergent expressions, possibly a generic property of all theories where the fundamental particles were regarded as mathematical points. String theory replaced points with one dimensional curved strings. The quantum corrections to gravity then give finite expressions.

There exist string theories with open strings, the strings has open ends, and closed strings where the string forms a loop. Today closed strings seem simplest and most promising.

In nature there is a distinction between left- and right-handedness (parity violation). Most superstring theories have this left-right asymmetry in ten-dimensions.

Left-right asymmetric theories tend to break down and give anomalies. The original symmetry structure can be chosen in a infinite number of ways, but only for a very few will the anomalies cancel. This canceling appears in the so called SO(32), and in the heterotic string theory, a $E_8 \otimes E_8$ symmetry.

Symmetries of particle physics currently accessible are part of one of the two E_8. The other E_8 symmetry describes a new kind of matter that does not interact, or only extremely weakly with ordinary matter. (one could imagine all sorts of objects, even galaxies made up of *shadow matter*, completely invisible to us except for gravitational effects.) There is no evidence of such shadow matter.

Theories of gravity describe the geometry of space and time. It will make sense to suppose that extra dimension exist, curled up into a tight little ball as a consequence of the geometry dictated by the theory, and sufficiently small not to be observed, (at the Planck scale). Each point in space is a little six-dimensional ball about 10^{-33}cm across.

The geometry and topology of the six-dimensional space play a crucial role in determining the properties of observable particles. (How many families etc.)

Superstring theory is no unique theory but a very large number of theories or solutions depending on how one chooses to curl up these extra dimensions.

The string can oscillate and vibrate in different ways, rotate and so forth. Each of these different modes of vibration or oscillation describes a particle (lepton, quark, or boson).

If one could do exact calculations and not only perturbation, one might single out one unique theory with no arbitrary parameters and no adjustable constants.

3.3 Neutrino Mass

Neutrinos may be massless, but only upper limits for masses are measured [30, 14, 24, 23].

In the standard electro-weak theory neutrinos are exactly massless. This is a postulate, based on the experimental observation or more correct; nonobservation of right-handed neutrinos in nature, and the observation of parity violation in weak interaction [35]. If this is a correct assumption, flavour conservation is an exact symmetry in the lepton sector.

Theoretically no fundamental symmetry dictates neutrinos to be massless. Beyond the Standard Model most gauge theory extensions of SM have some level of nonzero neutrino-mass, which may lead to lepton flavour violation.

If neutrinos are massive, then one may expect a hierarchy of masses among the different generations, with ν_τ being heavier than ν_μ and ν_e [31]. Massive neutrinos can mix with one another leading to lepton flavour violation. Massive neutrinos are also important for its impact on cosmology and astrophysics, where they have been considered as possible solutions to Dark Matter, solar neutrino, and atmospheric neutrino deficit, and other problems.

Experimental it is clear, that if massive, the scale of neutrino-mass is lower than that which characterizes all other known fermions. (But it's general agreed however that even a small value, for ν_τ in the 10 - 30 MeV/c^2 range, could have profound implications.)

If neutrinos are massive they can decay.

Recent results for the mass of;

$\boxed{\nu_e}$

The mass of the electron neutrino - m_{ν_e}, can in principle be measured by observing effects on electron energy spectrum from β decay, see figure 3. Given:

$$\frac{dn}{dE} = F(z,E)pE(E_o - E)\sqrt{(E_O - E)^2 - m_\nu^2} \tag{40}$$

F(z,E) - calculable Coulumb correction, E - electron Kinetic energy, p -momentum, E_o - end-point for m_ν=0.

If one chooses β decay with E_0 as small as possible, the mass of the electron neutrino m_{ν_e} calculated from $^3\mathrm{H} \rightarrow {}^3He + e + \nu_e$

gives the 1994 average of:

$$m_{\nu_e}^2 = (-54 \pm 30)\frac{eV^2}{c^4}.$$

From this one derives an upper limit at 95% CL of [14]

$m_{\nu_e} < 5.1$ eV.

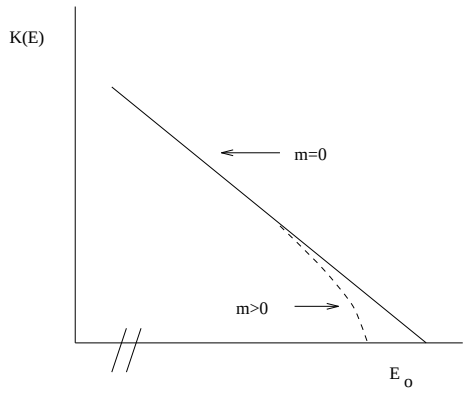

Figure 3: *Kurie plot K(E)=*$[\frac{i}{FpE} * \frac{dn}{dE}]$

(The m^2 is positive with only 3.5% probability, a problem not yet understood.)

ν_μ

The mass of the muon neutrino m_{ν_μ} calculated from the process $\pi^+ \rightarrow \mu^+ + \nu_\mu$

The combined result of muon-neutrino mass squared gives:
$m^2_{\nu_\mu} = -0.022 \pm 0.023 MeV^2$
consistent with zero from which one derives an upper limit at 90% CL of [14]:
$m_{\nu_\mu} < 160$ keV

ν_τ

Experimental limits on m_{ν_τ} has been based on studies of the end-point of the mass spectrum of the τ decay products. High multiplicity and heavy particle final states into 5π, 6π or KKπ provide best opportunity.

An analysis reported by the ALEPH group of 25 tau decays into 5π and 6π gives an upper limit at 95% CL [31];
$m_{\nu_\tau} < 23.8$ MeV

3.3.1 Neutrino mass in field theory.

Neutrinos can be described as Dirac or Majorana particles [30].

- Standard Model Dirac neutrinos:

  m_ν=0 and $\nu \neq \bar{\nu}$

Where ν has negative helicity and $\bar{\nu}$ has positive. In this picture ν with positive and $\bar{\nu}$ with negative helicity does not exist.

- Majorana neutrinos

  $\nu = \bar{\nu}$ and with two opposite helicity states of the same particle interacting differently with matter.

  Lepton number not conserved in the interaction.

STANDARD MODEL NEUTRINOS In the standard model only one helicity state of the neutrino per generation is present. Therefore it could not have a Dirac mass. Majorana mass terms requires one helicity state of a particle and uses the opposite helicity state of the antiparticle. However, this type of mass brakes lepton numbers by two units. The standard model conserves lepton number separately for each generation, or more precisely the quantum number B-L. (B is baryon number current, L is Lepton number current) Therefore neither of these mass terms can arise at any level in perturbation theory, or in the presence of non-perturbative effects. It can be shown that it is the B-L, rather than L which is relevant for this discussion [30]. The current of B-L is free of anomalies and is conserved. In processes or lagrangian terms that do not contain baryons, the conserved current effectively becomes a lepton number.

In the standard electro-weak $\mathrm{SU}(2)_L \otimes \mathrm{U}(1)_Y$ theory the leptons and quarks are arranged in left-handed doublets and right-handed singlets:

$$\begin{pmatrix} \nu \\ l^- \end{pmatrix}_L \; l_R$$

(*No ν_R exist in this model*)

The Higgs field

$$\Phi = \begin{pmatrix} \phi^+ \\ \phi^0 \end{pmatrix}$$

introduces the Charged lepton Dirac mass:

$$\lambda(\bar{\nu_L}, \bar{l_L}) \begin{pmatrix} \phi^+ \\ \phi^0 \end{pmatrix} l_R) + h.c. \rightarrow \lambda \langle \phi^0 \rangle \bar{l} l \tag{41}$$

(*Where λ is the Yukawa coupling, $\lambda\langle\phi^0\rangle = m_l$.*)
With no ν_R no Dirac mass for ν exist.

LEFT-RIGHT SYMMETRIC MODEL (LR) The Left-right symmetric model of weak interaction is an extension of the standard model which may manifest itself

in the multi-TeV energy range. In this model the left and right handed chiralities of fermions are assumed to play an identical role prior to symmetry breaking, or at high energies above all symmetry breaking scales. All left handed fermions must have a right handed partner. A consequence is the the existence of a right handed neutrino, and the theory automatically leads to massive neutrinos.

The smallest gauge group implementing LR are $\mathrm{SU}(2)_L \otimes \mathrm{SU}(2)_R \otimes \mathrm{U}(1)_{B-L}$ Right handed neutrinos are arranged in doublets:

$$\begin{pmatrix} \nu \\ l^- \end{pmatrix}_L, \begin{pmatrix} \nu \\ l^- \end{pmatrix}_R$$

A triplet Higgs is necessary to brake the symmetry so that:

$$SU(2)_L \otimes SU(2)_R \otimes U(1)_{B-L} \xrightarrow{\langle \Delta_R \rangle} SU(2)_L \otimes U(1)_Y \tag{42}$$

$$SU(2)_L \otimes SU(2)_R \otimes U(1)_{B-L} \xrightarrow{\langle \Phi \rangle} U(1)_{em} \tag{43}$$

(*Where $U(1)_{em}$ is the symmetry of QED, Δ_R the Higgs triplet (Δ_R^{++},Δ_R^{+},Δ_R^{0}), and Φ the Higgs bidoublet*

$$\begin{pmatrix} \phi_1^0 & \phi_1^+ \\ \phi_2^- & \phi_2^0 \end{pmatrix}$$

)

Possible Dirac mass terms for the LR model could be:

$$\lambda_D(\bar{\nu_L}, \bar{l_L})\sigma_2 \Phi^* \sigma_2 \begin{pmatrix} \nu_R \\ l_R \end{pmatrix} + h.c. \longrightarrow \lambda_D \langle \phi_2^{0*} \rangle \bar{\nu_L} \nu_R + h.c. \tag{44}$$

With possible Majorana mass terms:

$$\lambda_R((\bar{\nu_R})^c, (\bar{l_R})^c) i\sigma_2 \vec{\sigma} \begin{pmatrix} \nu_R \\ l_R \end{pmatrix} \Delta_R + h.c. \rightarrow \lambda_R \langle \Delta_R^0 \rangle (\bar{\nu_R})^c \nu_R + h.c. \tag{45}$$

More terms from for example another triplet Higgs (Δ_L) could exist.

In LR models with majorana neutrinos Z can couple to two different fermions. Unlike the situation in the standard model, Z has flavour changing neutral currents [30].

SEE-SAW-MECHANISM IN THE LR MODEL

A simple way to understand the smallness of neutrino mass is to assume it to be a majorana particle, and use the see-saw mechanism. (The mechanism of making on particle light at the expense of making another heavy.)

In a LR model the mass terms in the Lagrangian generally are:

$$L_{mass} = -m_D\bar{\nu}_L\nu_R - \frac{1}{2}(m_L(\bar{\nu}_L)^c + m_R(\bar{\nu_R})^c\nu_R) + h.c. = -\frac{1}{2}\bar{\nu}^c M\nu + h.c. \quad (46)$$

Where:

$$\nu \equiv \begin{pmatrix} \nu_L \\ (\nu_R)^c \end{pmatrix}, M = \begin{pmatrix} m_L & m_D \\ m_D & m_R \end{pmatrix}$$

The Higgs field hierarchy: $\langle\Delta_L^0\rangle \ll \langle\Phi\rangle \ll \langle\Delta_R^0\rangle$, indicating the magnitude of the mass matrix entries of: $0 \simeq m_L \ll m_D \ll m_R$

The See-saw mass matrix then becomes:

$$M = \begin{pmatrix} 0 & m_D \\ m_D & m_R \end{pmatrix} \quad (47)$$

And the Majorana mass eigenstates:

$$\nu \simeq \nu_L + (\nu_L)^c - \frac{m_D}{m_R}(\nu_R + (\nu_R)^c) \quad (48)$$

$$\nu \simeq \nu_R + (\nu_R)^c + \frac{m_D}{m_R}(\nu_L + (\nu_L)^c) \quad (49)$$

(*Where 48 is a light neutrino with mass* $\simeq \frac{m_D^2}{M_R} \ll m_D \simeq m_{l,q}$, *and 49 is a heavy neutrino with mass* $\simeq m_R \gg m_{l,q}$.)

If ν_R is in the the TeV region, one expect an eV-keV-MeV type spectrum for neutrinos. If $m_{\nu_e} \approx$10eV, one gets $m_{\nu_\mu} \approx$400keV, and $m_{\nu_\tau} \approx$160MeV.

The Lagrangian for a Dirac fermion is:

$$L = i\bar{\Psi}\gamma_\mu\delta^\mu\Psi - m_D\bar{\Psi}\Psi \quad (50)$$

With a Dirac mass term:

$$L_{mass}^D = -m_D\bar{\Psi}\Psi = -m_D(\bar{\Psi}_R\Psi_L + \bar{\Psi}_L\Psi_R) \quad (51)$$

(*Where* $\Psi_L = \frac{1}{2}(1-\gamma^5)\Psi$, $\Psi_R = \frac{1}{2}(1+\gamma^5)\Psi$, *and* $\Psi = \Psi_L + \Psi_R$)

The Dirac mass mixes chiral component Ψ_L and Ψ_R. But for neutrinos (Q=0) Majorana mass terms are also possible.

$$L_{mass}^M = -\frac{1}{2}m_M^L(\bar{\Psi}_L)^c\Psi_L - \frac{1}{2}m_M^R\bar{\Psi}_R(\Psi_R)^c + h.c. \quad (52)$$

(*Which does not mix* Ψ_L *and* Ψ_R)

Introducing the two-component Majorana states $\chi = \psi_L + (\psi_L)^c$ and $\eta = \psi_R + (\psi_R)^c$

The Lagrangian mass term then becomes

$$L^M_{mass} = -\frac{1}{2} m^L_M \bar{\chi}\chi - \frac{1}{2} m^R_M \bar{\eta}\eta \tag{53}$$

Where $\chi^c = \chi$, $\eta^c = \eta$

The Lagrangian mass term does not conserve additional quantum numbers Q,L,B,.....

$$\Psi \rightarrow e^{i\alpha}\Psi \Rightarrow \bar{\Psi}^c\Psi \rightarrow e^{2i\alpha}\bar{\Psi}^c\Psi \tag{54}$$

$\Psi^c \rightarrow e^{-i\alpha}\Psi^c$

Allowed only for neutral fermions

Lepton number violated

Neutrinos may be given a mass so that total lepton number is conserved by coupling to new fermions beyond those in the SM, but there are in general no reason for conserved total lepton number symmetry.

3.3.2 Models (examples)

A short description of some models are given below.

- SUPERSTRING INSPIRED STANDARD MODELS [13] Extending the Standard Model by adding new neutral fermions.

  In the Standard Model with the Weinberg-Salam Higgs doublet, the absence of right-handed neutrinos implies that neutrinos are exactly massless to all orders of perturbation theory A small but nonzero mass is possible if the B-L symmetry is broken at high energies so that the neutrino mass matrix is:

	ν_L	ν_R^c
ν_L^c	0	D
ν_R	D^T	M

  (*Where ν_L is a two-component Weyl SU(2) doublet field, the ν_R is an SU(2) singlet, the D a Dirac mass term proportional to the Higgs doublet vacuum expectation value, and M the Majorana mass*)

  M is a SU(2)$\otimes$U(1) singlet and expected to be much larger than D. This gives a heavy mass eigenstate M and a light eigenstate neutrino of mass m=-$DM^{-1}D^T$.

  A possible approach towards a complete unification of matter with all forces, including gravity, could be based on a low-energy limit of the heterotic superstring. In a phenomenologically viable model a problem like unacceptably large neutrino mass arises, originating from the lack of Higgs fields with appropriate quantum numbers, to provide the large Majorana mass needed in the neutrino mass matrix. A solution might be an new effective neutrino mass matrix:

	ν_L	ν_R^c	S^L
ν_L^c	0	D	0
ν_R	D^T	0	M^T
S_L^c	0	M	0

  (*Where the number and nature of the new fermions are model dependent.*)

  A wide class of theories lead to this neutrino mass matrix, not only string inspired ones. Theories based on this mass matrix may contain lepton flavour violation observable in Z factories like LEP

  In [13] consequences of this extended fermion sector in the framework of the minimal non-supersymmetric SU(2)$\otimes$U(1) gauge structure are analyzed.

  In the low energy structure relevant leptons are:

  $$\begin{pmatrix} \nu \\ e \end{pmatrix}_L \quad e_R \quad \nu_R S_L$$

  With completely standard quark in the chiral family. A light pair of Higgs doublets which break SU(2) and give fermion masses (via their Yukawa coupling to the two isospin channels) are assumed. The neutrino mass matrix determine

the structure of the leptonic weak interactions in the model. The neutrino mass matrix has a symmetry with three massless neutrinos and three heavy Dirac fermions. The charged lepton mass norm is arbitrary. and total effective global symmetry is total lepton number not individual lepton number, due to the effects of the heavy neutrinos. And determined by the mass scale M of the new fermions. M might arise from the vacuum expectation value of an SU(2)⊗U(1) singlet Higgs field also present in some superstring models.

In the model described, neutrinos are massless as a consequence of an exact symmetry, and new potential phenomenological manifestations can be realized, such as sizable *lepton flavour violation* at high energies.

This model is qualitatively similar to a standard gauge theory in which right-handed neutrinos are included, however with a very important difference; the conserved total lepton number ensuring massless neutrinos thereby allowing much higher values for $\frac{D}{M}$. The neutral coupling to the massless neutrinos are flavour dependent unlike in the Standard Model, and can change lepton flavour when it mixes the massless neutrinos to the heavy ones.

In this model upper limits on branching ratios of $\mathrm{Br}(Z^0 \rightarrow e\tau) \leq 3.4 \times 10^{-4}$, $\mathrm{Br}(Z^0 \rightarrow \mu\tau) \leq 4.2 \times 10^{-4}$, are given.

- EXTENDED ELECTRO-WEAK MODEL

Introducing a new neutral gauge field Z' heavier than Z^0, which couples to lepton-flavour-violating-current [34]. Z' will generally mix with the standard Z^0 and thereby give Z^0 a small but nonvanishing coupling to $e\bar{\mu}$, $e\bar{\tau}$, and $\mu\bar{\tau}$ in the form:

$$g\gamma_\mu[\frac{a_L}{2}(1-\gamma_5)+\frac{a_R}{2}(1+\gamma_5)] \tag{55}$$

where a_L and a_R are defined for each off-diagonal pair of leptons

Compared to the dominant standard coupling of Z^0 to $e\bar{e}$ of the exactly same form but a_L and a_R replaced by b_L and b_R. *where* $b_L \equiv -\frac{1}{2}+sin^2\theta_w$, *and* $b_R \equiv sin^2\theta_w$

From this one obtains for example:

$$\frac{B(Z^0 \rightarrow \mu\bar{e}+\bar{\mu}e)}{B(Z^0 \rightarrow \bar{e}e)} = \frac{|a_L|^2+|a_R|^2}{|b_L|^2+|b_R|^2} cos^2\theta_w \tag{56}$$

And so forth.

Very stringent experimental bounds are set for $\mathrm{B}(\mu \rightarrow ee\bar{e})$, from this also the bound on $\mathrm{B}(Z^0 \rightarrow \mu\bar{e}+\bar{\mu}e) < 10^{-12}$, which is too small to be measured. Rare τ decays have much less stringent bounds and therefore less severe bounds on $\mathrm{B}(Z^0 \rightarrow \mu\tau)$, and $\mathrm{B}(Z^0 \rightarrow e\tau)$. With some requirement on the heavy Z' couplings to the fermions, lepton-flavour-violating-current processes can occur at the level of $\sim 10^{-7}$, involving the τ lepton ($e\tau$, $\mu\tau$).

- SUPERSYMMETRIC STANDARD MODEL

A model with soft supersymmetric-breaking terms is described [26].

The Supersymmetric partners of leptons, the scalar leptons are given explicit arbitrary mass terms in the Lagrangian and allowed to mix with arbitrary angles. The resultant calculations are model independent.

The Lagrangian for leptons assumed here is L=L_{SGWS}+L_{break}

(*Where L_{SGWS} is the standard Supersymmetric Electro-weak Lagrangian, and L_{break} is the soft Supersymmetric-breaking terms.*)

In a Supersymmetric theory at least two Higgs doublets are needed to provide masses for the u and d quarks. Soft Supersymmetry breaking terms are then added. Mixing among the charged Higgs fermions *Higgsinos* and gauge fermions *gauginos* appear in conjugation with similar mixing between the neutral states.

TWO HIGGS DOUBLET MODEL:

- Two charged states *charginos* $\tilde{\chi}_i^+$
- Four neutral states *neutralinos* $\tilde{\chi}_j^0$

In general the left and right scalar leptons will mix. There will only be global lepton-family-number conservation and no $\tilde{e}$, $\tilde{\mu}$, and $\tilde{\tau}$ mixing. If there is mixing, a small effect in the nonsupersymmetric sector is expected, like radiative muon decay.

Only the two heaviest generations are let to mix significantly, and with little left-right mixing:

$\tilde{\mu}_L$ and $\tilde{\tau}_L$ with angle θ_L
$\tilde{\mu}_R$ and $\tilde{\tau}_R$ with angle θ_R
$\tilde{\nu}_\mu$ and $\tilde{\nu}_\tau$ with angle θ_ν

The largest cross section occur when the mass splitting between the mass eigenstates is large.

$$\frac{\sigma_{e^+e^-} \rightarrow \tau^+\mu^-}{\sigma_{e^+e^-} \rightarrow \mu^+\mu^-} = \frac{(|M_L|)^2 + (|M_R|)^2}{8\pi\alpha(cot^2 2\theta_W + tan^2\theta_W)} \tag{57}$$

The result for equation 57 in two extreme gaugino limits [26]:

1. Supersymmetric limit

   Eliminate the Supersymmetric-braking terms by letting M',M,$\mu \rightarrow 0$ and let ν_1=ν_2. The charged Supersymmetric partners are ruled out of mass less than $24\frac{GeV}{c}$. A large mass splitting, and maximal scalar lepton mixing are also assumed $\theta_\nu = \theta_L = \theta_R$=$\frac{\pi}{4}$.

   This could result in equation57 becoming as large as 3×10^{-6}, corresponding to at best a branching ratio for Br($Z^0 \rightarrow \tau^+\mu^-$)$\leq\sim10^{-7}$

2. Unmixed limit

   Higgs-fermion and gaugino sector disentangle from another. M$\rightarrow \infty$,M'$\rightarrow$0, $\mu \rightarrow$0, and θ_ν arbitrary.

   This gives a lower branching ratio than the first example.

Other theoretical papers predicting lepton flavour violation are listed in [21].

4 INSTRUMENTATION

In this section a description of the experiment used for this search, is given. A general introduction to CERN 4.1, the LEP collider 4.2 and the DELPHI detector 4.3 are presented.

4.1 CERN

European Organization for Nuclear Research or Conseil Européen pour Recherche Nucléaire, CERN, was founded in 1955 dedicated to research in nuclear physics [27].

The main project currently running at CERN is the Large Electron Positron collider - LEP.

At the same time several smaller research projects are running. From heavy ion experiments like ISOLDE at the Super Proton Synchrotron - SPS, to testing of apparatus for future projects like the Large Hadron Collider - LHC.

e^+e^- colliders:

Synchrotron radiation losses (equation 58) limit the energy which can be obtained in circular electron positron colliders. The only economically acceptable solutions for collision energies higher than LEP200 (close to 100GeV beam energy) are therefore linear colliders. The technique to build a 2 TeV e^+e^- like the proposed CLIC(at CERN), JLC(at KEK), and NLC(at SLAC) [18] colliders is out of reach in the near future, due to limitation in practical length, from the accelerating gradient and accelerator frequence, and also the need of a final focus system which has to provide extremely narrow beam dimensions in order to reach the necessary luminosity. But a lot of effort is put into attacking the challenges.

(Relativistic protons and electrons of the same momentum loses energy in the ratio $(\frac{m_e}{M_p})^4$).

$$\Delta E = \frac{4\phi e^2 \beta^2 \gamma^4}{3R} \tag{58}$$

(*Where the energy radiated per particle per turn* ΔE *is given by bending radius* R*, the particle velocity* β *and* $\gamma = (1-\beta^2)^{-\frac{1}{2}}$)

Hadron hadron colliders

LHC; a hadron hadron collider and the next main project at CERN, is to be installed in the existing LEP tunnel some years after the millennium. [18]

4.2 LEP

LEP[27] a 27km long circular e^+e^- accelerator and storage ring, is the last accelerator in a chain of five, handling the same electrons and positrons generated by the electron gun and the positron converter. The LEP injector consists of two lineacs of 200MeV and 600MeV, followed by a 600MeV Electron-positron Accumulator, which inject into the 3.5 GeV Proton Synchrotron(PS). PS is then used as injector for the 20 GeV Super Proton Synchrotron(SPS) the injector for LEP.

The beam energy at LEP was initial chosen to produce Z^0 particles, responsible for the weak force. The object was to test the Standard Model by studying the creation and decay of the Z^0.

At LEP200 the energy will be set to allow production of W^+W^- pairs to further study the Standard Model in a new domain.

LEP is in fact not completely circular but has 8 linear sections of approximately 1km each. At four of these sections both beams are focused into a interaction point inside one of the four detectors L3, OPAL, ALEPH and DELPHI to measure the properties of secondary particles from Z^0 decay.

LEP started working in August 1989 with only two plus two particle bunches with a separation of $\sim 90\mu s$ and about 10^{11} particles in each bunch. In 1990 it was upgraded to 4+4 bunches of 2^*10^{11} each, and in 1993 to 8+8 which it will run also under LEP200.

LEP gives contributions to a variety of physics issues:

- Very high precision measurements of the electro-weak parameters of the Standard Model. These measurements constrain the number of (light) neutrino families, the top quark mass, and the lower mass sector of whatever might exist beyond the Standard Model.
- QCD studies. Accurate measurement of the strong coupling constant, providing evidence for its q^2 dependence.
- Searches for new particles, like the Higgs boson and supersymmetric partners of known particles. Setting a lower limit on the standard Higgs boson above 50 GeV.
- Studies of short lived particles τ, and B hadrons, contributing to the lifetime and decay modes. Particular exploration of the B sector has been successful, with observation of individual B_s decay and evidence for B^0-$\bar{B}^0$ oscillations.

LEP200 will contribute with:

- New particle searches, like supersymmetric model predicted low-mass Higgs. With radiative corrections upper limit of 150 GeV. The reach of LEP200 in this regime will be approximately 100 GeV.
- Direct study of the ZWW coupling, which interferes destructively with neutrino exchange in the t-channel, and is of fundamental importance for the understanding of the electro-weak interactions.
- Precision measurement of the W mass.

4.2.1 Accelerating system

The RF acceleration system at LEP consists of 128 five-cell copper cavities. Each accelerating cavity is coupled to a spherical low-loss storage cavity, so that the electromagnetic power continuously oscillate between the two sets of cavities, with the power in the accelerating cavities at its peak at the instant of the passage of the beam bunches. The power loss due to heating of the copper cavity walls is greatly reduced, since the electromagnetic power spend half of its time in the very-low-loss storage cavities.

4.2.2 Bending and focusing

The electromagnetic guide field system of LEP consists of dipoles, quadrupoles, horizontal and vertical dipole correctors, rotated quadrupoles, and electrostatic dipole deflectors. About three quarters of the LEP circumference is occupied by bending and focusing magnets grouped in so called 'cells'. A cell consist of magnets in the following order: a defocusing quadrupole, a vertical orbit corrector, a group of six bending dipoles, a focusing sextupole, a focusing quadrupole, a horizontal orbit corrector, a second group of six bending dipoles, and finally a defocusing sextupole, all at a length of 79.11 m. Each of LEP's eight arcs contains 31 of these cells.

The bending field of the dipoles has been made as low as about 0.1 T so as to increase the bending radius and thereby reduce the amount of synchrotron radiation.

The quadrupole magnets, which produce fields linear with the transverse position, act as magnetic lenses and focus the beam. The sextupoles produce a field which is quadratic in transverse displacement, and they are used to compensate the dependence of the focusing strength on the beam energy.

A set of superconducting quadrupoles with a very strong field gradient focuses the transverse beam dimension in the centre of the four detectors to increase the luminosity.

When LEP is to be upgraded to LEP200 one of the main renewal is going to be the installation of superconducting bending magnets with a field of maximum 10T. The technological challenge to achieve this has been considerably, and is the main reason for LEP200 being postponed at least 2 years.

4.2.3 Vacuum system

A LEP fill might take several hours, during this time each of the 10^{12} particles in the beam will have traveled the 26.67 km of vacuum chamber about 500 million times. To minimize particle losses due to collisions with gas molecules, the whole vacuum chamber must be pumped down to very low pressure. The achieved static pressure for LEP is 8×10^{-12} Torr. In the presence of the beam the pressure rises to about 10^{-9} Torr. This is due to gas desorption from inner wall of the vacuum-chamber, provoked by the synchrotron radiation from the beam.

4.3 The DELPHI Detector

The detector is described in detail in ref [4]. A short description is given below; DEtector with Lepton, Photon and Hadron Identification, DELPHI (figure 4) is formed as a barrel around the beam-pipe with the beam interaction point in the center. The detector is symmetric forward backward due to LEP being a e^+e^- collider and therefore the momentum in the detector system being zero. The detector has a radius more than 4 m and a length of more than 10 m, and a total weight of 3500 tons. The different types of detectors are placed as hollow cylinders inside each other. To bend the trajectories of the charged particles, and thereby measure their momentum, the DELPHI contains the largest superconducting solenoid built, which produces uniform magnetic field of 1.2 tesla.

DELPHI is an advanced detector which, as well as having high precision and granularity has the specific ability, using the Ring Imaging Cerenkov technique, to differ between various secondary particles. It also has an advanced silicon strip micro-vertex detector to detect very short lived particles.

In this search only the barrel implying only the region between $\theta = 45^o$ and $\theta = 135^o$ was used. The description below is therefore of the barrel and not the forward region.

DELPHI DETECTOR-TYPES:

- Going from the interaction-point and out

  1. VD

     The Vertex Detector is a tracking device (appendixB.1), its main objective is to get good resolution as close as possible to the interaction point to be able to tag secondary vertexes which is important for several purpose.

     The original two layers of silicon microstrip detectors at radii 9 and 11 cm were operating until the end of 1990. In 1991 a new beam pipe of smaller radius was installed around the interaction point and made it possible to insert a third layer at radius 6.3 cm.

     The Microvertex detector was replaced with a partly new detector in 1993 composed of three layers at at radii 6.3, 9.0, and 11.3 cm. The Closer, Inner and Outer layers cover polar angles in the range 25^0-155^0, 36^0-144^0 and 43^0-137^0, respectively. Closer and Outer layer consist of double sided double metal strip detectors providing both Rϕ and z coordinates. The Inner layer only providing Rϕ coordinates and being made up of one sided strip detectors from the old detector.

     The precision reached by interpolating within the cluster shape is better than 10 microns in Rϕ and z coordinates. The strip width in Rϕ is 50 microns, the z pitch varies between 50-150 microns.

  2. ID

The Inner Detector is a tracking and triggering detector (appendix B.1) with purpose of giving fast information for vertex reconstruction and trigger. It consists of two concentric layers:

(a) The JET-chamber section with Cylindrical drift, subdivided into 24 sectors of 15^0 in ϕ, at radii 11.8-22.3 cm and of length 40 cm. Each sector consist of 24 sense wires, measuring drift-time, Giving 24 Rϕ-points per track.

(b) The Trigger-layers consist of 5 Cylindrical MWPC, each equipped with 129 anode wires parallel to the beam axis and 192 cathode strips forming full circles at constant z at radii 23-28 cm with a length of 50 cm.

Full angular coverage is down to 30^0-150^0 in θ. The JET resolution is of the order 60 microns in R-ϕ, and about 1.5 mrad in the angle ϕ. The two-track separation is of order 1mm.

3. TPC

The DELPHI Time Projection Chamber is a drift chamber (appendix B.1.3). The TPC is a cylinder of 2x1.3 m situated between the radii 0.29 m and 1.22 m. It consist of two drift volumes separated by a 20kV plate producing an electric field of 150 Vcm^{-1}. TPC is filled with a mix of 80% Ar and 20% CH4. A charged particle crossing the TPC produces by ionization around 70 electrons per cm of gas. These primary electrons then drift in the direction of the proportional chamber.

The TPC is the principal tracking device of DELPHI. Divided into 2x6 sectors with 192 sense wires and 16 circular pad rows each. This gives a maximum of reconstructed 16 space points for a track, and 192 $\frac{dE}{dx}$ measurements can be performed on the track. The TPC covers a region corresponding to $\sin\theta > 0.2$. The Rϕ-resolution is 0.23mm and the z 0.9mm.

4. RICH

The Ring Imaging Cerenkov Counter is a particle tagging devise based on Cerenkov light from particles (appendix B.3). Cerenkov counters is based on the fact that when high energy charged particles traverse a dielectric media, part of the light emitted by exited atoms appears in the form of a coherent wavefront at a fixed angle with respect to the trajectory. The radiation is produced when the velocity of the particle exceeds $\frac{c}{n}$, where n is the refractive index of the medium.

The RICH is special for the DELPHI detector in LEP and was constructed first of all to give good hadron identification over a wide momentum range. Due to some problems the RICH was first operating during the 93 running.

The barrel Ring Imaging Cerenkov Counter is constructed as 3.5m long cylinder with inner ϕ = 246cm and outer ϕ = 394 cm divided into two halves by a central support wall. It consists of both gas and liquid radiators. The liquid radiator boxes with 1cm liquid and quartz windows

are mounted near the inner radius. Drift tubes are constructed entirely from quartz plates and serves to detect UV-photons both from the liquid and the gas radiators, and are placed between them. The gas radiator placed near the outer radius is equipped whit parabolic mirrors to focus Cerenkov-photons into ring images in the drift tubes.

5. OD

   The Outer Detector is composed of 24 modules 4.7 meters long and each consisting of 145 drift tubes in 5 layers. It is situated at a radii of 198-206cm. The OD gives 3 space points plus 2 r-ϕ points per track. The accuracy in the r-ϕ coordinate is of 0.11mm and in z of 4.4cm.

   A charged particle crossing the tube produces electrons which drift toward the wire (appendix B.1.3). The wire is at a high voltage of 4.4kV, and gives a signal with short rise time and high amplitude.

   OD provide fast trigger information in both Rϕ and z, and is used together with TPC to improve the momentum resolution. ID trigger data are correlated with the OD ones in order to reduce the rate due to cosmic and gas events.

6. HPC

   High density Projection Chamber(appendix B.2) situated inside the solenoid between a radii of 208-260cm and have a length of 254cm. It consists of 144 independent modules, arranged in 6 rings of 24 modules each. Each module is a trapezoidal box with ranging from 52 to 64 cm, a hight of 47 cm, and a length of 90 cm except for modules in the first and last rings which are somewhat shorter. The box is filled with 41 layers of a fiberglass-epoxy support(0.1mm) with lead wires glued to both sides. The gap between each layer is filled with 80% argon and 20% methane. The 10th sampling gap at about 4.5 radiation length(shower maximum) is filled with a scintillator plane instead of gas and is used for first level trigger.

   Each sampling gap ends in a cathode which is divided into segments(2-8cm long), which are connected to their neighbours(above or below) in groups of 3-6. The result is 128 pads in 9 rows defining the granularity in r and ϕ.

   A electromagnetic particle showers in the lead and ionizes the gas. The charge drifts to one end of the box, where it is collected by a proportional chamber with pad readout.

   The HPC measures the three-dimensional charge distribution induced by electromagnetic showers.

7. TOF

   The Time Of Flight detector consists in a single layer of 192 scintillation counters along the beam axis. Each counter has a dimension of

20x345x2cm^3 and is provided with a Photo Multiplier(PM) tube in both ends.

A particle crossing a scintillator generates a light pulse propagating to both ends where the puls reaches a PM. The PM converts the light puls into a electronic puls which gives information about arrival time and charge.

8. HCAL

   The barrel Hadron Calorimeter is a sampling gas detector covering polar angles between 42.6^0 - 137.4^0. It consist of 24 sectors with 20 layers of limited streamer mode detectors inserted into 2 cm slots between 5 cm iron plates in each sector. The detectors are wire chambers which consists of a plastic chatode forming 8 cells of 9×9 mm^2 with one anode wire in each. The detectors vary in length from 40 to 410 cm, operating with Ar/CO2/i-butan 10/60/30%. The HV of each detector can be disconnected individually to reduce dead zones in case of a defect.

   The readout boards are segmented into pads, shaped to form towers pointing towards the interacting point, which pick up the streamer charges. Pads of 5 adjacent layers are combined into a tower. Each tower cowers an angular region of $\Delta\phi$=3.75^0 and $\Delta\theta$=2.96^0 in the barrel. The dimension of a typical tower in the barrel are $25\times25\times35$ cm^3.

   The resolution is about $\frac{120\%}{\sqrt{E}}$

9. MUB

   The DELPHI Barrel Muon chamber consist of 1372 drift chambers arranged into 24 sectors and 2 additional sectors between the legs of the detector. The drift chambers operate with Ar/CH_4/CO_2 (85.5/8.5/6%).

   Each chamber can provide up to three signals which can be used to give space points for a particle passing through the chamber. The accuracy of MUB when space points are associated to extrapolated tracks are in r-ϕ of 2mm and in z of 80mm for dimuons.

10. SAT

    Small Angle Tagger was used for luminosity determination by measuring the Bhabha rate in the polar angle 43< θ <135 mrad, corresponding to a cross section of 27.12±0.04 nb. The SAT was removed from the experiment at the end of 1993, and replaced by the STIC detector.

11. VSAT

    the DELPHI Very Small Angle Tagger detects electron and positron coming from Bhabha scattering between 5 and 7 mrad corresponding to a cross section of about 400nb. VSAT produces information about energy deposition, and position information in xy.

    VSAT consist of 4 calorimeter modules each composed of 12 silicon diodes separated by tungsten absorbers of two radiation length thickness. Three silicon strip planes with 1 mm pitch are placed at 5, 7, and 9 radiation

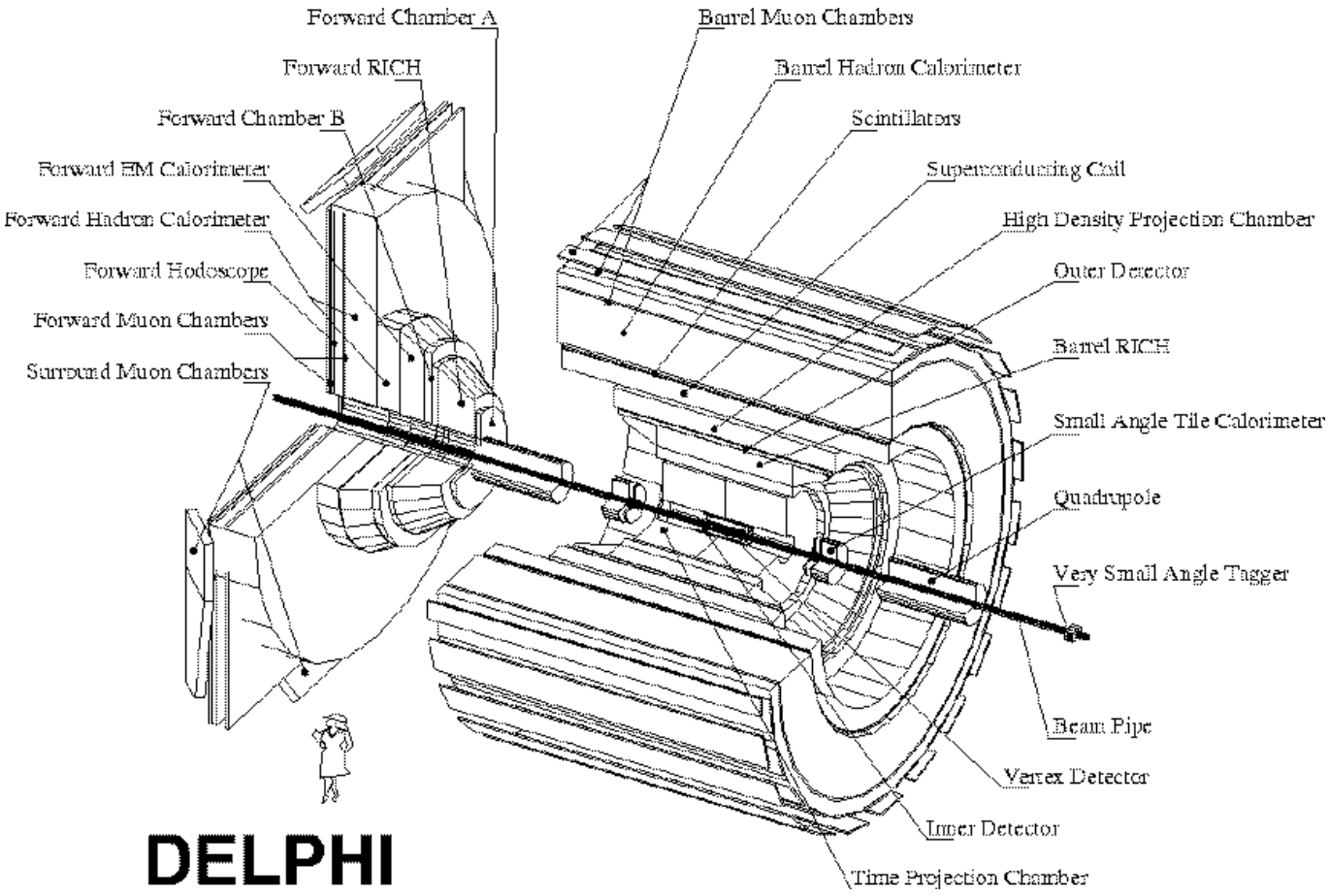

Figure 4:

lengths into the modules and used for shower position measurement in x-y.

The accuracy in energy at 45GeV is 5% and in xy of 170 microns. The expected systematic error in relative luminosity measurement is 0.1%.

5 ANALYSIS

In this section the search for lepton flavour violating events in the three decay channels $Z^0 \rightarrow \mu\tau$ (section 5.4), $Z^0 \rightarrow$eτ (section 5.5), and $Z^0 \rightarrow \mu$e (section 5.6) is described. In each section first a set of preselection - and detector status cuts with corresponding luminosities are described. Then the particle selection cuts are described, and the result of the search for each channel.

5.1 Signature and Background

In a search for lepton flavour violating Z^o decays one looks for final state particles violating the conservation rules given for each of the three lepton families.

$$\begin{pmatrix} \nu_e \\ e \end{pmatrix} \begin{pmatrix} \nu_\mu \\ \mu \end{pmatrix} \begin{pmatrix} \nu_\tau \\ \tau \end{pmatrix}$$

In this thesis a direct search for lepton flavour violation was done by searching for the three decay modes $Z^o \rightarrow \mu\tau$, $Z^o \rightarrow \mu$e, and $Z^o \rightarrow \tau$e forbidden by the Standard Model.

Since the tau leptons decay so fast, within 0.1 mm of the interaction point, also producing hadrons in the final state, not only leptons have to be identified. A good single particle identification is therefore essential.

The expected experimental signature of $Z^o \rightarrow \mu$e, $Z^o \rightarrow \mu\tau$ and $Z^o \rightarrow$eτ is an electron or muon with energy close to beam energy recoiling against a different type of lepton. In the case of the τ the signal will typically be a multiprong event or a e, μ or π with missing energy.

Background arises from both incorrectly reconstructed $e^+e^-, \mu^+\mu^-$ events and $\tau^+\tau^-$ events with one of the taus decaying into electron or muon, escaping with almost all the energy of the tau.

No official DELPHI particle identification routines were used in this search.

5.1.1 Monte Carlo

So called Monte Carlo (MC) simulated events were generated using the ordinary DELPHI chain ([2] [1]) , based on BABAMC [15], DYMU3 [22], and KORALZ [33]. The MC was used to study Standard Model Background from e^+e^-, $\mu^+\mu^-$ and $\tau^+\tau^-$

A modified version of KORALZ was used to generate signal events for all the three decay modes, which were used for efficiency calculation. 19,778 events in the $Z^o \rightarrow \mu$e channel, 18,521 events in the $Z^o \rightarrow \mu\tau$ channel, and 17,021 events in the $Z^o \rightarrow$eτ channel were produced.

5.2 Preselection

Using leptonic DST's event [1] sample, some cuts were applied to make sure the different detectors were operating at a sufficient level to give lowest possible rate of misinterpretation from for example detector failure. This was done by cutting in variable indicating the detector status, set for each detector, for each run, during data taking.

- DETECTOR STATUS using the DELPHI run selection files [11].

  For each event in the process of putting the data on tape the status of each detector is indicated by giving it a number between 0. and 9.

  0. Detector is not in central partition.

  1. Less than half of the Detector is in central partition.

  2. Half of the Detector is in central partition.

  3. - 6. More than half of the Detector is in central partition.

  7. The full Detector is in central partition.

  8. The full Detector is in central partition. but shaky. (for instance H.V. are not always on)

  9. The status of the detector is unknown.

- Only data from the volume defined by $|\cos\theta| < \frac{\sqrt{2}}{2}$ were used.
- A cut in impact point to suppress background from cosmic muons was applied.
- A cut in the number of charged tracks was used to suppress hadronic events.
- Runs without any luminosity information found in the official luminosity files [10] were removed from the sample.
- In the eτ channel events with a leading track in one of the hemispheres, pointing towards a dead module in the HPC, were excluded.

The exact cut value for these variables should be set to minimize background from misinterpretation of tracks, from for example particles passing not operating detector modules, or from cosmics.

But at the same time a good statistic is very important, and therefore one should lett as much luminosity as possible through the selection routine.

5.2.1 Luminosity

Luminosity was calculated from all runs with SAT Luminosity information found on the official luminosity files [10] passing the detector quality cuts.

A total integrated Luminosity for 1991 to 1993 data for the $\mu\tau$ channel of 62880 nb^{-1}, for the eτ channel of 65980 nb^{-1}, and for the μe channel of 61900 nb^{-1} were obtained. Corresponding to 2.174×10^6, 2.269×10^6 and 2.137×10^6 Z^0's for the $\mu\tau$, eτ, and μe channels respectively.

5.3 Lepton identification

To search for lepton flavour violation, an efficient way of tagging single leptons is needed. This is made more difficult since the tau lepton has a mean lifetime of 0.3×10^{-12} making it decay close to the interaction point(10μm), and to final states frequently containing muons or electrons.

5.4 $Z^0 \to \mu\tau$ channel

In the $\mu\tau$ channel the signature would be a high momentum muon in one hemisphere and an identified τ final state in the other. No muonic tau decay were accepted, and different selection routines were applied for electronic and hadronic tau final states.

Preselection
In the $\mu\tau$ channel the following preselection cuts were applied.

- Detector status
  1. Time projection chamber(TPC) status
     $5 \leq TPC \leq 7$
  2. Hadronic Calorimeter(HAD) status
     $5 \leq HAD \leq 7$
  3. Muon Chambers(MUB) status
     $5 \leq MUB \leq 7$
- Barrel; only data from the volume defined by $|\cos\theta| < \frac{\sqrt{2}}{2}$ corresponding to 61.9% of 4π for leptonic data.
- Impact point less than 1.5mm from interaction point.
- The number of charged tracks more than 1 but less than 11.

5.4.1 Luminosity in the $\mu\tau$ channel

Luminosity was calculated from all events with SAT Luminosity information passing the detector quality cuts.

- Luminosity 1991 for the processes $\mu\tau$
  1. Energy point 88.464GeV Luminosity 634$\pm$2.5nb^{-1}
  2. Energy point 89.453GeV Luminosity 549$\pm$2.2 nb^{-1}
  3. Energy point 90.211GeV Luminosity 580$\pm$2.3 nb^{-1}
  4. Energy point 91.229GeV Luminosity 5047$\pm$20 nb^{-1}
  5. Energy point 91.952GeV Luminosity 625$\pm$2.5 nb^{-1}
  6. Energy point 92.952GeV Luminosity 537$\pm$2.1 nb^{-1}

7. Energy point 93.701GeV Luminosity 581±2.3 nb^{-1}

Integrated Luminosity
of 8560±34 nb^{-1}

- 1992 Integrated Luminosity at Energy point 91.340 GeV
of 21130±80 nb^{-1}

- 1993

1. Energy point 89.485GeV Luminosity 8505±34 nb^{-1}
2. Energy point 91.295GeV Luminosity 13208±52 nb^{-1}
3. Energy point 93.076GeV Luminosity 9001±36 nb^{-1}

Integrated Luminosity
of 30710±120 nb^{-1}

This gives a total integrated Luminosity for the $\mu\tau$ channel of 60400±210 nb^{-1}
Corresponding to 2174000±19000Z^0's

5.4.2 Single Muon identification

Muon identification is based on two very important factors; Associated hit in muon detector and very high momentum (figure: 30).

The muon identification efficiency was calculated from running a sample of Monte Carlo muons through the single muon identification routine.

- To select single muons in the $\mu\tau$ channel the following cuts were applied:

  1. One charged track in hemisphere

     Should remove multiprong events from tau decay, cosmics and quark events.

  2. Muon chamber hit

     At least one associated hit in muon chambers for a muon was required This requirement should remove from the sample almost 100% of electrons but will contain taus decaying to muon, and some hadronic events which showers into a muon chamber.

     Muon-chambers has an acceptable coverage between 52^o to 128^o except for the crack at 90^0. Outside this region some extra constrains are needed in search involving muons.

     The requirement of good muonchamber coverage for a search involving muons, is important to avoid background from muons which pass holes in the muon-chambers to be interpreted as non-muons, and thereby give muon-pairs which are accepted as lepton flavour violating $\mu\tau, \tau \rightarrow$h events.

     In this thesis the search was done down to 45^o but only with additional cuts for the tau in the region below 52^o

  3. Normalized momentum

     $0.97 < p/E_{beam} < 1.45$

     In tau decay $\tau \rightarrow \mu\bar{\nu}_\mu\nu_\tau$ neutrinos will escape with some of the tau energy, leaving less energy to the muon (figure: 30).

     To select muons and suppress $\tau\tau$ background, where one tau decay into a muon, a very strict cut in momentum normalized(p) was applied, only letting particles with close to beam-energy pass. The normalized momentum spectra for muons, taus, and electrons are shown in figure 30.

     The upper cut avoids problems due to wrongly reconstructed momenta.

  4. Hadronic energy per fired layer in HCAL

     $0.03 < EHL < 3.1$

     The Hadronic Calorimeter - HCAL gives four layers of energy information. The EHL variable was calculated from the associated energy deposited in HCAL for the track, divided on the number of layers with any associated energy.

Hadronic final states from tau decays will shower in the HCAL, sometimes even into the MUB, but also often in less than all four layers of HCAL.

Plotting EHL (figure: 33) for muons, electrons, and a sample of hadrons from tau decays, taken from Monte Carlo simulated events, shows a characteristic higher value for hadronic final states than for muons and electrons.

The upper cut was set to suppress background from tau pairs (table: 3, 4), the lower to ensure hadronic energy associated to the muon track.

The efficiency calculated from a sample of Monte-Carlo simulated $\mu^+\mu^-$ events and found to be 45.7% in barrel.

5.4.3 Single Tau identification in the $Z^0 \to \mu\tau$ channel

Single Tau identification is made more complicated due to its decay to the two other leptons and therefore the possible critical problem of distinguish between for example an electron from $Z^0 \to e^+e^-$ and an high energy electron from tau decay. In this thesis all taus decaying into muons were excluded in the $\mu\tau$ channel search.

The search for a single tau in the $\mu\tau$ channel was split into two depending on the tau final state, one with hadronic final state and one with electron final state.

The problem of distinguishing an electron from tau decay from an electron from an electron pair was of course not a critical problem, since in the $\mu\tau$ it would in both cases indicate lepton flavour violation, but the problem would at least indicate some extra errors in the calculation of upper limit.

A Particle identified as a $\tau \to e\nu_e\bar{\nu_\tau}$ was not run trough the $\tau \to h..$ selection routine to avoid double counting.

- SINGLE TAUS IN THE $Z^0 \to \mu\tau$, $\tau \to E\nu_e\bar{\nu_\tau}$ DECAY MODE WERE SELECTED BY THE FOLLOWING CUTS:

  (Accepting no tau decay to muons; ($Z^0 \to \mu\nu_\mu\bar{\nu_\tau}$)

  1. Acolinearity

     Acol$> 0.5^o$

     The conservation of lepton number in the standard model, and experimental upper limit on lepton flavour violation existing, justify an assumption of missing energy neutrinos in tau decay (figure: 34).

     And therefore also justifies a cut in acolinearity even if this means cutting in both hemispheres at the same time.

     The acolinearity cut suppress background from muon-pairs where one of the muons were stopped before MUB (figure: 5).

     Acolinearity should also remove background from electron-pairs, however this background is very unlikely since one of the electrons then has to be tagged as a muon. The only possibility for this to happen could be from detector error, or a cosmic muon involved.

At the same time it also reduces the efficiency since it removes taus where the final state lepton or hadrons carries a very high fraction of the energy, but this seems unavoidable because of the difficulties of distinguishing it from μ pairs already mentioned.

2. Normalized Electromagnetic energy HPC

   $\frac{E_{HPC}}{E_{beam}} > 0.02$

   To select electron final states, a cut in E_{HPC} was used (figure: 31). This should suppress background from muons and to some extent from hadrons (figure: 6). The less dangerous background from $\tau \to \pi^0\pi^{\pm}$... with a small opening angle could pass this cut.

3. Normalized momentum

   $\frac{p}{E_{beam}} < 0.95$

   This cut was set to suppress background from μ pairs where the muon stops before the second layer of HCAL and maybe radiates a γ with pair production giving a high energy electron as the leading track.

4. Cracks in HCAL and Muon chambers

   $|90 - \theta| > 0.5^0$

   In this thesis all events with a leading track within 0.5^0 of the 90^0 crack were removed.

   The Hadronic calorimeter is built in modules which means there will be dead regions on the border of two modules. The particles are generally not going parallel with the borders, and there will only be small regions where particles cross such dead regions, going from one module into another. The border section at θ=90^0, on the other hand, will be a possible source for misinterpreting because here the particles are parallel with the border sections, and only bent in the ϕ direction, and therefor easily might go undetected passing this crack.

   The same goes for the Muon Chambers which also have less or no coverage in the θ=90^0 region.

5. No energy deposition in second third and fourth HCAL layers

   This cut should suppress background from μ pairs and hadronic events since most of them deposit energy in more than one layer of HCAL (figure 8)

6. No muon chamber hits

   Also to suppress background from μ pairs.

- To select Taus in $Z^o \to \mu\tau$, $\tau \to$ hadronic final states the following cuts were applied:

  (No $\tau \to \mu\nu_\mu\bar{\nu_\tau}$ was accepted.)

  1. Acolinearity

     Acol $> 0.5^o$

The same argument as for tau decaying to electron final state applies here. The cut in acolinearity (figure: 34) was set to suppress background from μ pairs, where one of the muons does not fire the MUB.

Might also suppress background from electron-pairs, very unlikely anyway, where one of the electrons showers into HCAL, which is not to unusual (figure: 35), especially in regions around cracks in the HPC.

To further suppress muon pair background the acolinearity cut was strengthened to 0.8 under two additional conditions:

(a) $EHL < 4.0$ (figure: 12).

(b) $\frac{p}{E_{beam}} > 0.9$ (figure 10, 11).

Both this cuts were aimed to suppress background from muon pairs where one of the muons was stopped before MUB, giving typical high energy low acolinearity events (figure: 10(c)). This cut should not affect the signal efficiency considerably since the signal tau decaying to hadronic final state typical are high acolinarity low momentum events (figure: 10(b)).

The signal MC (figure: 12(b)) contains all tau final states not only hadronic and therefore indicates a worse effect on the efficiency than the cut in fact makes since hadronic energy for hadrons are in average somewhat higher than the leptonic final states.

2. Hadronic energy per fired layer HCAL

   $EHL > 3.1$

   The requirement of hadronic energy per fired layer to be grater than 3.1 , was in the tau decaying to hadronic final state a very important cut to suppress background from muon pairs. Hadrons, mainly pions showers in HCAL depositing large energy inside few layers, while muons penetrates HCAL and continue into MUB and deposit moderate energy in all layers of HCAL. This, and the requirement of no MUB hit, suppress as good as all muon background.

   The cut was strengthened to $EHL > 4.0$ if the track was closer than 1.0^o from the ϕ cracks in Muon Chambers, because a higher rate of muons in this region go undetected by the MUB.

3. Cracks in MUB

   If $\theta < 52^0$ or $\theta > 128^0$ then H_{3-4}=0.

   To avoid background from $\mu^+\mu^-$ where one of the muons falls into a θ crack in muon chambers, this additional requirement of no Hadronic energy deposition in third and fourth layer of HCAL, was used outside the barrel region $52^0 - 128^0$.

4. No Muon Chamber hits

   The most important muon suppression cut.

5.4.4 Result of the $Z^0 \to \mu\tau$ channel search

Efficiency is calculated from running a sample of Monte Carlo simulated $Z^0 \to \mu\tau$ events through the same routine as data, finding an efficiency of (18.6±0.9)% in the 4π region.

Remaining number of events after each cut are shown in table 3, and 4. Some examples of events passing the $Z^0 \to \mu\tau$ selection are shown in figures 14, 15, and 16

$\mu(\tau \to$e)	Ev. a. cut	$(\tau \to$e)μ	Ev. a. cut
Preselection cuts	156985	-	156985
μ id. cuts		$\tau \to$e id. cuts	
Charged tracks	135175	ACOL	83793
MUB	50167	E_{HPC}	36604
p	26781	p	31294
EHL	25641	H2+h3+h4	25688
$\tau \to$e id. cuts		MUB	25613
ACOL	4280	θ	25580
E_{HPC}	229	μ id. cuts	
p	126	Ch. track	20750
H2+h3+h4	19	MUB	1912
MUB	11	p	21
θ	11	EHL	14

Table 3: $\mu\tau, \tau \to e\nu\bar{\nu}$ channel. The table show the number of events remaining after a given cut.

$\mu(\tau \rightarrow$h)	Ev. a. cut	$(\tau \rightarrow$h)μ	Ev. a. cut
Preselection cuts	156985	-	156985
μ id. cuts		$\tau \rightarrow$h id. cuts	
Charged tracks	135175	ACOL	83779
MUB	50167	EHL	13165
p	26781	θ	12755
EHL	25641	MUB	11924
$\tau \rightarrow$h id. cuts		μ id. cuts	
ACOL	4269	Ch. track	7954
EHL	53	MUB	1562
θ	39	p	7
MUB	2	EHL	2

Table 4: $\mu\tau, \tau \rightarrow$hadronic final states. The table shows the number of events remaining after a given cut.

Data	Seen	$\mu^+\mu^-$ MC	e^+e^- MC	$\tau^+\tau^-$ MC	4π Eff MC %
1991	1	1.1±0.7	0.0	2.5±0.7	18.3±0.9
1992	10	7.4±1.4	0.0	6.7±1.2	18.7±0.9
1993	18	7.2±2.4	0.0	6.1±1.6	18.6±0.9

Table 5: $Z^o \rightarrow \mu\tau$

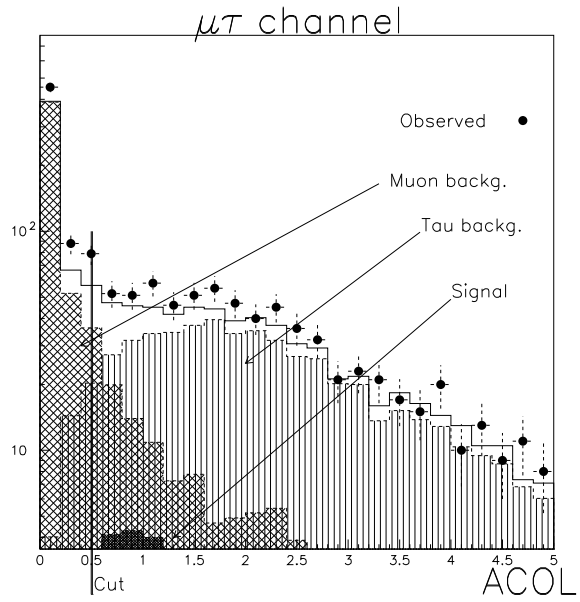

Figure 5: Acolinearity distribution leading track for events(black dots), and background($\mu^+\mu^-$cross-hadched, $\tau^+\tau^-$ vertical lines) tagged as single muons in the opposite hemisphere. The the tau selection cut is indicated. A signal of order 10^{-4} is plotted(black).

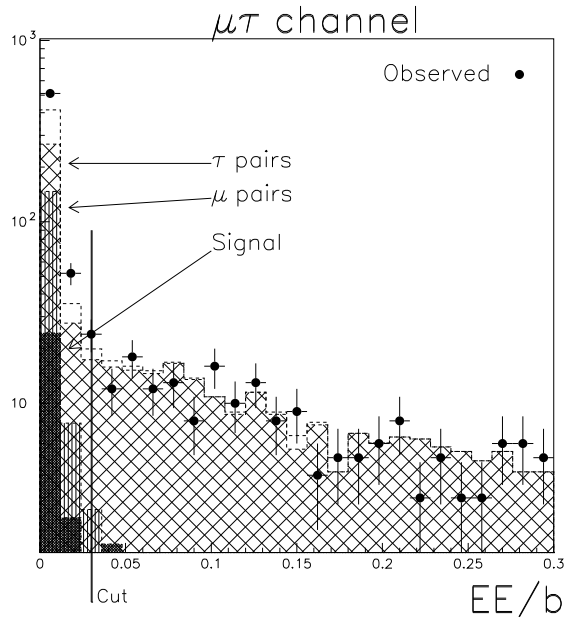

Figure 6: Normalized HPC energy distribution leading track for events(black dots), and background($\tau^+\tau^-$cross-hadched, $\mu^+\mu^-$ vertical lines), tagged as single muons in the opposite hemisphere. The $\tau \rightarrow$e selection cut is indicated. A signal(black) of order 10^{-4} is plotted.

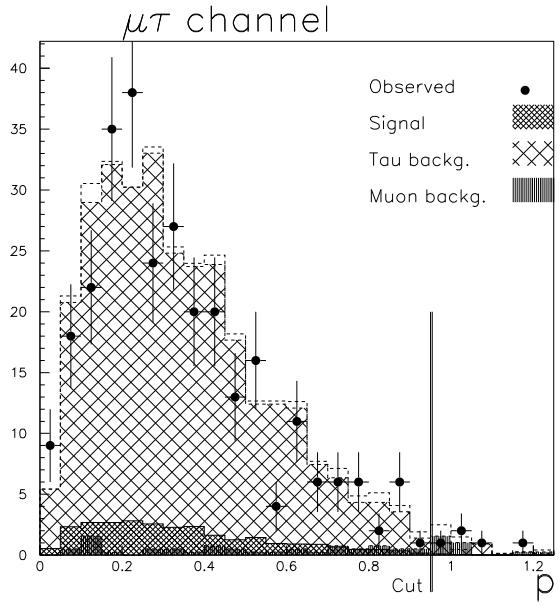

Figure 7: Normalized momentum (p) distribution leading, track for events(black dots), and background($\tau^+\tau^-$cross-hadched, $\mu^+\mu^-$ vertical lines), tagged as single muons in the opposite hemisphere. The $\tau \rightarrow$e selection cut is indicated. A signal(grey) of order 10^{-4} is plotted.

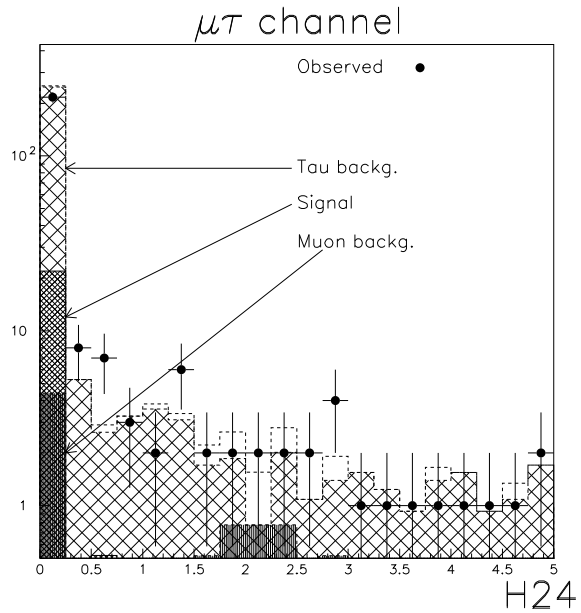

Figure 8: Energy distribution for the sum of second, third, and fourth layers of HCAL for the leading track, when a muon is tagged in opposite hemisphere. Events(black dots), and background($\tau^+\tau^-$cross-hadched, $\mu^+\mu^-$ vertical lines). The $\tau \rightarrow$e selection cut is indicated. A signal(grey) of order 10^{-4} is plotted.

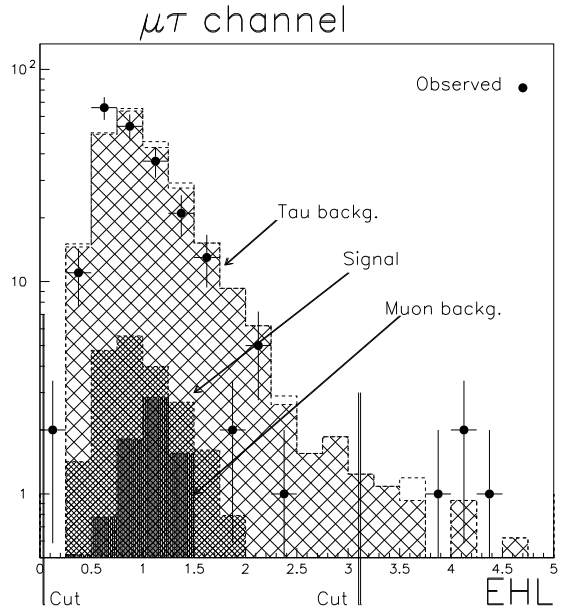

Figure 9: HCAL energy per layer with energy distribution for leading track events(black dots), and background($\tau^+\tau^-$cross-hadched, $\mu^+\mu^-$ vertical lines) tagged as $\tau \rightarrow$e in the opposite hemisphere. The cut in the single μ routine is indicated. A signal(grey) of order 10^{-4} is plotted.

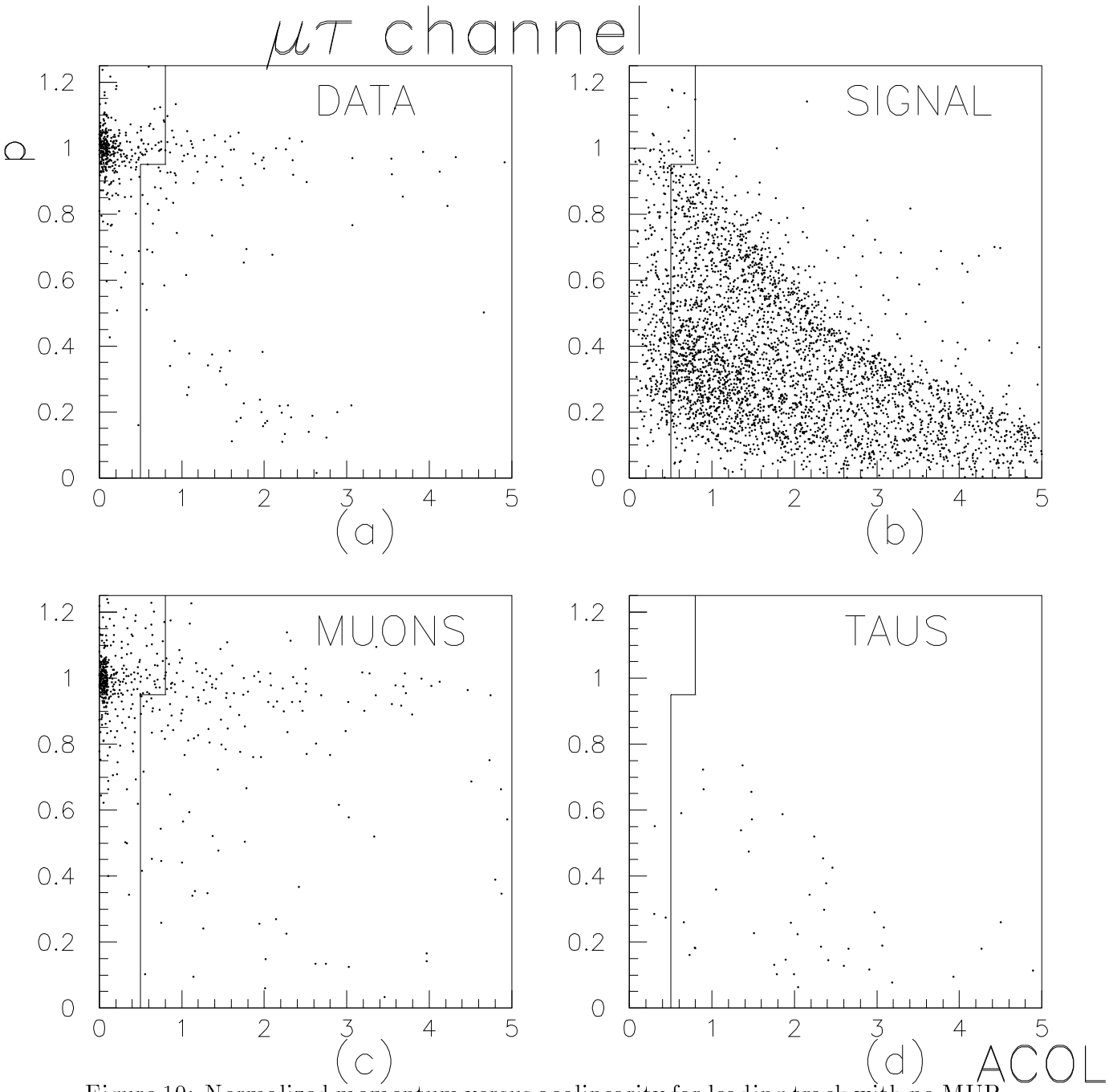

Figure 10: Normalized momentum versus acolinearity for leading track with no MUB hit when having an identified muon in the opposite hemisphere. (a) for Data, (b) for signal MC, (c) for Muon pair MC, and (d) for tau pair MC. The $\tau \rightarrow$h cut is indicated for the $\mu\tau$ channel.

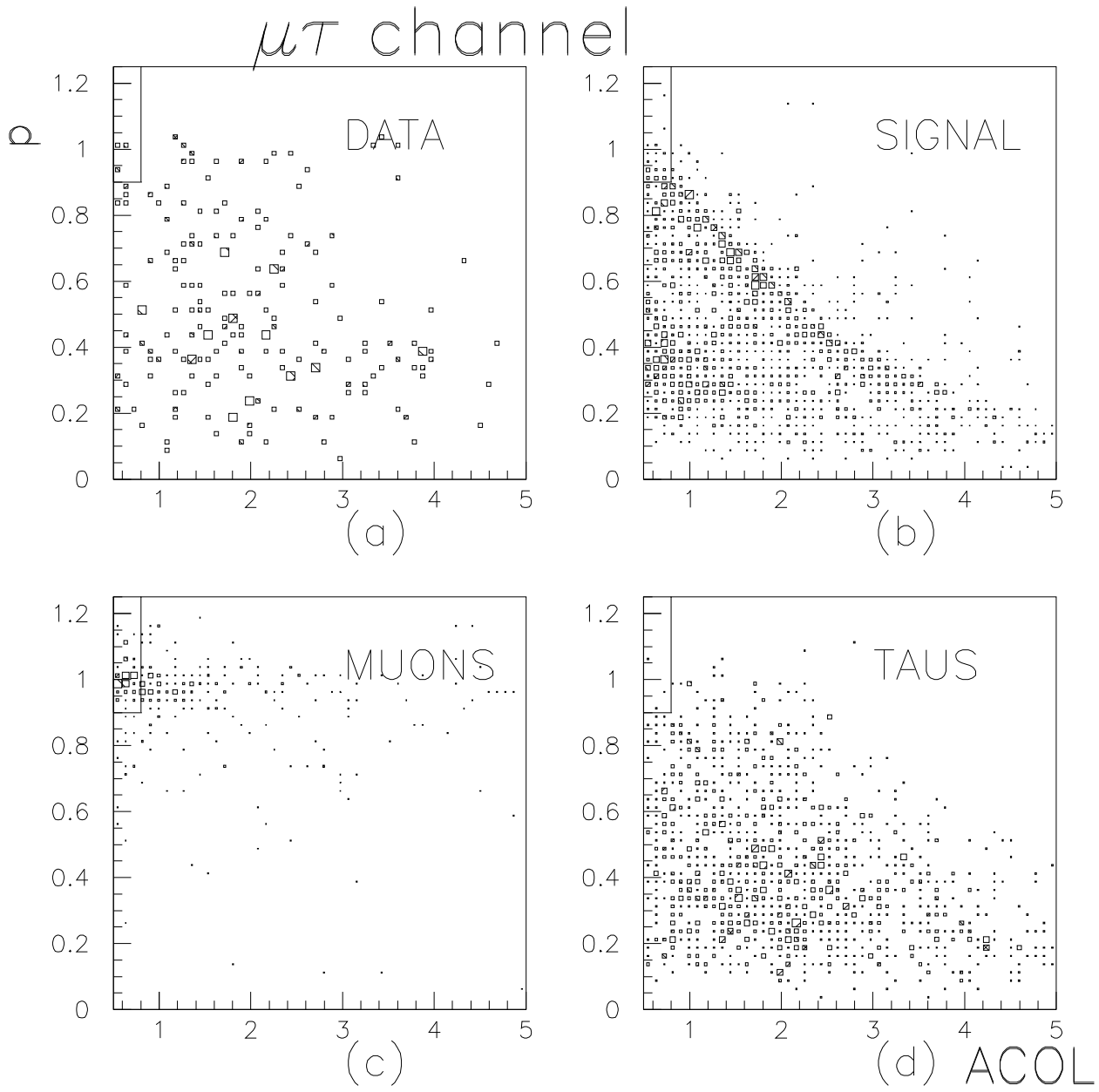

Figure 11: Normalized momentum (p) for leading track versus acolinearity when a muon is tagged in opposite hemisphere. The additional cut in the $\tau \rightarrow$h selection is indicated.

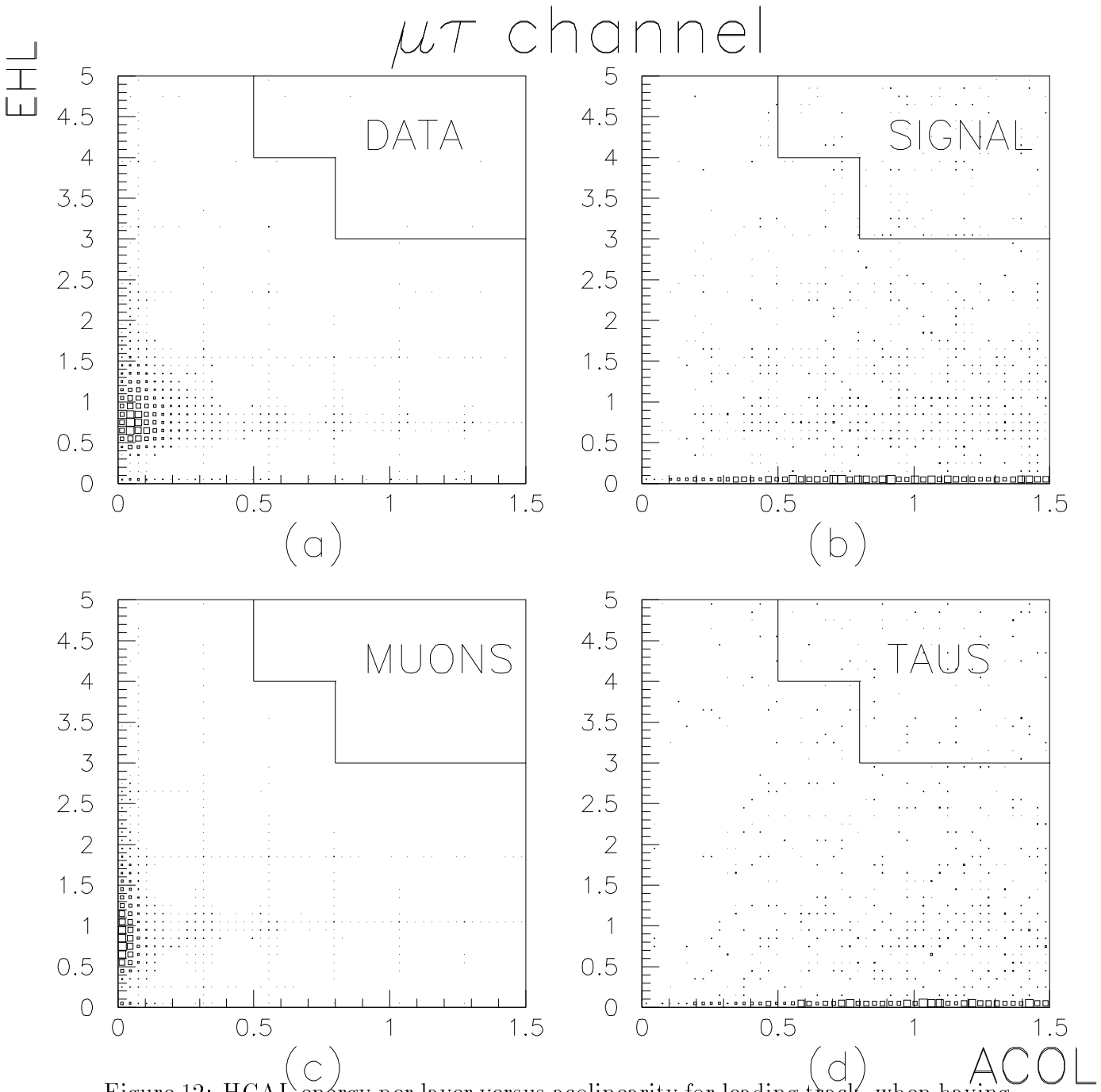

Figure 12: HCAL energy per layer versus acolinearity for leading track, when having an identified muon in the opposite hemisphere. (a) for Data, (b) for signal MC, (c) for Muon pair MC, and (d) for tau pair MC. The $\tau \rightarrow$ hadronic final state cut is indicated for the $\mu\tau$ channel.

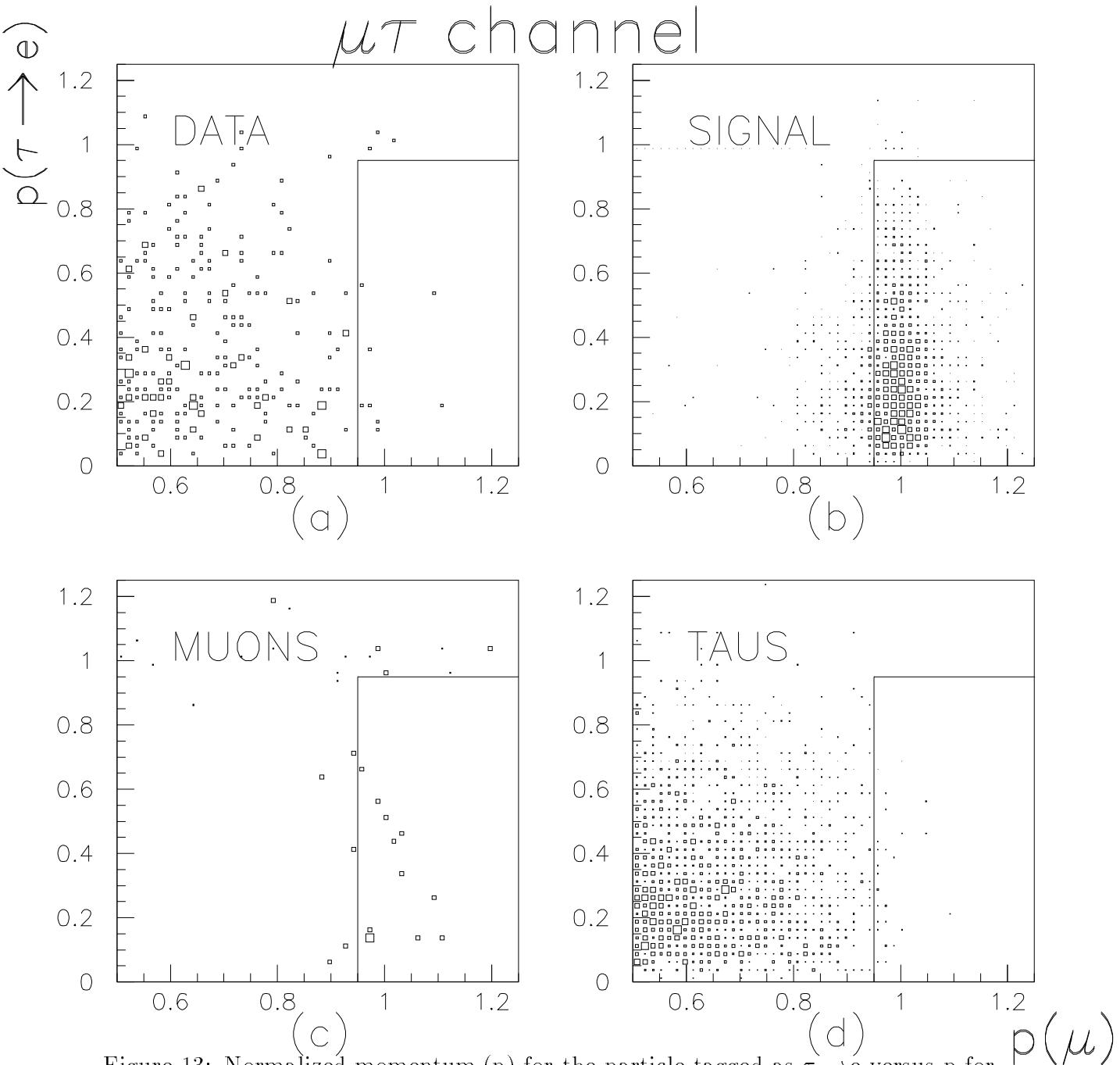

Figure 13: Normalized momentum (p) for the particle tagged as $\tau \rightarrow$e versus p for the particle tagged as muon in the opposite hemisphere.

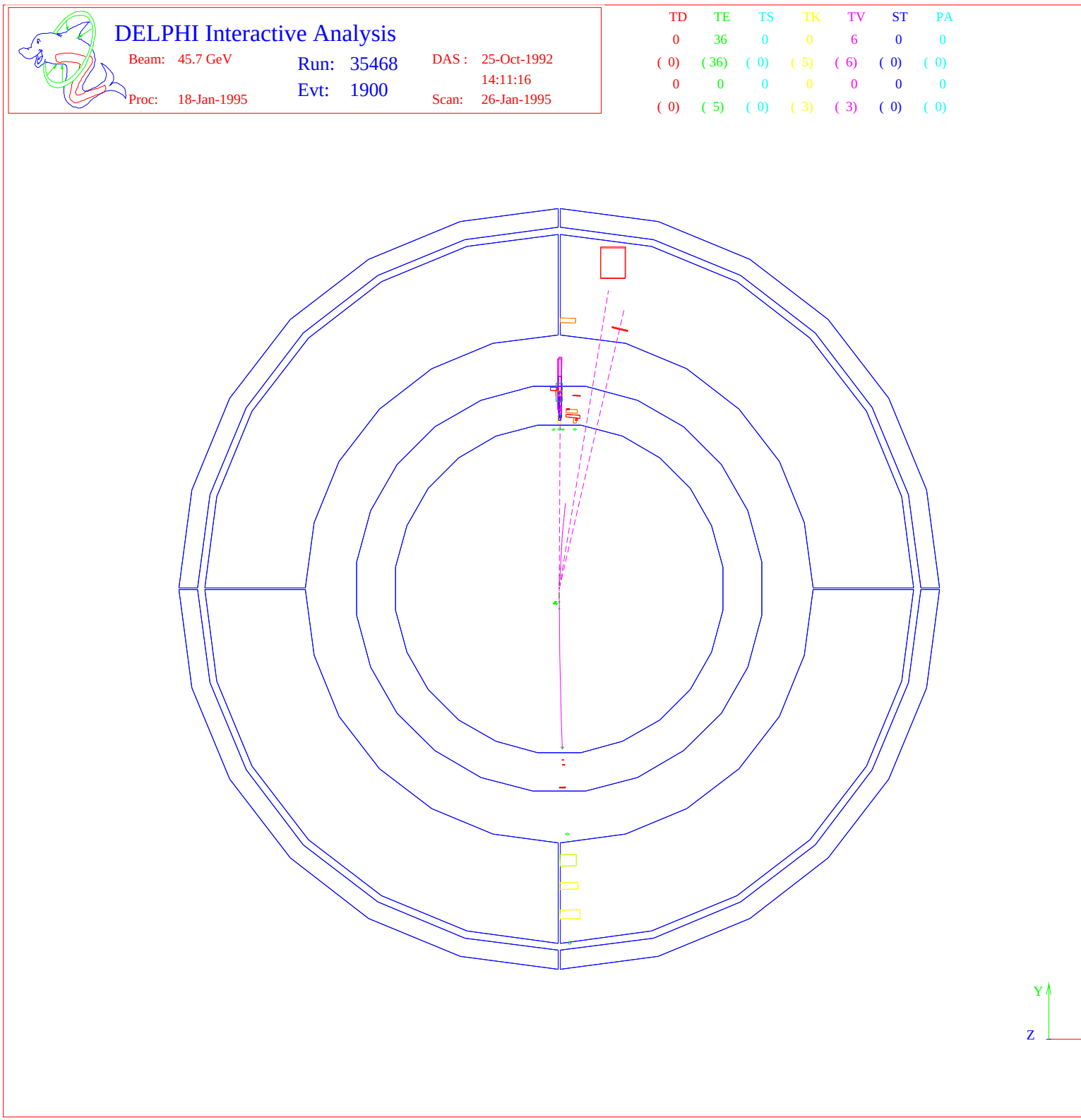

Figure 14: Event classified as $\mu\tau$. probably a tau-pair with one high energy muon and a multi prong event in opposite hemisphere.

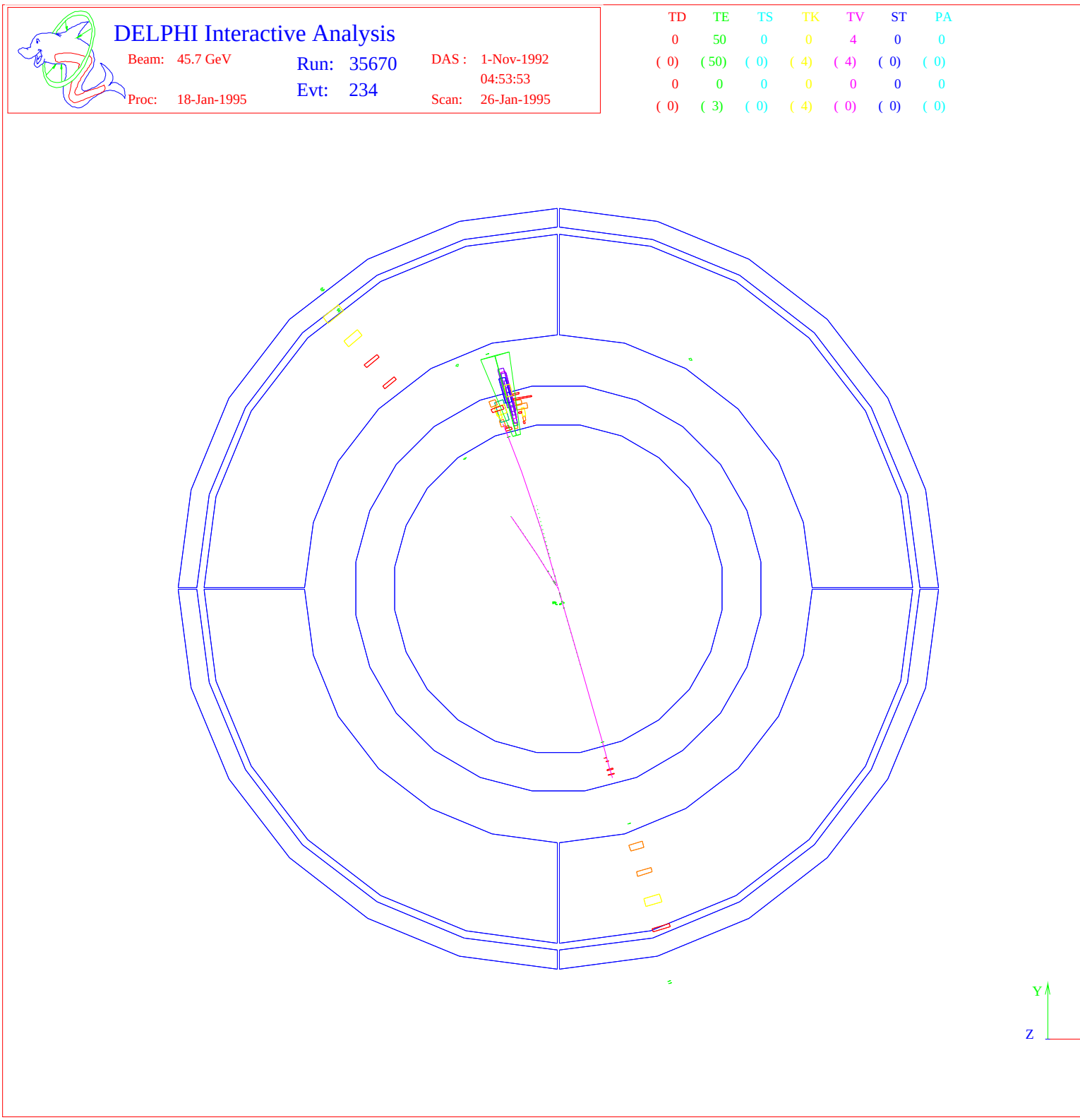

Figure 15: Event classified as $\mu\tau$. Probably a muon pair where one of the muons has radiated a high energy γ with pair production resulting in leading track being a electron with acolinearity higher than 0.5^0.

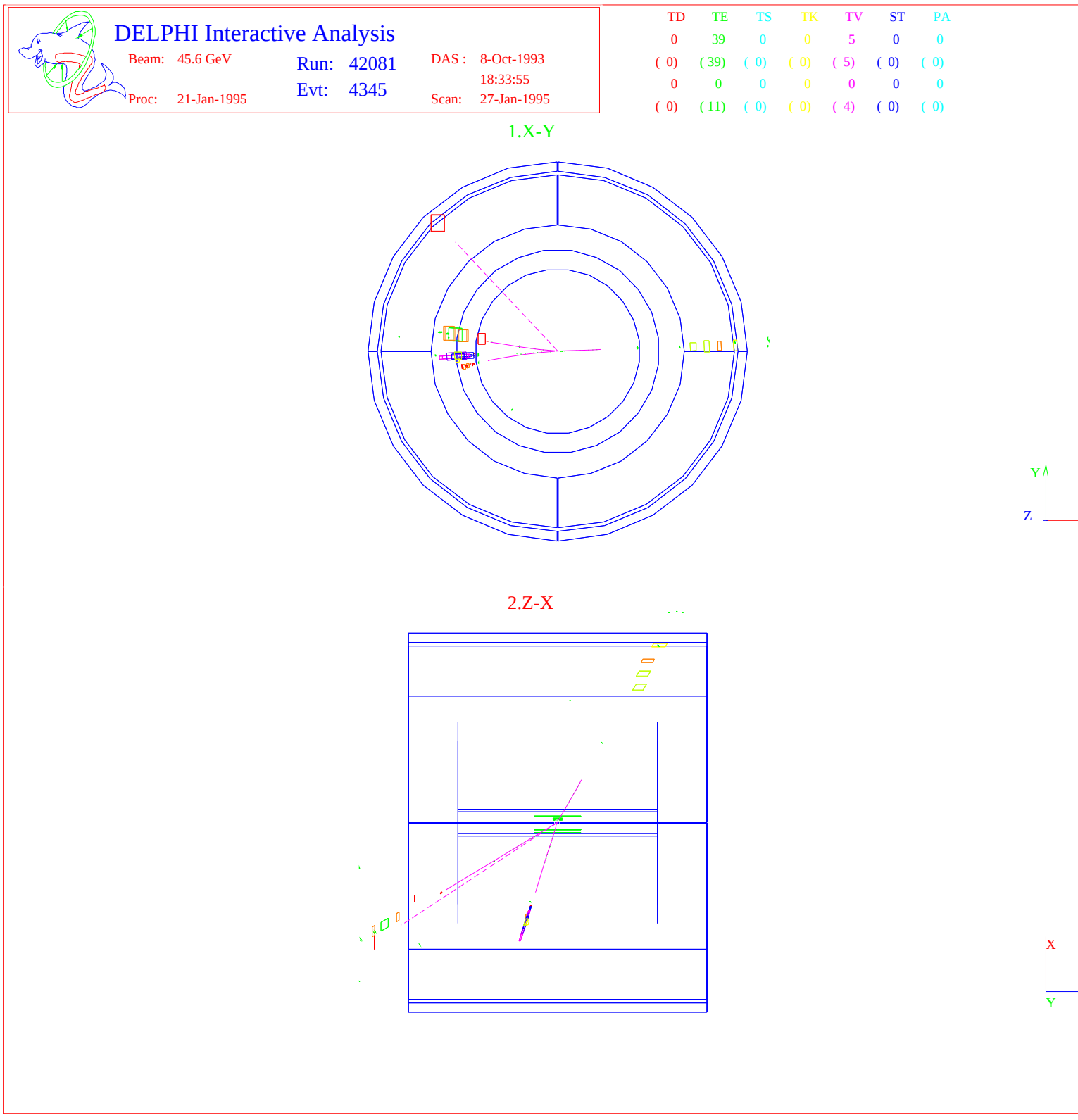

Figure 16: Classified as a $\mu\tau$ event. Hit in MUB in forward chambers for a low energy track indicating a muon pair where one muon radiates, and then pair production.

5.5 $Z^0 \rightarrow e\tau$ channel

Th following preselection cuts were applied in the $e\tau$ Channel:

- Detector status (see section: 5.2)

  1. Time projection chamber status: $5 \leq TPC \leq 7$
  2. Hadronic Calorimeter status: $5 \leq HAD \leq 7$
  3. Electromagnetic Calorimeter status: $5 \leq HPC \leq 7$

- Impact point less than 1.5mm from interaction point.

- The number of charged tracks more than 1 but less than 11.

- Dead elements in HPC were removed:

  An electron passing the HPC without or with very low detector response, and then showering into HCAL, could easy be mistaken for a tau decaying to a hadron. Therefor it was essential to remove from the sample tracks passing a module not operating correct. This was done by selecting a sample from data of electrons passing the following cuts:

  1. High Normalized HPC energy:$\frac{E_{HPC}}{E_{beam}} > 0.95$ in one hemisphere.
  2. Low acolinearity:ACOL<0.5
  3. No energy deposition in HCAL or MUB both hemispheres.

  This should give a sample of e^+e^- with very low background from tau pairs and possibly, if existing, lepton flavour violating events.

  Plotting the HPC module number if the leading track in opposite hemisphere does not give a response in the HPC, should not have any preference for any module, if the events are tau-pairs or lepton nonconservation background. A preference will indicate a malfunctioning or dead module (figure 17). The run number information on these events, indicates for which period the module has been dead.

  The following HPC module numbers were excluded for the runs indicated:

  - Module 114 for run number from 21911 to 28734
  - Module 78 for run number from 21921 to 28734
  - Module 89 for run number from 33539 to 36269
  - Module 58 for run number from 37026 to 39243
  - Module 113 for run number from 37456 to 42565
  - Module 137 for run number from 39245 to 43039

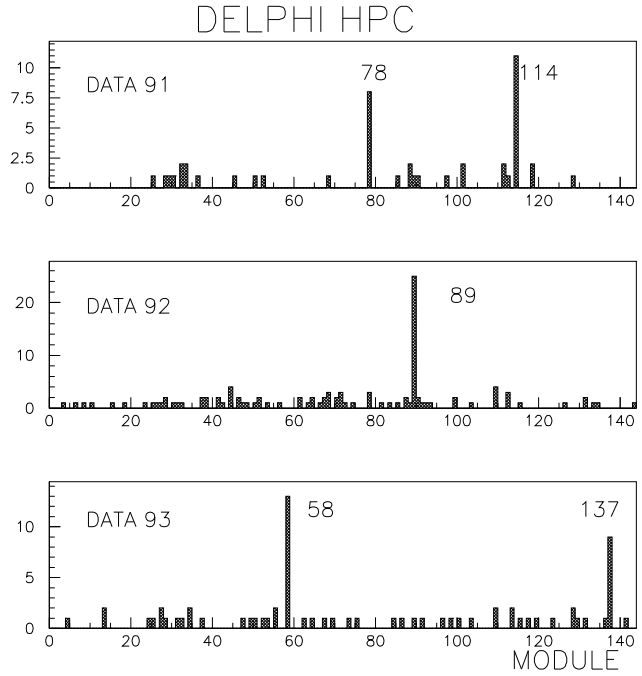

Figure 17: Dead elements in the HPC.

5.5.1 Luminosity in the eτ channel

Luminosity were calculated from all events with SAT Luminosity information passing the detector quality cuts.

- Luminosity 1991 for the processes eτ :

  1. Energy point 88.464GeV Luminosity 706$\pm$2.8 nb^{-1}
  2. Energy point 89.453GeV Luminosity 620$\pm$2.5 nb^{-1}
  3. Energy point 90.211GeV Luminosity 593$\pm$2.4 nb^{-1}
  4. Energy point 91.229GeV Luminosity 5525$\pm$22.1 nb^{-1}
  5. Energy point 91.952GeV Luminosity 668$\pm$2.7 nb^{-1}
  6. Energy point 92.952GeV Luminosity 617$\pm$2.5 nb^{-1}
  7. Energy point 93.701GeV Luminosity 670$\pm$2.7 nb^{-1}

  Integrated Luminosity of 9400$\pm$38 nb^{-1}

- 1992 Integrated Luminosity at Energy point 91.340 GeV of 22670$\pm$90 nb^{-1} at

- 1993

  1. Energy point 89.485GeV Luminosity 9239$\pm$37 nb^{-1}
  2. Energy point 91.295GeV Luminosity 14903$\pm$60 nb^{-1}
  3. Energy point 93.076GeV Luminosity 9774$\pm$39 nb^{-1}

Integrated Luminosity of 33920±130 nb^{-1}

A total integrated Luminosity in the eτ channel of 65980±220 nb^{-1}

5.5.2 Single Electron identification

The signature of a high energy electron would be a charged track with an associated shower close to beam energy in the HPC. Ideal there should be no energy deposition after the HPC but this is not true, and quite a high fraction of electrons will shower into first layer of HCAL, especially around cracks in HPC (figure 35).

- To select single electrons the following cuts were applied:

  1. One charged track in the hemisphere

     Should remove multiprong events from tau decay, cosmics and quark events.

  2. Normalized electromagnetic energy HPC

     $\frac{E_{HPC}}{E_{beam}} > 0.97$

     An electron would deposit close to all its energy in the HPC (figure 31, and 18), therefore a very high cut in normalized HPC energy can be applied, without losing to much efficiency, and still suppress all background from muon pairs and a high fraction of taus decaying to electrons, which is the dangerous background in this channel.

     The same argument as for the $\tau \rightarrow \mu\nu_\tau\nu_\mu$ background applies here for the suppressing of $\tau \rightarrow e\nu_\tau\nu_e$.

     Also possible background from the decay $\tau \rightarrow \pi^0\pi^\pm$..... should be suppressed.

     The $\pi^0 \rightarrow \gamma\gamma$ decay where the two gamma showers in the HPC are to close to be resolved as multitrack, and this possibly close to a $\pi^\pm$ could give a signal very similar to that of an electron.

  3. Electromagnetic energy on momentum

     $\frac{E_{HPC}}{p} > 0.4$

     To further suppress muons radiating, and hadrons this cut in HPC energy on momentum was used (figure 32, and 20).

  4. Hadronic energy first layer

     $H1 < 0.95$

     Optimal no electrons should penetrate into hadronic calorimeter but a fraction of electrons does so. Showering into HCAL, electrons will have deposited most of its energy in HPC, and therefor only give a small energy depositions. The cut was set to suppress Hadronic final state taus (figure 19).

     Because of the structure of HPC some electrons will pass through the gap between the modules without any detectable energy deposition and penetrate into first and some even second layer of HACL giving a very high hadronic energy deposition in first layer.(figure: 35, 36).

The efficiency finding electrons, calculated on e^+e^- MC was 24.5% (4π).

5.5.3 Single tau identification in the $Z^0 \rightarrow e\tau$ channel

Like in the $\mu\tau$ channel (section: 5.4.3) the single tau identification in the eτ channel is made more complicated due to its decay to electron and thereby the problem of distinguish between an electron from $Z^0 \rightarrow e^+e^-$ and an high energy electron from tau decay.

In this thesis all taus decaying to electron were excluded in the eτ channel.

- SINGLE TAUS IN $Z^0 \rightarrow e\tau$, $\tau \rightarrow \mu\bar{\nu}_\mu\nu_{tau}$ AND $\tau \rightarrow$ HADRONIC FINAL STATE DECAY MODE WERE SELECTED BY THE FOLLOWING CUTS:

  Accepting no decay to electrons ($\tau \rightarrow e\bar{\nu}_e\nu_{tau}$)

  1. Acolinearity Acol> 0.4

     The acolinearity cut was set to suppress background from electron-pairs, where one of the electrons showers into the HCAL, and thereby could be tagged as hadrons from tau decay (figure: 34).

  2. Normalized HPC energy
     $\frac{E_{HPC}}{E_{beam}} < 0.1$
     Since not accepting taus decaying to electrons, the leading charged track in tau decays should deposit most of its energy in the HCAL for hadrons, and muons even partly outside the detector. Therefore to further suppress background from e-pairs showering into HCAL a cut in normalized E_{HPC} energy was applied (figure: 31, 21).

  3. Energy in second layer of HCAL
     $H_2 > 0$
     Electrons showering into HCAL were also suppressed by demanding energy in second layer of HCAL.

  4. HPC ϕ crack
     If the track passed closer than 1^o from a HPC ϕ crack, energy in third layer of HCAL was required.
     The problem of electrons passing cracks Between HPC modules and therefore showering further into HCAL (figure: 35,36), was met by a requirement of hadronic energy in third HCAL layer, if the track was close than 1^o from a HPC module border.

5.5.4 Result of the $Z^0 \rightarrow e\tau$ channel search

Efficiency is calculated from running a Monte Carlo simulated sample of $Z^0 \rightarrow e\tau$ through the same routine as data, finding an efficiency of $(7.8 \pm 0.5)\%$ in the 4π region.

Plot of events tagged as eτ are shown in figures 22, and 23.

$e\tau$	Ev.a cut	τe	Ev.a cut
Preselection cuts	160792	-	160792
e id. cuts		τ id cuts	
Charged tracks	138453	Acol	89695
E_{HPC}	22911	E_{HPC}	59209
$\frac{E_{HPC}}{p}$	22721	H2	31063
H1	22015	ϕ +	31100
τ id cuts		e id. cuts	
Acol	6261	Charged tracks	25239
E_{HPC}	562	E_{HPC}	11
H2	14	$\frac{E_{HPC}}{p}$	10
ϕ +	6	H1	10

Table 6: eτ channel. The table shows the number of remaining events after a given cut.

Data	Seen	$\mu^+\mu^-$ MC	e^+e^- MC	$\tau^+\tau^-$ MC	4π Eff MC %
1991	2	0	0	3.2±0.8	8.0±0.5
1992	6	0	1.0±0.3	6.4±1.0	7.8±0.5
1992	8	0	1.0±0.3	7.2±1.5	7.7±0.5

Table 7: $Z^o \rightarrow e\tau$

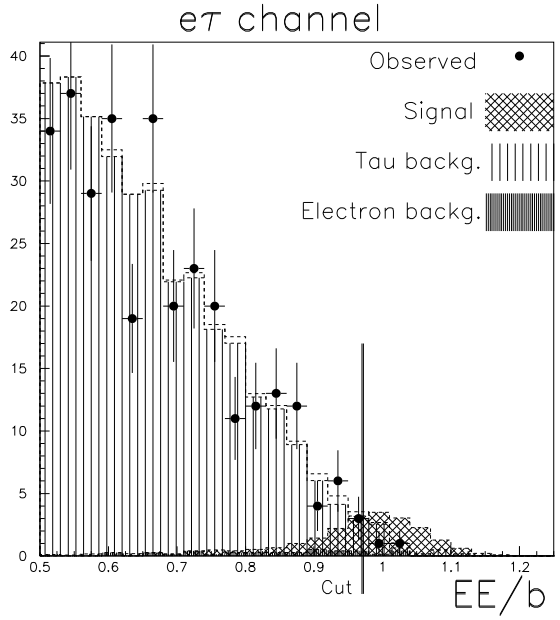

Figure 18: HPC energy distribution for leading track for events and background($\tau^+\tau^-$vertical lines, e^+e^- black), with an identified tau in opposite hemisphere. The electron cut and a signal (cross-hatched) of the order of 10^{-4} are indicated.

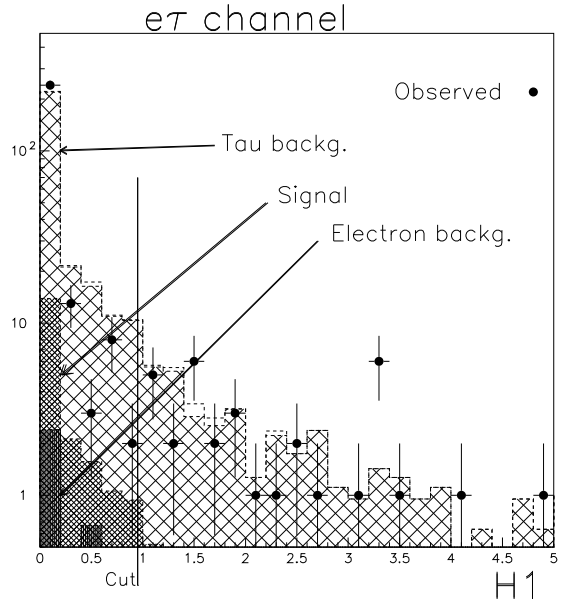

Figure 19: Energy deposition leading charged track in first layer of HCAL for event with a tagged tau in opposite hemisphere. Background from e-pairs (black), and τ-pairs(cross-hadched) are plotted. The electron cut and a signal(grey) of the order of 10^{-4} are indicated.

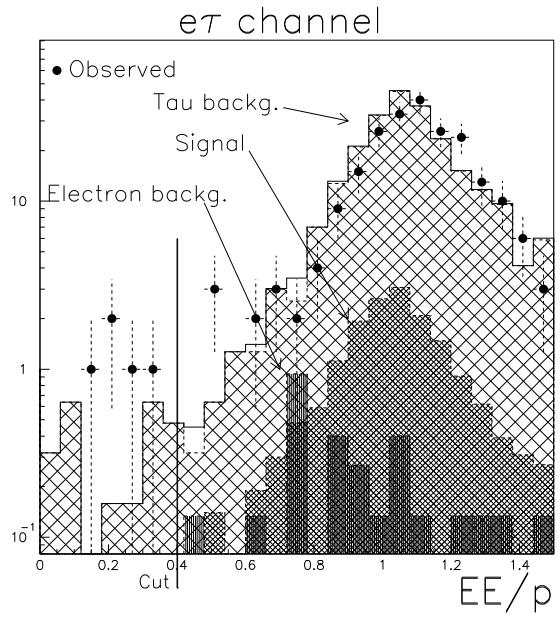

Figure 20: $\frac{EE}{p}$ distribution leading track for event with a tagged tau in opposite hemisphere. Background from e-pairs (black), and τ-pairs(cross-hadched) are plotted. The electron cut and a signal(grey) of the order of 10^{-4} are indicated.

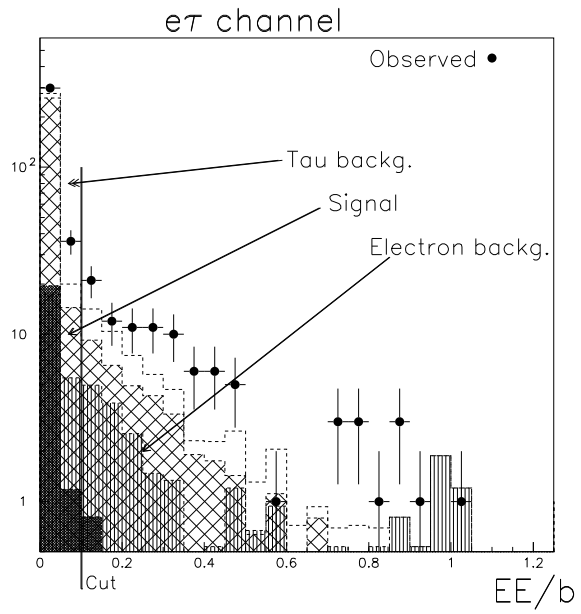

Figure 21: HPC energy distribution for leading track for events(black dots) and background($\tau^+\tau^-$cross-hadched, e^+e^-vertical lines), with an identified electron in opposite hemisphere. The tau cut and a signal(black) of the order of 10^{-4} are indicated.

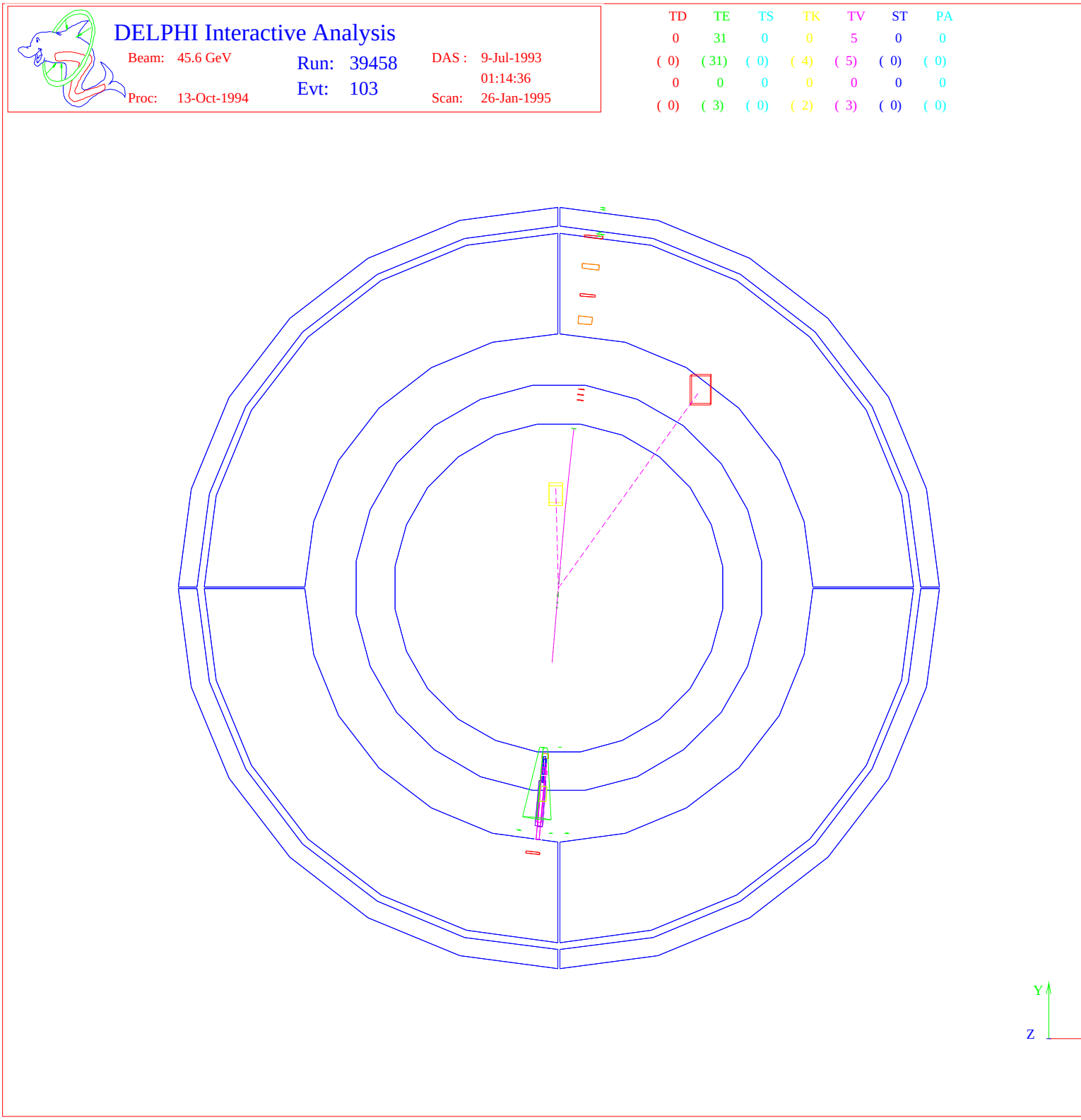

Figure 22: Classified as an $e\tau$ event. Probably a tau-pair with a high energy electron.

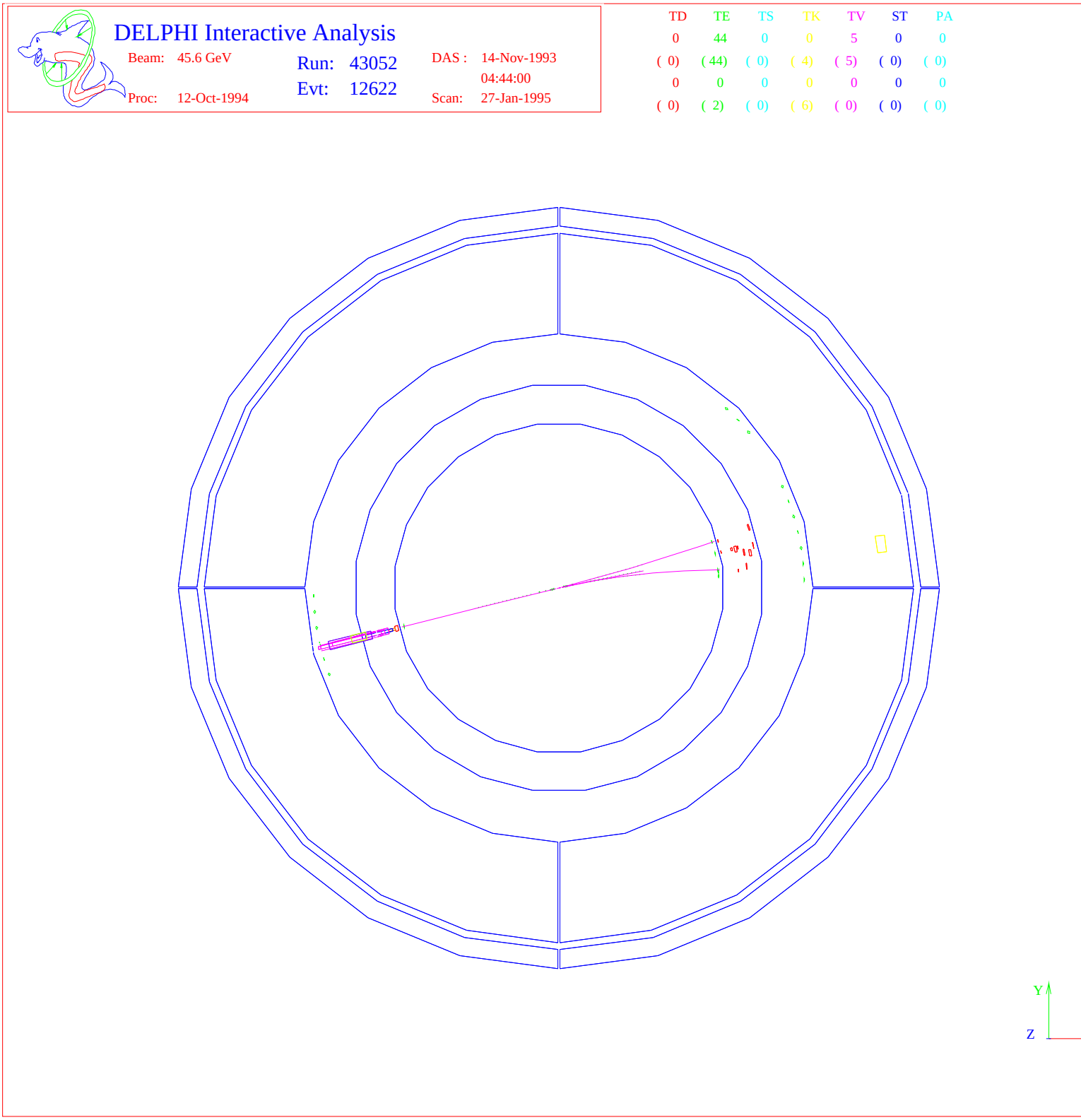

Figure 23: Classified as an eτ event. A possible tau-pair event.

5.6 $Z^0 \rightarrow \mu$e channel

The signature of μe event should be a single beam energy electron recoiling against a beam energy muon, a clean low background event.

Before the single particle tagging some preselection cuts were applied to reject events with bad detector status, containing cosmic background, or tracks outside the barrel area, similar to the $\mu\tau$ and eτ channels.

The following preselection cuts were used in the μe Channel:

- Detector status
  1. Time projection chamber status $5 \leq TPC \leq 7$
  2. Electromagnetic Calorimeter status $5 \leq HPC \leq 7$
  3. Muon Chambers status $5 \leq MUB \leq 7$
- Impact point less than 1.5cm from interaction point.
- The number of charged tracks had to be more than 1 but less than 11.

5.6.1 Luminosity in the μe channel

Luminosity were calculated from all events with SAT Luminosity information passing the detector quality cuts.

- Luminosity 1991 for the μe channel:
  1. Energy point 88.464GeV Luminosity 639$\pm$2.6 nb^{-1}
  2. Energy point 89.453GeV Luminosity 549$\pm$2.2 nb^{-1}
  3. Energy point 90.211GeV Luminosity 593$\pm$2.4 nb^{-1}
  4. Energy point 91.229GeV Luminosity 5218$\pm$20 nb^{-1}
  5. Energy point 91.952GeV Luminosity 625$\pm$2.5 nb^{-1}
  6. Energy point 92.952GeV Luminosity 550$\pm$2.2 nb^{-1}
  7. Energy point 93.701GeV Luminosity 581$\pm$2.3 nb^{-1}

  Integrated Luminosity of 8756$\pm$35 nb^{-1}
- 1992 Integrated Luminosity at Energy point 91.340 GeV of 21430$\pm$86 nb^{-1} at
- 1993
  1. Energy point 89.485GeV Luminosity 8585$\pm$34 nb^{-1}
  2. Energy point 91.295GeV Luminosity 14076$\pm$56 nb^{-1}
  3. Energy point 93.076GeV Luminosity 9060$\pm$36 nb^{-1}

  Integrated Luminosity of 31720$\pm$120 nb^{-1}

A total integrated Luminosity of 61900$\pm$210 nb^{-1}

5.6.2 Electrons in the μe channel

Electrons in the μe channel were selected by using similar cuts to the cuts used in the eτ channel. The background from tau pairs will almost vanish compared to the two other channels since single beam energy leptons were required in both hemispheres. Therefore the cuts could be less strict, giving much higher efficiency and less total background.

- SINGLE ELECTRONS WERE SELECTED BY TH FOLLOWING CUTS:

  1. one charged track in the hemisphere

     To suppress background from multiprong events from tau decay, cosmics and quarkevents.

  2. Normalized HPC energy

     $\frac{E_{HPC}}{E_{beam}} > 0.86$

     Since background from taus decaying to electrons were less important, due to not accepting taus in the opposite hemisphere, the cut in normalized HPC energy was set considerably lower than in the eτ channel. (figure 24)

  3. No energy in second, third or fourth HCAL layer and low in first

     H_1 <3.3 GeV, H_{2-4}=0

     The same argument as in the eτ channel, only that the value was set higher because of less problems with background (figure 26).

  4. No MUB hits

     Same as for the eτ channel.

  The efficiency of this single electron tagging was calculated from running a sample of Monte Carlo generated e^+e^- through the same selection routine. The single electron efficiency was found to be 73.0% in barrel.

5.6.3 Muons in the μe channel

Like the electrons in this channel the muons were selected by similar cuts to those used in the $\mu\tau$ channel, but with less strict cuts.

- SINGLE MUONS IN THE μE CHANNEL WERE SELECTED USING THE FOLLOWING CUTS:

  1. One charged track in hemisphere

     To suppress background from multiprong events from tau decay, and quarkevents.

  2. Muonchamber hit

     To suppress background from tau decaying to hadronic final states. (figure 27)

3. Normalized momentum

   $\frac{Momentum}{E_{beam}} > 0.86$

   Suppress background from tau decaying to muon final state.

4. Energy per layer in HCAL

   $0.03 < EHL < 3.9$

   Also to suppress background from tau decaying to hadronic final states. (figure 28)

EFFICIENCY The single muon efficiency was calculated from running a sample of Monte Carlo simulated Standard Model $\mu^+\mu^-$ through the same selection routine, and found to be 77.5% in barrel.

5.6.4 Result of the $Z^0 \to \mu$e channel search

The efficiency for finding the lepton flavour violating μe events was calculated from running a sample of Monte-Carlo simulated $Z^0 \to \mu$e trough the same routine and found to be (35.5±1.5)% (4π)

A plot of normalized HPC energy distribution for the electron versus normalized momentum distribution for the muon for events, and background passing the μe selection cuts $\frac{E_{HPC}}{E_{beam}}$ set to 0.5 are shown in figure 29

μe	Event a. cut	eμ	Event a. cut
Preselection cuts	154516	-	154516
μ id. cuts		e id. cuts	
Charged tracks	133063	Charged tracks	133063
MUB	49415	MUB	83648
p	36497	$\frac{E_{HPC}}{E_{beam}}$	35409
EHL	34390	H1	35304
e id. cuts		H24	35230
Charged tracks	33849	μ id. cuts	
MUB	2027	Charged tracks	33102
$\frac{E_{HPC}}{E_{beam}}$	0	MUB	26
H1	0	p	5
H24	0	EHL	0

Table 8: eμ channel. The table shows the number of remaining events after a given cut.

Data	Seen	$\mu^+\mu^-$ MC	e^+e^- MC	$\tau^+\tau^-$ MC	4π Eff MC %
1991	0	0	0	0.1±0.1	35.4±1.5
1992	0	0.5±0.3	0	0.5±0.3	35.5±1.5
1993	0	0.4±0.4	0	0.6±0.4	35.4±1.5

Table 9: $Z^o \rightarrow e\mu$

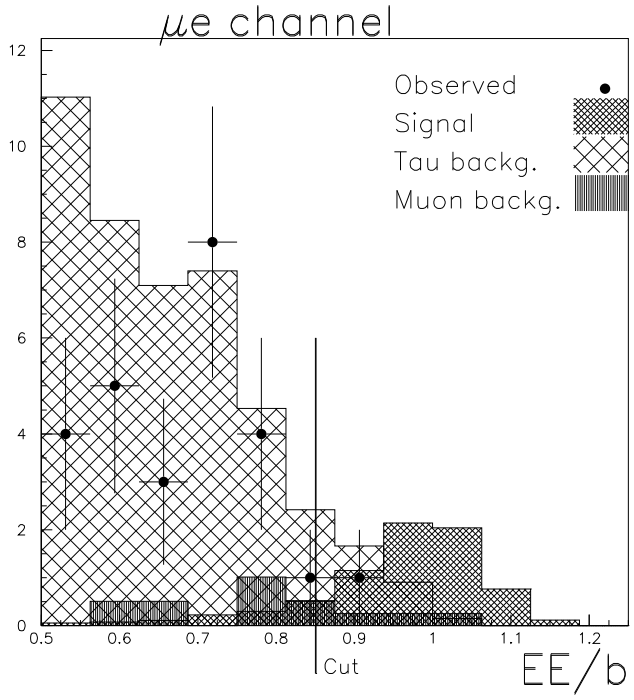

Figure 24: Normalized HPC energy distribution for leading track, when a muon is tagged in the opposite hemisphere. Events(black dots), background($\tau^+\tau^-$cross-hadched, $\mu^+\mu^-$black), and a signal(grey) are plotted. The cut in the electron selection routine is indicated.

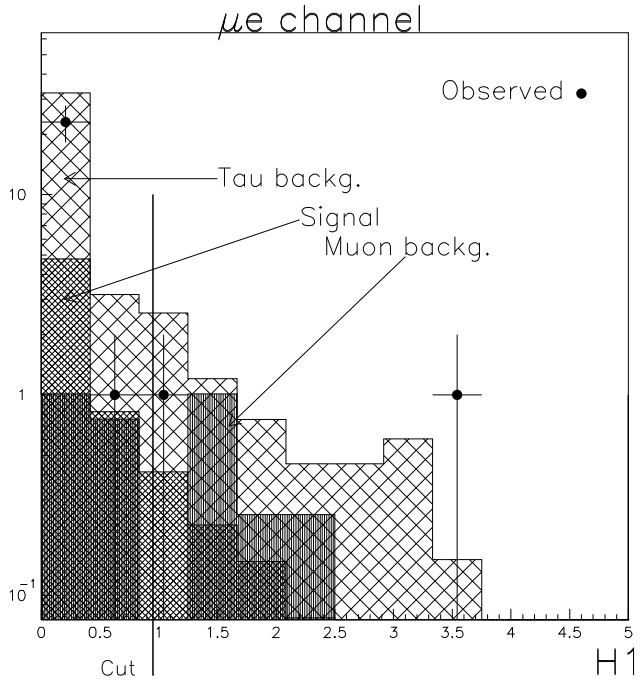

Figure 25: HCAL energy in first layer distribution for leading track when a muon is tagged in the opposite hemisphere. Events(black dots), background($\tau^+\tau^-$cross-hadched, $\mu^+\mu^-$black), and a signal(grey) are plotted. The cut in the electron selection routine is indicated.

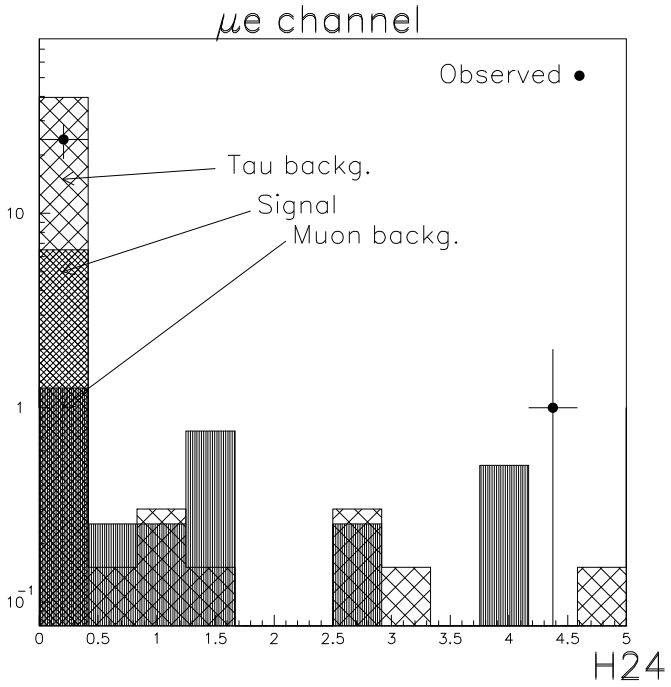

Figure 26: The sum of HCAL energy in second, third, and fourth layers distribution for leading track, when a muon is tagged in the opposite hemisphere. Events(black dots), background($\tau^+\tau^-$cross-hadched, $\mu^+\mu^-$black), and a signal(grey) are plotted.

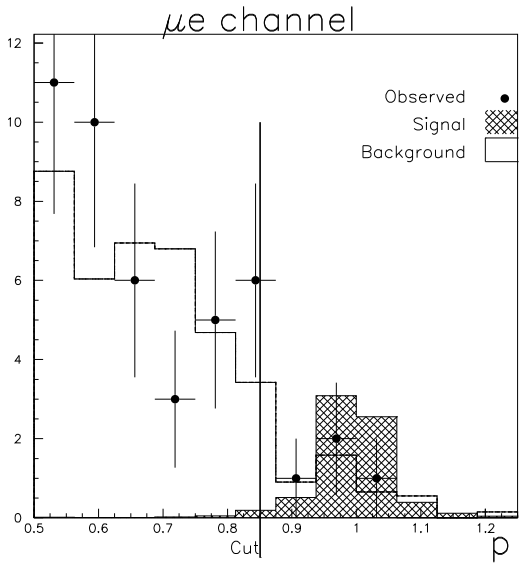

Figure 27: Normalized momentum distribution for leading track, when an electron is tagged in opposite hemisphere. A signal(grey) is indicated. The muon selection routine cut is indicated.

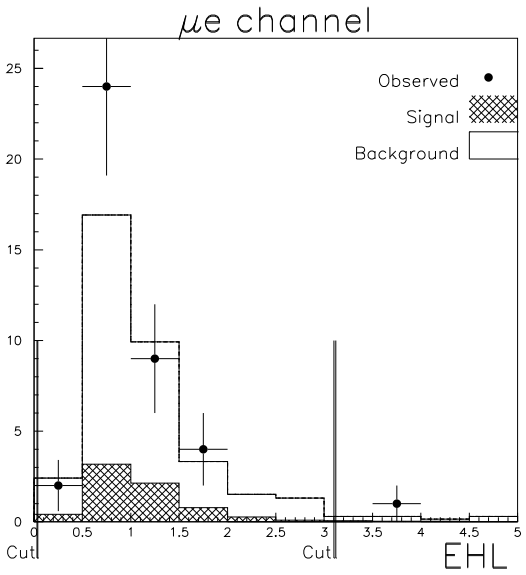

Figure 28: HCAL energy per layer with energy deposition, when an electron is tagged in opposite hemisphere. The observed events(black dots) are above the expected background(histogram), but just slightly more than a 1 σ fluctuation.

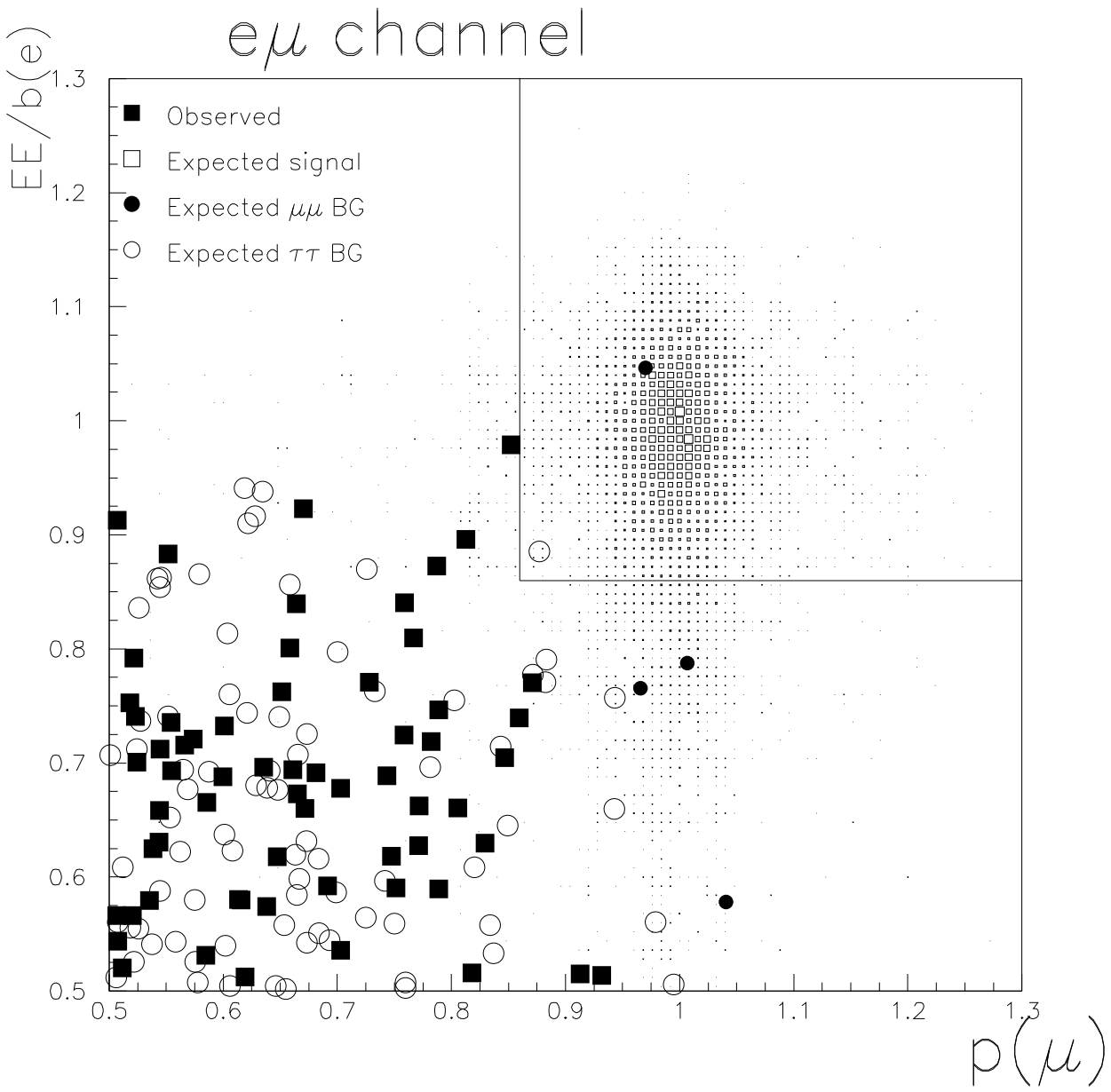

Figure 29: Normalized momentum for a tagged muon versus normalized HPC energy for a tagged electron in the same event. The eμ channel cut is indicated. Background is scaled to data, using only 15.1% of the total $\tau^+\tau^-$(open quadrangles) MC, and 25.5% of all $\mu^+\mu^-$(black circles) MC.

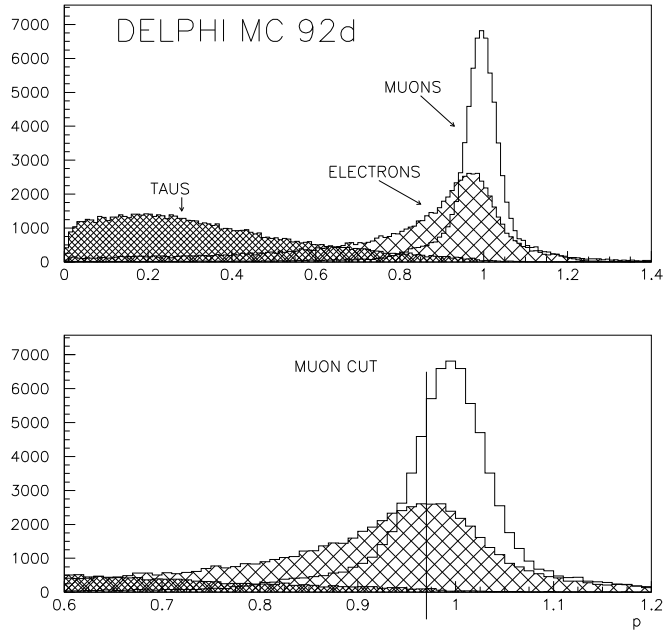

Figure 30: Normalized momentum Monte Carlo simulated $\mu^+\mu^-$, $\tau^+\tau^-$, and e^+e^- events for the 92d processing. In (b) the $\mu\tau$ channel μ cut is indicated.

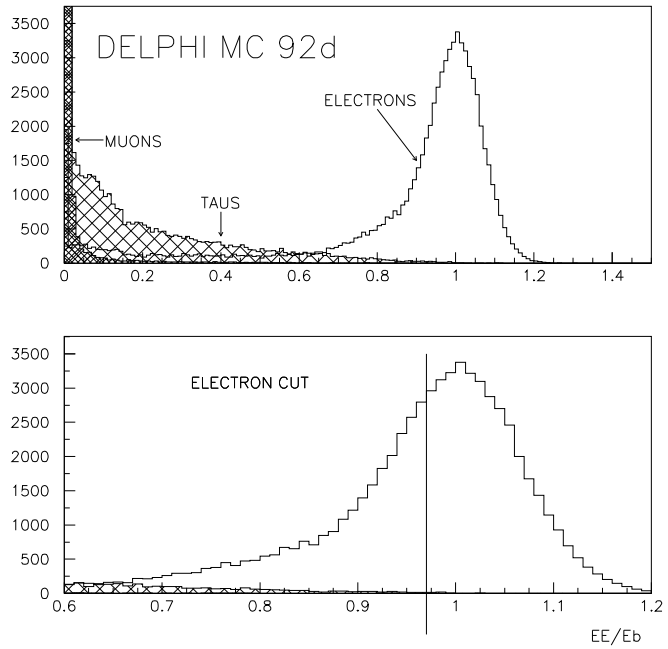

Figure 31: Normalized HPC energy Monte Carlo simulated $\mu^+\mu^-$, $\tau^+\tau^-$, and e^+e^- events for the 92d processing. In (b) the electron cut in the $e\tau$ channel is indicated.

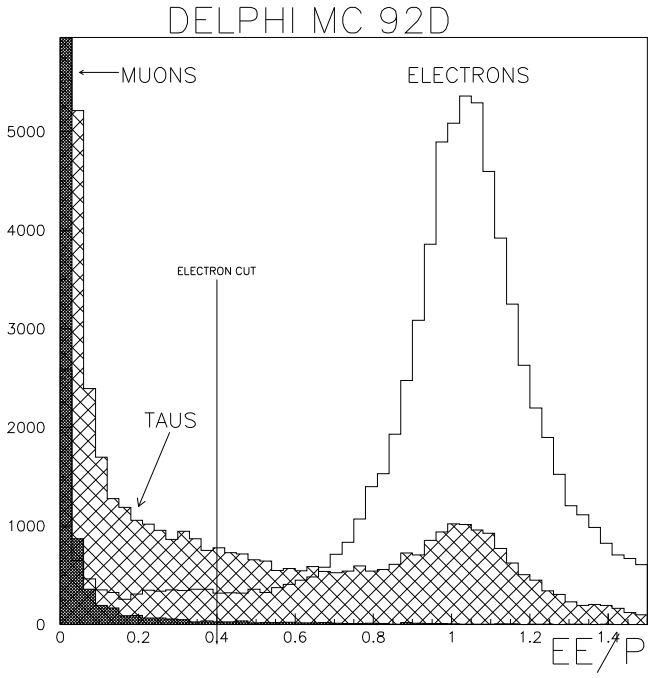

Figure 32: HPC energy Monte Carlo normalized to momentum simulated $\mu^+\mu^-$, $\tau^+\tau^-$, and e^+e^- events for the 92d processing. The electron cut in the $e\tau$ channel is indicated.

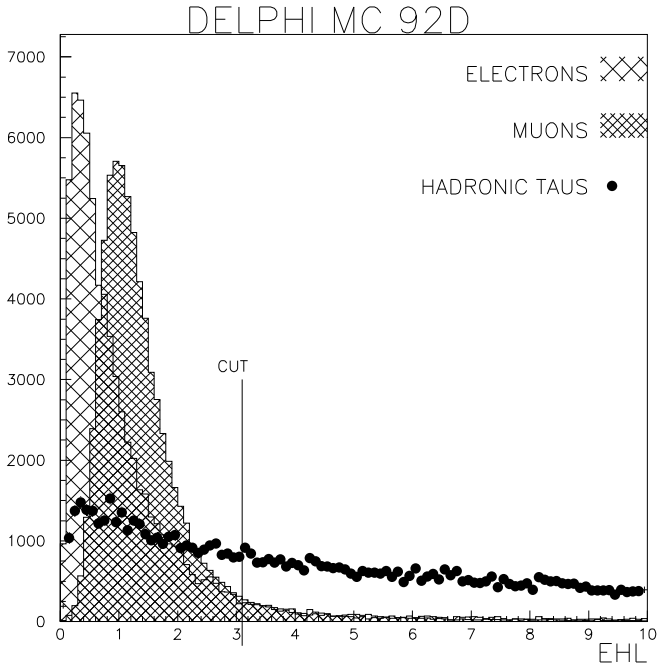

Figure 33: HCAL energy per layer, Monte Carlo simulated $\mu^+\mu^-$, and hadronic $\tau^+\tau^-$ events, 92d processing. The hadronic tau final state sample was selected demanding no MUB hit and low HPC energy. The cut in the $\mu\tau$ channel is indicated.

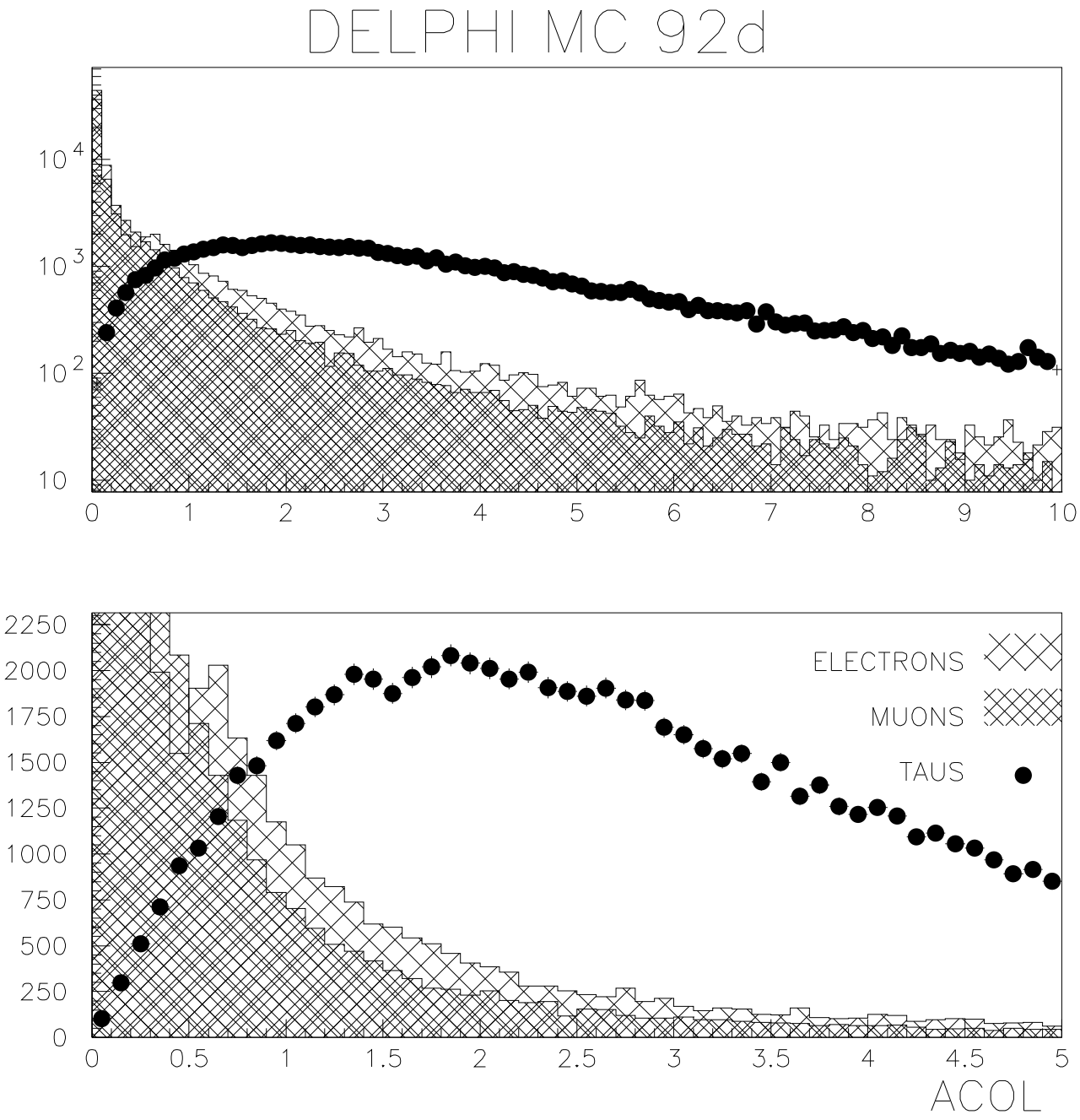

Figure 34: Acolinearity, Monte Carlo simulated $\mu^+\mu^-$, and hadronic $\tau^+\tau^-$ events, 92d processing.

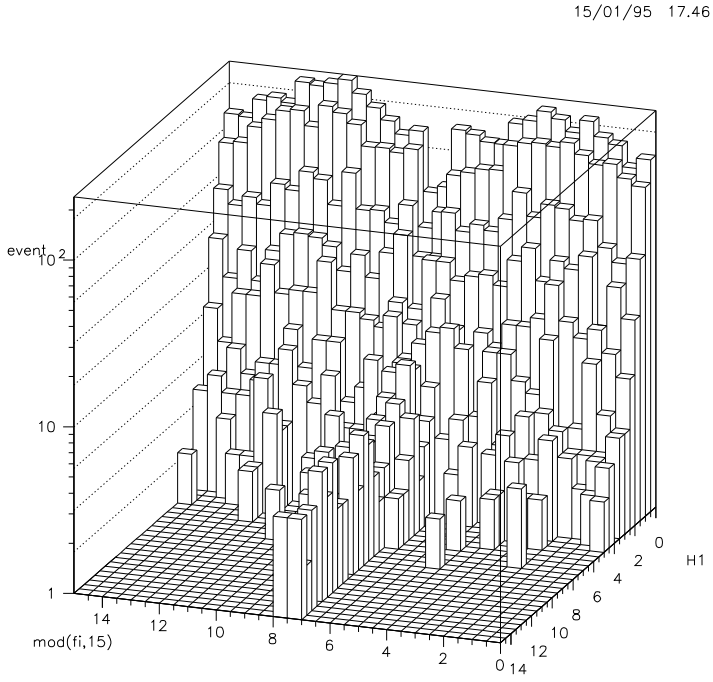

Figure 35: MC Electrons showering into first layer of HCAL versus the position of the track in the HPC module. The border section between two modules is in the middle of the figure,(at (mod(fi,15)=7.5).

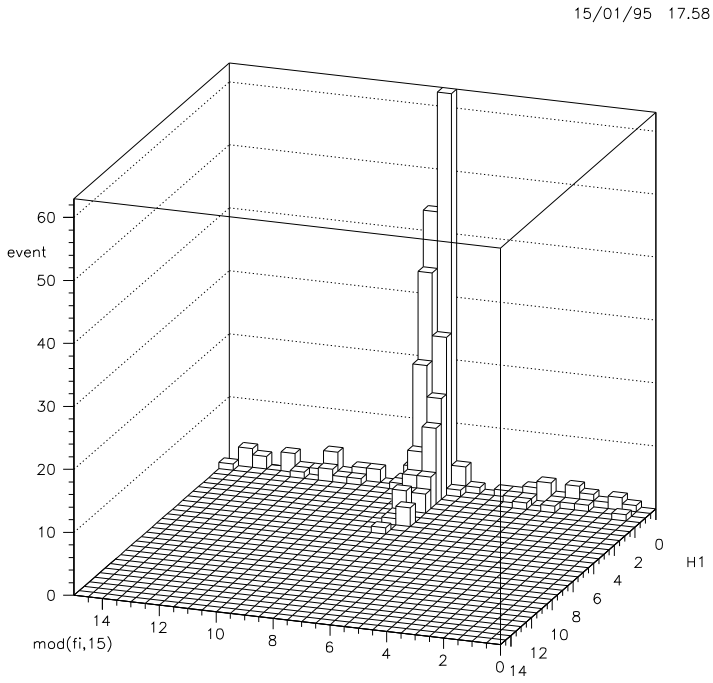

Figure 36: MC Electrons showering into second layer of HCAL versus the position of the track in the HPC module. The border section between two modules is in the middle of the figure, (at (mod(fi,15)=7.5).

6 Upper limits on branching ratios

In this section the process of estimating the background is described (section 6.1).

Also the calculation of Upper limits on branching ratios (section:6.2),

and smearing of MC to data used for background and efficiency calculations are described (section 6.4).

Data was collected in the DELPHI detector during LEP runs, and written on DST tapes, using the DELANA package [1].

In this thesis real data and Monte Carlo simulated leptonic events from the 91E($\tau^+\tau^-$ only), 91F(not $\tau^+\tau^-$), 92D and 93B processing were used.

6.1 Background estimate

Background was estimated from running samples of Monte Carlo(MC) simulated events through the same routine as data. A number $N_{l\bar{l}}^{MC}$ of events accepted as background in the $\mu\tau$, eτ and μe channels were obtained for each of the three MC simulated Standard model lepton pairs $\mu^+\mu^-$, e^+e^-, $\tau^+\tau^-$ event samples.

The number of Background events $N_{l\bar{l}}^{MC}$ passing the selection was scaled to data, giving a scaled background $B_{l\bar{l}}$:

$$B_{l\bar{l}} = \sum_{y=1}^{3} \frac{N_{l\bar{l}}^{MC} \sum_i L_i^{Data} \sigma_i \varepsilon_\theta}{n_{l\bar{l}}^{MC}} \tag{59}$$

(Where L_i^{Data} is the Luminosity at energy point i, σ_i the cross section at the energy point i, $n_{l\bar{l}}^{MC}$ is the number of generated MC events, and the factor ε_θ from equation 60 originates from that the MC are generated over less than 4π.)

Monte Carlo simulated events are generated in different regions of the detector which gives a scaling factor corresponding to the fraction of the full 4π:

$$\varepsilon_\theta = \frac{\int_{\theta_1}^{\theta_2}(1 + cos^2\theta + \frac{8}{3}A_{fb}cos\theta)dcos\theta}{\int_0^{180}(1 + cos^2\theta + \frac{8}{3}A_{fb}cos\theta)dcos\theta} \tag{60}$$

Where θ_1, θ_2 are the boundary within the events are generated, and A_{fb} is the forward backward asymmetry.

Upper limit on branching ratios calculated from equation 61 depend on the background. A too high background estimate will give a too low upper limit and might hide a signal. A too low estimate could fake signal.

Background estimated using the scaling of equation 59 was too high (figure 41, and 42). Therefor, to obtain a better correspondence between estimated background and observed events, an additional scaling was applied.

BACKGROUND FROM $\tau^+\tau^-$

The normalized momentum - (p) distribution for a sample passing the $\mu\tau$ channel cuts, (except for using P>0.5 in the μ identification), was used. All background

satisfying 0.5<P<0.9 were then assumed to be from τ-pairs. The extra scaling factor $\eta^y_{\tau\bar{\tau}}$ for year y was then:

$$\eta^y_{\tau\bar{\tau}} = \frac{N^y_O}{N^y_{\tau\bar{\tau}}}$$

(*Where N^y_O is the number of observed events in the region 0.5<p<0.9, and $N^y_{\tau\bar{\tau}}$ is the estimated number of τ-pairs in the same region scaled.*)

The extra scaling factors obtained are given in table 10.

BACKGROUND FROM $\mu^+\mu^-$

Subtracting the taus obtained after the extra scaling from the observed events, the rest were assumed to be μ-pairs, and a possible signal (fig 69). The muon background was then scaled down to data using:

$$\eta^y_{\mu\bar{\mu}} = \frac{N^y_O}{N^y_{\mu\bar{\mu}}}$$

this time using the region 0.9<p<1.1. (*Muon background was only scaled down; to prevent a too low upper limit, not up, not to destroy a signal.*)

The extra scaling factors obtained are given in table 10.

y	$\eta^y_{\tau\bar{\tau}}$	$\eta^y_{\mu\bar{\mu}}$
1991	0.885	0.3±0.2
1992	0.887	0.5±0.5
1993	0.915	1.0

Table 10: Extra scaling factors for background

6.2 Branching ratio upper Limit

Using a confidence interval of 95%, and using the formula for a Poisson process with background, in the absence of errors: (appendix: A.1) [19]:

$$95\% = 1 - \frac{e^{(\mu_B+N)} \sum_{n=0}^{n_0} \frac{(\mu_B+N)^n}{n!}}{e^{\mu_B} \sum_{n=0}^{n_0} \frac{\mu_B^n}{n!}} \tag{61}$$

Where μ_B is the expected background, n_0 the number of observed events, and N the upper limit.

To include error estimate the upper limit definition are extended to include integrals over the variables μ_B, and N:

$$1 - CL = \int dP(\mu_B) \int dP(N) \frac{e^{(\mu_B+N)} \sum_{n=0}^{n_0} \frac{(\mu_B+N)^n}{n!}}{e^{\mu_B} \sum_{n=0}^{n_0} \frac{\mu_B^n}{n!}} \tag{62}$$

6.3 Optimization

The aim of this search was; to first search for a signal of lepton flavour violation, and then if not finding such a signal, establish an upper limit for the processes searched for. In the search there are some obvious limitations which constrains the possible limit to reach.

- Number Z^0 produced.
- The efficiency of getting the events on tape, which just like the number Z^0 produced, was a parameter not possible to influence in this search.
- The DELPHI Detector: The detector has limitations due to resolution, impurity, dead areas and so on.
- The Monte Carlo:

Working with these limitation the goal was to reach the lowest possible upper limit or a clear as possible signal.

Since all variables in an event more or less are dependent the n variables can be considered a n-dimensional cut space, and the task will be to find the minima. The best way of obtaining the minima would then be to use all variables, and by varying all cuts simultaneously, in some intelligent way, go towards the minima, and avoiding the false ones.

This seams like a formidable and resource consuming task, and involves problems like the Monte-Carlo inconsistence, and how to not miss a signal, to be solved. a much simpler approach was used in this thesis.

Only one cut at the time was optimized, holding all other cutvalues fixed. Calculating the upper limit for the branching ratio at 95% confidence level, a dependence between the cutvalue and upper limit was obtained. This was repeated for all the cutvariables, and also for different fixed values for the cuts not varied, (to in a simple way try to simulate the full optimalization process described before).

To avoid to optimize for background the estimated background - (B^{MC}) was also set to be equal the number of observed events - (N^O) if $B^{MC} > N^O$.

Some examples of this optimization process are given in figures 43, 44, 45, 46, 43, 48, and 47.

6.4 Smearing of Monte Carlo

Good agreement between Data and MC is important for several reasons. Background was calculated from MC, and to be able to interpret the results of the search, it was important to get this estimate as correct as possible.

A to high background estimate might hide a result, which with a correct estimate would indicate lepton flavour violation. On the other hand a to low estimate could fake lepton flavor violation. Both scenarios quite unpleasant.

The efficiency was calculated from samples of Monte Carlo simulated events, and was thereby also dependent on a good data - Monte Carlo agreement.

In this thesis only the main cut variables are studied, even if there were some disagreement in several of the cut variables. But the influence on the result was assumed to mainly origin from the main variables, the electromagnetic energy for electron, and momentum for muons.

6.4.1 Smearing of Momentum

Normalized momentum(p) and hit in MUB were the main variable to select muons and suppressing tau background, both in the $\mu\tau$ and the μe channels. Small variations in p, around beam energy, influenced strong on efficiency and background, while other muon selection cuts were much less sensitive to variations. Therefore a good agreement in the momentum peak around beam energy, was essential.

Samples of muons from data and Monte Carlo generated muon-pairs were selected, and the width and the position of the MC, were compared to the data sample.

The μ-pair sample was selected by demanding;

1. Only one charged track per hemisphere, to suppress multiprong quark events.
2. Hit in muon-chambers both hemispheres, to suppress τ-pair background.
3. Acolinearity less than 0.5. To further suppress τ-pair background.
4. To remove the low energy tail in data mainly consisting of taus decaying into muons, high energetic muons is required in both hemispheres; $\frac{p}{E_{beam}}$ >0.75 in hemisphere one, and $\frac{p}{E_{beam}}$ >0.75 in hemisphere two

Unsmeared μ-pair Monte Carlo simulated events shows disagreement both in the location and shape of the characteristic muon momentum peak (fig 69).

To change the position of the top, a constant t_k multiplied with the momentum, was used. More energetic tracks will be less bent in the magnetic field and therefore have less of the curve inside the tracking detectors corresponding to a bigger error in momentum than less energetic tracks.

The width of the momentum was smeared by adding a variable, consisting of the result of two gaussian distributed functions, equation 63. The smearing was also made energy dependent by multiplying with the normalized momentum.

$$(1-c)\frac{1}{\sqrt{\pi}\sigma_1}e^{\frac{-x^2}{2\sigma_1^2}} + c\frac{1}{\sqrt{\pi}\sigma_2}e^{\frac{-x^2}{2\sigma_2^2}} \tag{63}$$

Each year was smeared independent

- MC 1991_F smeared to Data 1991_E: c=0.04, σ_1 = 0.012, σ_2=0.16, t_k=0.993
- MC 1991_F smeared to Data 1991_F: c=0.07, σ_1 = 0.023, σ_2=0.16, t_k=0.9952
- MC 1992_D smeared to Data 1991_F: c=0.05, σ_1 = 0.021, σ_2=0.16, t_k=0.993
- MC 1992_D smeared to Data 1992_D: c=0.10, σ_1 = 0.023, σ_2=0.16, t_k=0.9952

- MC 1992_D smeared to Data 1992_D: c=0.10, σ_1 = 0.020, σ_2=0.16, t_k=0.996
- MC 1993_B smeared to Data 1993_B: c=0.07, σ_1 = 0.023, σ_2=0.16, t_k=0.9952

(It might be argued that it is $\frac{1}{p}$ which is Gaussian distributed and should be smeared if smearing with a Gaussian. And to avoid shifting of sign for low energy instead of the more possible for high energy tracks. The later because high energy tracks are less bent in the magnetic field and the charge harder to establish.

In this thesis no cuts in charge were applied, which makes the later less important, and secondly; the momentum was smeared not with a Gaussian, but a function of two Gaussians.

6.4.2 Smearing of Electromagnetic energy

Normalized HPC energy was the main variable in electron selection and background suppression in both the eτ and the μe channels. Small variations in the E_{HPC} variable resulted in big variation in efficiency and background.

Samples of electrons were selected and the width and position of the MC were then fitted to the data sample.

The electron sample was selecting demanding:

1. Only one charged track per hemisphere. Suppress multiprong quark events.
2. No energy in any of 2.,3., or 4. layer of Hadronic calorimeter, both hemispheres. To suppress muons and hadron.
3. Acolinearity less than 0.5. Suppress tau decaying to electrons.
4. No muon chamber hits, both hemispheres. to further suppress muons. getting through cut 2.
5. Electromagnetic energy normalized to beam energy greater than 0.75 in both hemispheres. To remove the lower tail in data mainly consisting of taus decaying to electrons.

A correction is done both to the the position by multiplying the raw value of electromagnetic energy deposition with a constant k_1, and smeared by adding a gaussian distributed Energy dependent variable (eq:64).

$$v = v_1 \frac{E_{HPC}}{E_{beam}} k_2 \tag{64}$$

Where v_1 is a gaussian distributed variable with mean zero and sigma one. ee is electromagnetic energy in HPC and E_{beam} is beam energy.

The energy dependence in smearing avoids problems in the low energy region. Each processing is smeared separate:

- MC 1991_E smeared to data 1991_F: k_1=1.011, k_2=0.11.

- MC 1991_F smeared to data 1991_F: k_1=1.012, k_2=1.5.
- MC 1992_D smeared to data 1991_F: k_1=1.006, k_2=1.5.
- MC 1992_D smeared to data 1992_D: k_1=1.012, k_2=1.2.
- MC 1992_D smeared to data 1993_B: k_1=0.996, k_2=1.3.
- MC 1993_B smeared to data 1993_B: k_1=1.012, k_2=1.5.

6.4.3 Smearing of the angle dependence in HCAL energy distribution.

A correction of the angle dependence of HCAL energy was done by multiplying the associated HCAL energy for each leading track in the region $52< \theta < 128$ with $\sin^2\theta$.

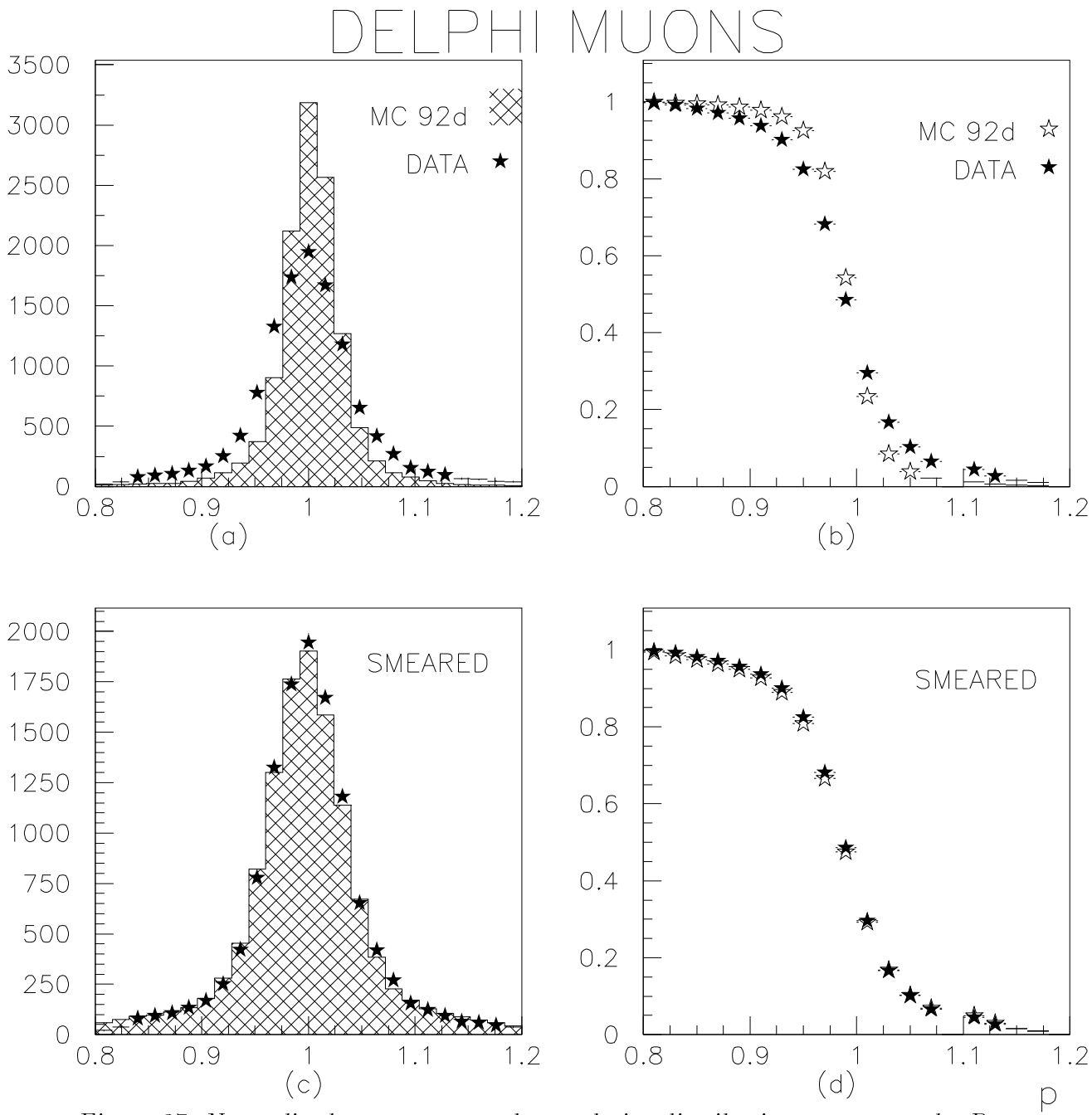

Figure 37: Normalized momentum and cumulative distribution muon samples Data and Monte Carlo 92d. Smeared MC in (c) and (d).

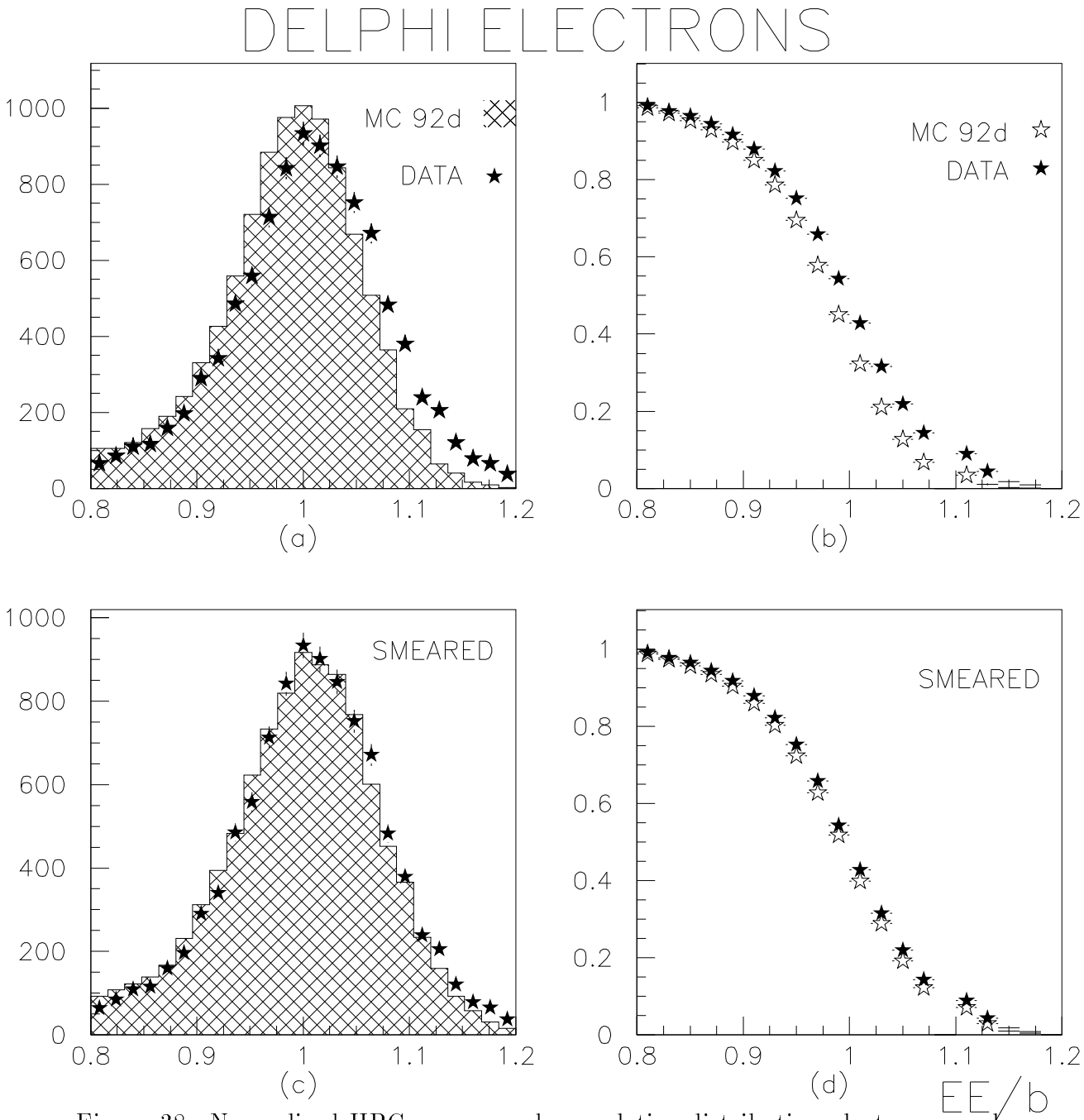

Figure 38: Normalized HPC energy and cumulative distribution electron samples Data and Monte Carlo 92d. Smeared MC in (c) and (d).

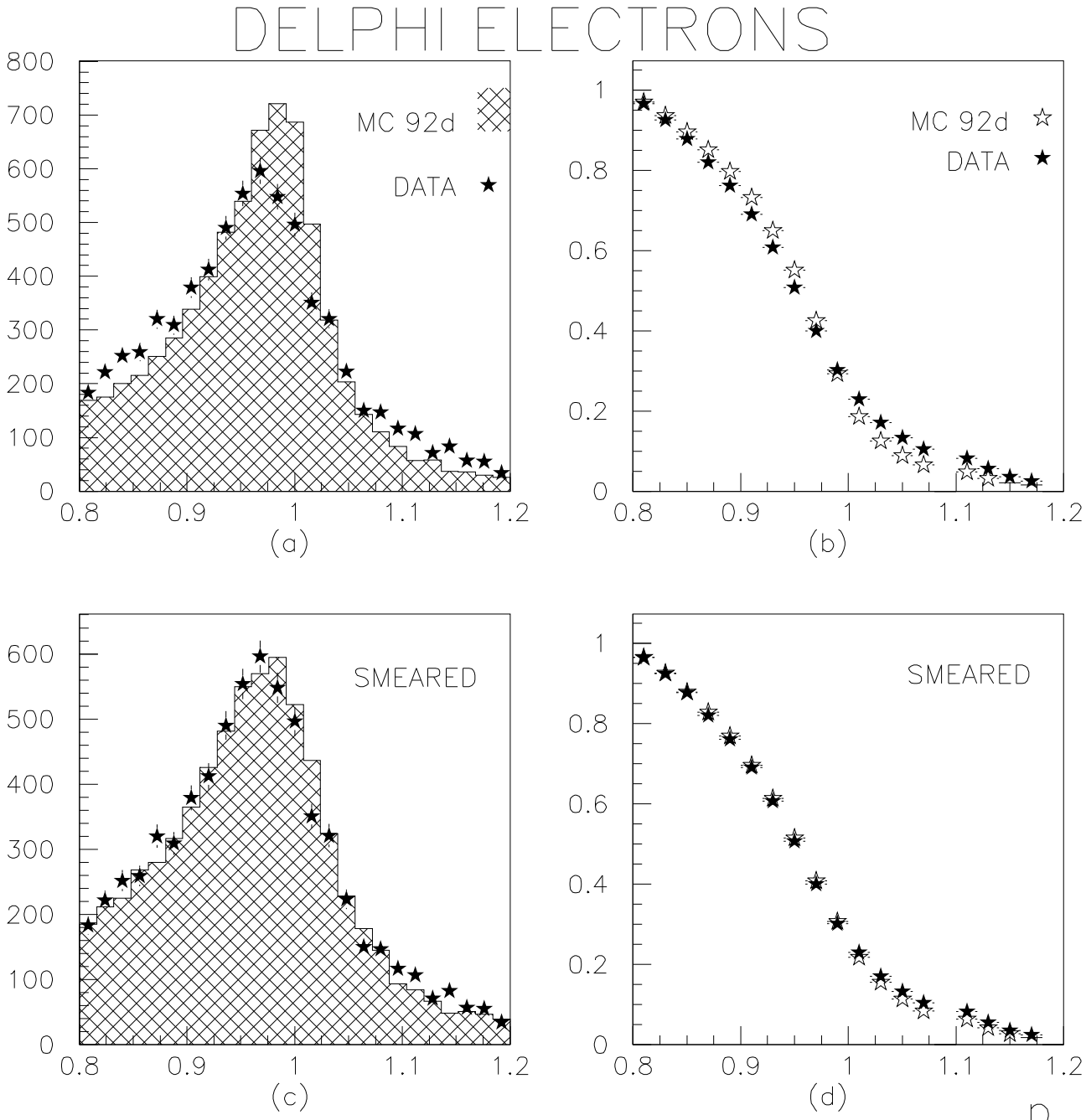

Figure 39: Normalized momentum and cumulative distribution electron samples Data and Monte Carlo 92d. Smeared MC in (c) and (d).

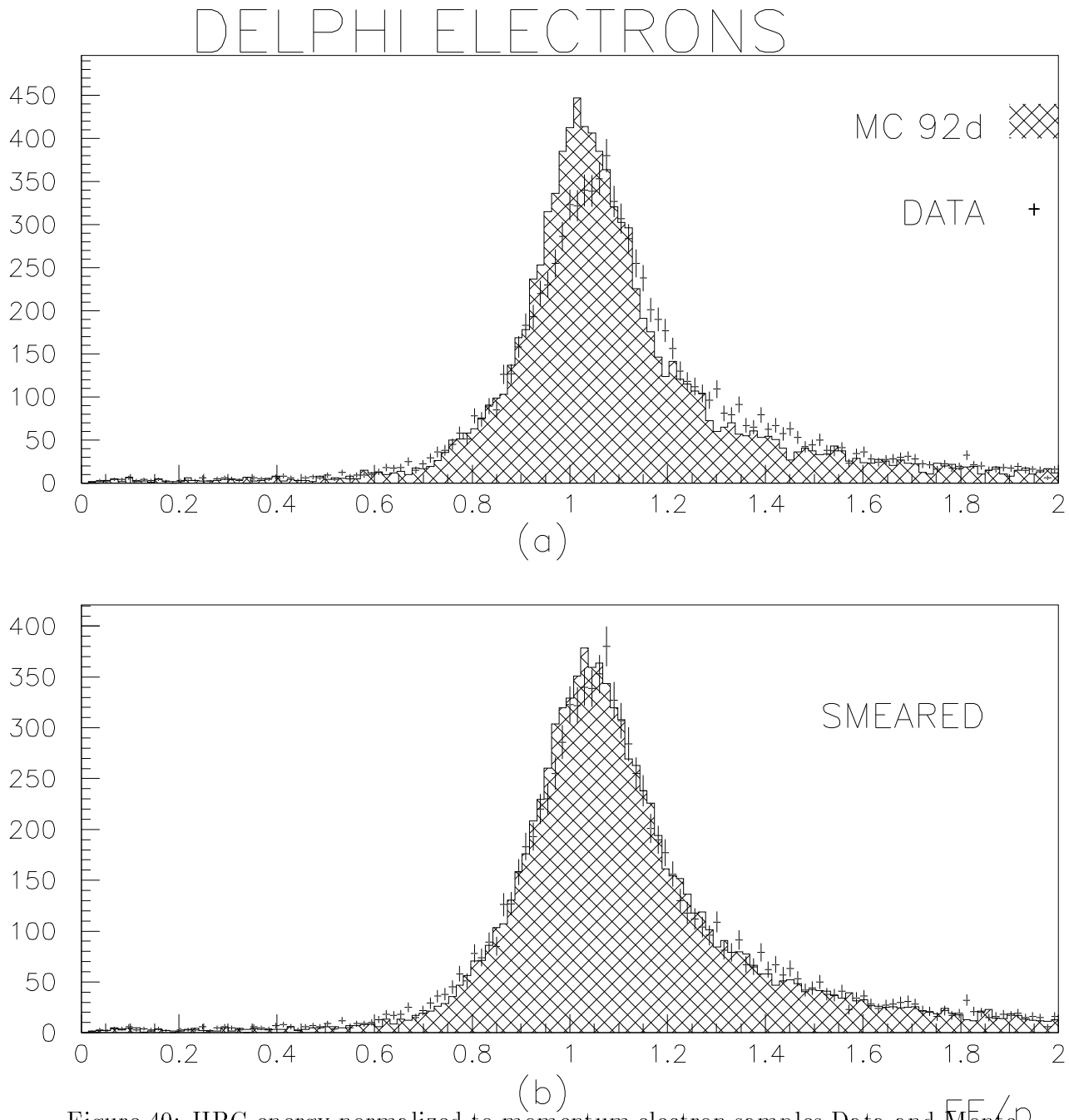

Figure 40: HPC energy normalized to momentum electron samples Data and Monte Carlo 92d. Smeared MC in (c) and (d).

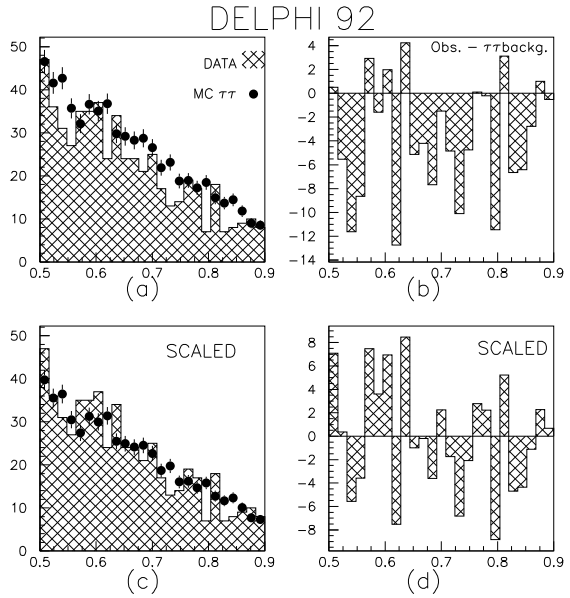

Figure 41: Normalized momentum distribution: (a) observed event(histogram), and MC 92d smeared tau-pair background. (b) observed event subtracted tau-pair background. (c) Same as a only after scaling tau-pair background to data. (d) Same as c but tau scaled.

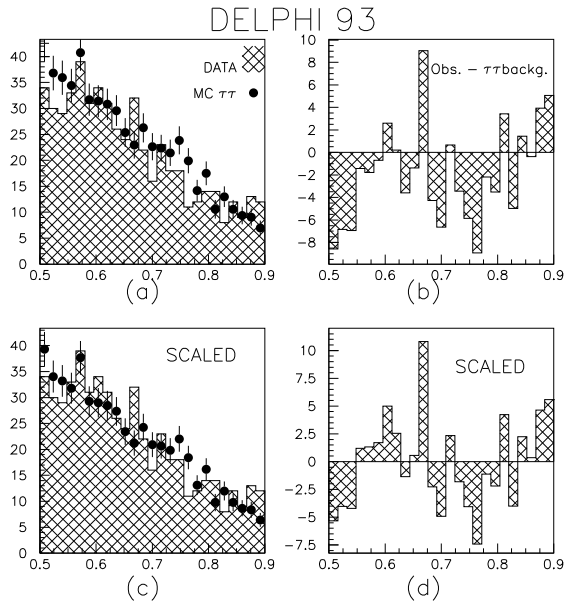

Figure 42: Normalized momentum distribution: (a) observed event(histogram), and MC 93b smeared tau-pair background. (b) observed event subtracted tau-pair background. (c) Same as a only after scaling tau-pair background to data. (d) Same as c but tau scaled.

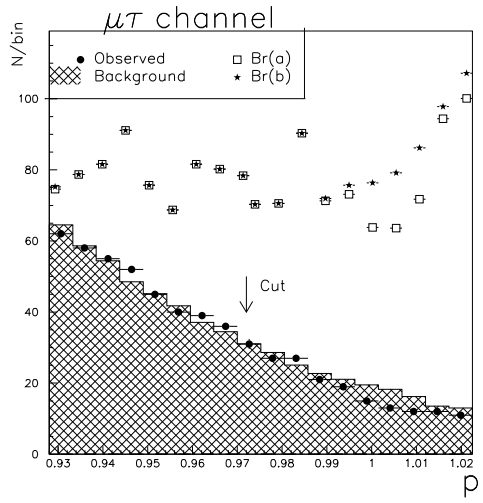

Figure 43: Number of observed events N_o(black dots) and background N_b (cross-hatched) varying with the normalized momentum cut for muons. Upper limit (95% CL) multiplied with the number of Z^0 (Br[$Z^0 \to \mu\tau$]$\times N_z$) - Br(a) normal procedure (open quadrangles), - Br(b) using observed events also as background whenever $N_b > N_o$ (black stars).

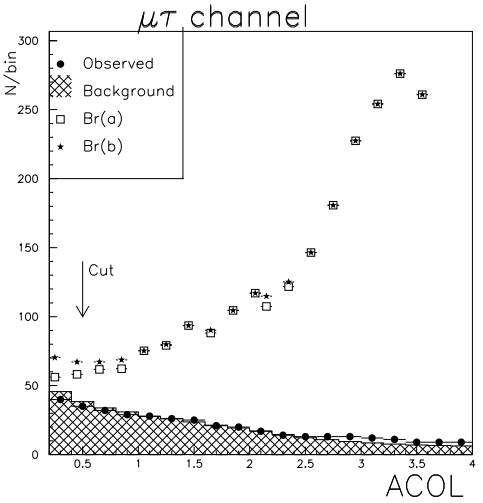

Figure 44: Number of observed events N_o(black dots) and background N_b (cross-hatched) varying with the acolinearity of the event. Upper limit (95% CL) multiplied with the number of Z^0 (Br[$Z^0 \to \mu\tau$]$\times N_z$) - Br(a) normal procedure (open quadrangles) - Br(b) using observed events also as background whenever $N_b > N_o$.

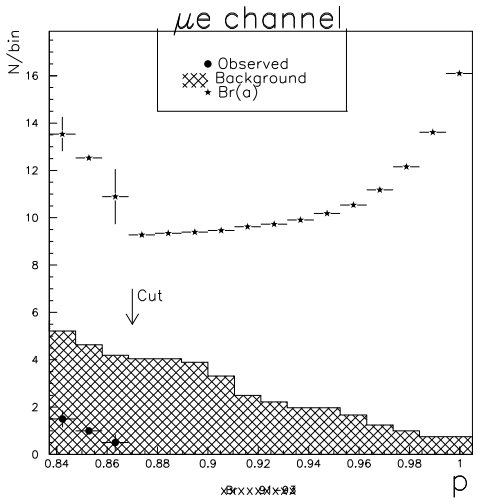

Figure 45: Number of observed events N_o(black dots) and background N_b (cross-hatched) varying with the normalized momentum cut for muon identification. Upper limit (95% CL) multiplied with the number of Z^0 (Br[$Z^0 \rightarrow \mu\tau$]$\times N_z$) - Br(a) using observed events also as background whenever $N_b > N_o$ (black stars) to avoid false minima.

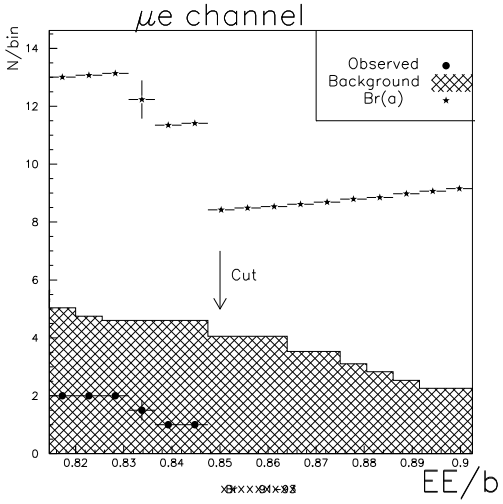

Figure 46: Number of observed events N_o(black dots) and background N_b (cross-hatched) varying with the normalized HPC energy cut for electron identification. Upper limit (95% CL) multiplied with the number of Z^0 (Br[$Z^0 \rightarrow \mu\tau$]$\times N_z$) - Br(a) using observed events also as background whenever $N_b > N_o$ (black stars) to avoid false minima.

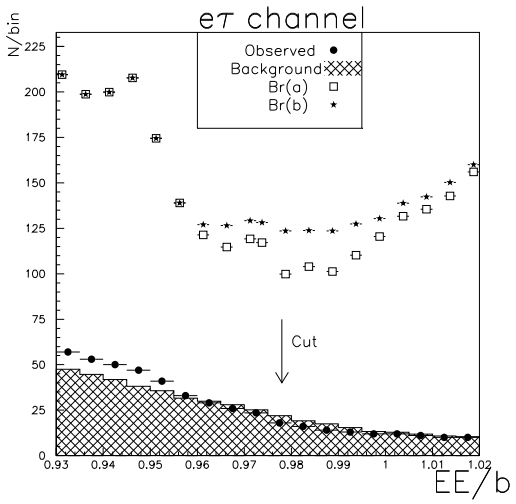

Figure 47: Number of observed events N_o(black dots) and background N_b (cross-hatched) varying with the normalized HPC energy cut in the electron tag. Upper limit (95% CL) multiplied with the number of Z^0 (Br[$Z^0 \to \mu\tau$]$\times N_z$) - Br(a) normal procedure (open quadrangles), - Br(b) using observed events also as background whenever $N_b > N_o$ (black stars).

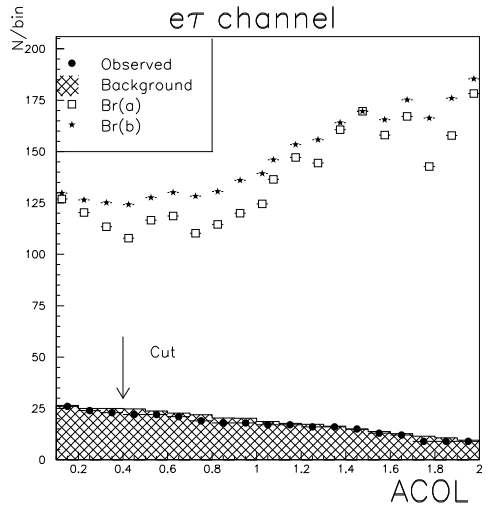

Figure 48: Number of observed events N_o(black dots) and background N_b (cross-hatched) varying with the acolinearity of the event. Upper limit (95% CL) multiplied with the number of Z^0 (Br[$Z^0 \to \mu\tau$]$\times N_z$) - Br(a) normal procedure (open quadrangles), - Br(b) using observed events also as background whenever $N_b > N_o$ (black stars).

7 SUMMARY AND CONCLUSION

No evidence for lepton flavour violation were found. The number of events are consistent with background in all channels. Upper limits at 95% confidence level were set for for the three channels $\mu\tau$, eτ, and μe (table 11)

Upper limits can at least in the $\mu\tau$ channel be slightly improved by a likelihood analyzes.

The results obtained in this thesis are comparable with the results obtained by OPAL and ALEPH, but not competing with the results presented in table 1 by the L3 collaboration. This is due to L3's better use of the forward region, and better momentum and energy resolution.

- -	$Z^0 \to \mu\tau$	$Z^0 \to$eτ	$Z^0 \to \mu$e
Background			
MC $\tau^+\tau^-$	15.3±1.6	16.8±2.0	1.3±0.5
MC e^+e^-	0	2.0±0.5	0
MC $\mu^+\mu^-$	15.7±2.0	0	0.9±0.5
4π eff.	18.6±0.9%	7.8±0.5%	35.5±1.5%
obs.	29	16	0
pred 95% C.L	11.3	8.3	3.0
Br 95% C.L	2.9×10^{-5}	4.8×10^{-5}	0.40×10^{-5}

Table 11: *Results of the search at 95% CL*

A APPENDIX

A.1 Upper limit on a signal in the presence of a background

Assume μ_0 events observed and μ_B to be the expected mean background with S as the unknown mean signal.

The confidence level (CL) is defined as the probability that the true signal is less than the upper limit.

The likelihood $L(s)ds$ is the probability of obtaining the experimental results μ_0 if the true value of S is between$S$ and S+ds. The likelihood for observing μ_0 events if the true signal is S:

$$L(s) = N\frac{e^{-(\mu_B+S)}(\mu_B+S)^{\mu_0}}{\mu_0!} \tag{65}$$

for $0 \leq S < \infty$

The normalization N can be determined from the requirement

$$\int_0^\infty L(s)ds = 1 \tag{66}$$

Which gives:

$$N = \frac{\mu_0!}{\int_0^\infty e{-}(\mu_B+S)(\mu_B+S)^{\mu_0}ds} \tag{67}$$

The confidence level of an upper limit l on S is then the probability that S<l:

$$CL = \int_0^l L(s)ds = \frac{\int_0^l e{-}(\mu_B+S)(\mu_B+S)^{\mu_0}ds}{\int_0^\infty e{-}(\mu_B+S)(\mu_B+S)^{\mu_0}ds} = 1 - \frac{e{-}(\mu_B+l)\sum_{\mu_0}^{n=0}\frac{(b+l)^n}{n!}}{e^{-b}\sum_{\mu_0}^{n=0}\frac{b^n}{n!}} \tag{68}$$

The factor $e^{-b}\sum_{\mu_0}^{n=0}\frac{b^n}{n!}$ in equation 68 results from the fact that no more than μ_0 background events can be observed.

A.2 Branching Ratio

The branching ratio for a signal:

$$Br(Z^0 \to xy) = \frac{N_s}{\epsilon^s_{xy}N^{Z^0}} \tag{69}$$

Where N_s *is the number of observed signal events,* ϵ^s_{xy} *is the efficiency for observing the signal, and* N^{Z^0} *is the number of* Z^0 *which is used in the analysis*

The N_s is then replaced in the presence of background with an upper limit at a given confidence level of a signal S calculated from equation 68

B DETECTORS OF HIGH ENERGY PHYSICS

Particle detectors are the instruments used to measure the kinematic properties of particles and quanta i.e. their four-vector. [3] [20] In order to detect a particle it has to interact with the material of the detector. It can interact with an atomic nucleus via the strong interaction if it is a hadron, or by the weak interaction if it is a neutrino. If the energy is sufficiently high, new particles my be produced as a first step in a detection process.

To be detected the particle has to transfer energy to the medium they are transversing. This can occur via the process of ionization or excitation of the constituent atoms which can be detected for example as charged ions in an gas counter, scintillation light, Cerenkov radiation, etc.

The Bethe-Bloch formula for the mean rate of ionization loss of a charged particle:

$$\frac{dE}{dx} = \frac{4\pi N_0 z^2 e^4}{mv^2}\frac{Z}{A}\left[ln\left(\frac{2mv^2}{I(1-\beta^2)}\right) - \beta^2\right] \tag{70}$$

Where m is the electron mass, z and v the charge and velocity of the particle, N_0 Avogadro's number, Z and A the atomic number and mass number of the atoms in the medium, x the path length in the medium, and I an effective ionization potential averaged over all electrons.

Part of the energy loss of a relativistic particle may be reemitted from excited atoms in the form of coherent radiation at a particular angle, so called Cerenkov radiation B.3.

The main energy loss results in formation of ion pairs in the medium. The incident particle produces primary ionization in atomic collisions. Electrons with high energy produced in this process can themselves produce ions in traversing the medium. The total number of ion pairs is 3-4 times the number of primary ionization, and is proportional to the energy loss of the incident particle in the medium. The average energy loss has a very characteristic dependence on the velocity of the incident particles.

Electron also lose energy in traversing a medium in the process of radiation loss or *bremsstrahlung* (eq: 71). The nuclear electric field decelerates the electron and the energy appears in the form of a photon with a spectrum of approximate form of $\frac{dE'}{E'}$ where E' is the photon energy. For a relativistic electron the average energy loss is given by:

$$-\frac{dE}{dx} = \frac{E}{L_R} \tag{71}$$

Where L_R is the radiation length given by:

$$\frac{1}{L_R} = 4\left(\frac{\hbar}{mc}\right)^2 Z(Z+1)\alpha^3 n_a ln\left(\frac{183}{Z^{\frac{1}{3}}}\right) \tag{72}$$

Where n_a is the atom density per cm^3

The rate of ionization energy loss of fast electrons is approximately constant, while the average radiation loss is proportional with the energy, it follows that at high energy radiation loss dominates. Radiation losses are much smaller than ionization losses for all other particles than electrons and positrons at all but very high energies.

The energy lost in Coulumb collision with nuclei is neglectable since $\frac{dE}{dx}$ in equation 70 is inversely proportional to the target mass. Coulumb scattering is on the other hand important because it limits the precision with which the direction of the particle can be determined.

Photons have a high probability of being absorbed or scattered through large angels by the atoms in matter.

Detector used in high energy physics are aimed to identify the particles. This can be done from simultaneous measurement of velocity by time-of-flight or Cerenkov radiation, momentum, and rest mass from the observation of decay modes if the particle is unstable and from its observed interaction with mater via strong, electromagnetic, or weak forces.

Neutral particles are detected trough their decay and/or interaction with matter leading to secondary charged particles.

No single detector is general able to meet all this requirements so a combination of detector types has to be used.

B.1 Tracking of charged particles

Tracking detectors register the ionization trail left by the passage of the charged particle. The medium must permit the transport of the ionization charge.

B.1.1 Solid-state ion chambers:

Semiconductor Detectors Silicon strip/microstrip detectors is based on semiconductor technology. A particle crossing the medium releases energy and produces electron-hole pairs. In the presence of an electric field, electrons and holes separate and are collected at the electrodes giving a signal proportional to the energy loss of the incident charged particle. Semiconductor detectors has a very good spatial resolution but limited ability to withstand radiation.

B.1.2 Proportional Counters

A Proportional Counter Consist of a gas-filled tube of metal or glass maintained at a negative potential, with a fine central anode wire at a positive potential. The electric field in the gas for a potential difference V_0 is then:

$$E(r) = \frac{V_0}{rln(\frac{r_1}{r_2})} \tag{73}$$

Where r_1 and r_2 is the radius of the anode wire and gas tube respectively

An electron liberated by ionization will drift towards the anode and gain energy. If the energy exceeds the ionization energy of the gas new ions are produced and a chain of such processes leads to a shower of electrons and positive ions. The gas amplifying factor is typical of the order of 10^5 independent of the number of primary ions.

Wire chambers A multiwire proportional counter consist of many parallel anode wires stretched in a plane between two cathode plans with the different anode wires acting as independent detectors.

B.1.3 Drift Chambers/Time Projection Chamber(TPC)

To achieve good spatial resolution over large areas using Proportional Counters an enormous number of wires and amplifiers are required. Instead this can be achieved for low interaction intensity, like in e^+e^- colliders, by drifting the electrons from the primary ionization in a low field region before reaching the high-field amplification region near the anode wire. The collection time of the avalanche then gives a measure of position. Very large volume(100m^3) drift chambers have been built.

B.2 Energy measurement of electrons, photons, and hadrons

The energy measurement of particles and quanta provides complementary information to momentum determination. For neutral particles and photons it is the only methode of obtaining information on their kinematical properties. Shower calorimeter Energy and position of secondaries from high-energy interaction can be measured by total-absorbtion. Incident particles interact in a large detector mass, generate secondary particles, which again generates new particles until the energy of the incident particle appears as ionization or excitation in the medium.

For high energy electrons and photons the combined result of bremsstrahlung and pair production gives a cascade shower. Pair production and photon radiation will increase exponential with the depth in the medium, reaching its maximum and then cease abrupt when the particle energy get below ionization energy in the medium.

Hadron shower result from anincident hadron undergoing an inelastic nuclear collision with production of secondary hadrons, which again interact inelastic to produce hadrons and so on.

Compared with electromagnetic shower detectors, hadron calorimeter are large. In a hadron cascade roughly 30% of the incident energy is lost by the breakup of nuclei, nuclear excitation, and evaporation neutrons and photons, and does not give an observable signal.

B.3 Cerenkov Counters

Cerenkov Counters are based on the Cerenkov effect. When an high-energy charged particle traverses a dielectric media parts of the light emitted by excited atoms form

a wave front at a fixed angle with respect to the trajectory. Such radiation appears whenever the particle velocity βc exceeds $\frac{c}{n}$ where n is the refractive index of the medium. The wavefront forms a cone about the trajectory axis:

$$cos\theta = \frac{ct/n}{\beta ct} = \frac{1}{\beta n} \tag{74}$$

Cerencov radiation appears as a continues spectrum. In a dispersive medium but n and θ will be functions of the frequency ν. The numbers of photons at a particular frequency or wavelength is proportional to $d\nu$ or $\frac{d\lambda}{\lambda^2}$.

Measurement of the angle 74 provides a direct measurement of the velocity βc.

B.4 Readout methods for calorimeter

Scintillation Counters The excitation of the atoms of certain media by ionizating particles result in luminescence which can be recorded by a photomultiplier. The scintillator can be of inorganic single crystals, organic liquids and plastics, and also in liquids and gases.

Inorganic crystal scintillator are doped with activator centers. Ionizing particles traversing the crystal will produce free electrons and holes, which move around until captured by an activator center. This transforms into an excited state and decays with emission of visible light over a broad spectrum.

In organic materials molecules are exitated which decay with emission of light in the UV region. The light is then shifted to the blue region via fluorescent excitation of dye molecules known as wavelength shifters, incorporated into the scintillator medium.

The light from the medium is recorded by photomultiplier tube consisting of a photocathode where electrons are liberated by the photoelectric effect.

References

[1] 89-49 PROG. *DELANA USERS GUIDE.*

[2] 89-67 PROG 142. *DELSIM USERS GUIDE.*

[3] G.Shaw B.R.Martin. *PARTICLE PHYSICS.* John Wiley & Sons, 1992.

[4] DELPHI colab. *THE DELPHI DETECTOR AT LEP.* Nucl.Instr A303, 1991. (233-276).

[5] ARGUS Collab. *SEARCH FOR LEPTON NUMBER AND LEPTON FLAVOUR VIOLATION IN TAU DECAYS.* Phys.lett.B 185, 1987. (228).

[6] DELPHI Collab. *A SEARCH FOR LEPTON FLAVOUR VIOLATION IN Z^0 DECAYS.* Phys.Lett.B 298, 1993. (247).

[7] L3 Collab. *SEARCH FOR LEPTON FLAVOUR VIOLATION IN Z DECAYS.* CERN-PPE/93 – 151, (Phys.Lett.B), August 9. 1993.

[8] OPAL Collab. *A SEARCH FOR LEPTON FLAVOUR VIOLATION IN Z DECAYS.* Phys.Lett.B 254, January 17. 1991. (293).

[9] OPAL Collab. *A SEARCH FOR LEPTON FLAVOUR VIOLATION Z^0 DECAYS.* CERN-PPE 95-043, 1995. (preprint).

[10] DELPHI public area files. *LUMINOSITY91.RES, SATLUM92.07JUL93, LUMI93.30NOV93.*

[11] DELPHI public area files. *RUNQUALI.SUMARY91, RUNQUALI.SUMARY92, RUNQUALI.SUMARY93.*

[12] D.J.W.F.Valle. *HIGH LUMINOSITIES AT LEP.* CERN report, 11 march 1991. (98).

[13] T. Bowcock et al. (CLEO). *SEARCH FOR NEUTRINOLESS DECAYS OF THE τ LEPTON.* Phys.Rev.D 41, Feb. 1 1990. (805).

[14] J.Bernabeu et. all. *LEPTON FLAVOUR NON-CONSERVATION AT HIGH ENERGIES IN A SUPERSTRING INSPIRED STANDARD MODEL.* Phys.Lett.B 187, 26 March 1987. (303).

[15] E.W.Otten. *DIRECT NEUTRINO MASS MEASUREMENTS.* Nucl. Phys. B (Proc. Suppl.) 38, 1995. (26-35, and references therin).

[16] R.Kleiss F.A.Berends, W.Hollik. *BABAMC.* Nucl.Phys. B304, 1988. (712).

[17] A.D.Martin F.Halzen. *QUARKS AND LEPTONS.* John Wiley & Sons, 1984.

[18] G.Shaw F.Mandel. *QUANTUM FIELD THEORY.* John Wiley & Sons, 1993.

[19] G.Flogge. *FUTURE RESEARCH IN HIGH ENERGY PHYSICS.* CERN 94-04, 30 June 1994. (and references therein).

[20] Particle Data Group. *PARTICLES AND FIELDS.* Phys. Rev. D, 1 August 1994.

[21] Donald H.Perkins. *INTRODUCTION TO HIGH ENERGY PHYSICS.* Addison-Wesly Publishing Comp.,Inc., 1987.

[22] I.Vorobiev. *SEARCHES FOR LEPTON FLAVOUR CHANGING NEUTRAL CURRENT USING* τ. Nucl.Phys.B(Proc. Suppl.) 40, 1995. (513-522, and references therein).

[23] R.Zitoun J.E.Campagne. *DUMY3.* Z.Phys.C43, 1989. (469).

[24] L. Di Lella. *CURRENT PROBLEMS IN NEUTRINO PHYSICS.* CERN, Summer school, lecture, July 1993. (Unpublished).

[25] Jukka Maalampi. *PHYSICS OF MASSIVE NEUTRINOS.* Nordic School in High Energy Physics Phenomenology, June 11-17 1994. (Unpublished).

[26] Kari Marvik. *SEARCH FOR FOR LEPTON FLAVOUR VIOLATION IN* τ*-DECAY USING THE DELPHI DETECTOR.* Dept. of Physics, University of Bergen, April 21 1994. (Cand.Scient. thesis).

[27] M.J.S.Levin. $e^+e^- \rightarrow \tau^+\mu^-$ *DUE TO SCALAR-LEPTON MIXING.* Phys.Rev.D 36, 1 September 1987. (1329).

[28] J.Brown P.C.W.Davis. *SUPERSTRINGS, a theory of everything ?* Cambridge University Press, 1988.

[29] R.Kleiss. *INTRODUCTION TO THE STANDARD MODEL.* CERN Summer school, 1993. (Unpublished).

[30] P.B.Pal R.N.Mohapatra. *MASSIVE NEUTRINOS IN PHYSICS AND ASTROPHYSICS.* World Scientific, Singapore, 1991.

[31] R.Stroynowski. *SUMMARY TALK.* Nucl.Phys.B(Proc. Suppl.) 40, 1995. (513-522 and references therein).

[32] W. Betl et. al. SINDRUM Collab. *SEARCH FOR THE DECAY* $\mu^+ \rightarrow e^+e^+e^-$. Nucl.Phys.B 260, 1985. (1).

[33] Z.Was S.jadach, B.F.L.Ward. *THE MONTE CARLO PROGRAM KORALZ VERSION 3.8, FOR THE LEPTON OR QUARK PAIR PRODUCTION AT LEP/SLC ENERGIES.* CERN-TH 5994/91, Comp.Phys.Commun.66, 1991. (276).

[34] S.Myers. *THE JOHN ADAMS MEMORIAL LECTURE.* CERN, 26 November 1990.

[35] N.Nakagawa T.K.Kuo. *LEPTON-FLAVOUR-VIOLATING DECAYS OF Z^0 AND τ*. Phys.Rev.D 32, 11 July 1985. (306).